

See discussions, stats, and author profiles for this publication at: <https://www.researchgate.net/publication/259335711>

25th Anniversary Article: Ordered Polymer Structures for the Engineering of Photons and Phonons

ARTICLE in ADVANCED MATERIALS · JANUARY 2014

Impact Factor: 17.49 · DOI: 10.1002/adma.201303456 · Source: PubMed

CITATIONS

31

READS

149

7 AUTHORS, INCLUDING:



Jae-Hwang Lee

University of Massachusetts Amherst

41 PUBLICATIONS 396 CITATIONS

[SEE PROFILE](#)



Jonathan Phillip Singer

Rutgers, The State University of New Jersey

26 PUBLICATIONS 535 CITATIONS

[SEE PROFILE](#)



Seog-Jin Jeon

Rice University

23 PUBLICATIONS 750 CITATIONS

[SEE PROFILE](#)



Edwin L Thomas

Rice University

620 PUBLICATIONS 24,357 CITATIONS

[SEE PROFILE](#)

25th Anniversary Article: Ordered Polymer Structures for the Engineering of Photons and Phonons

Jae-Hwang Lee,* Cheong Yang Koh, Jonathan P. Singer, Seog-Jin Jeon, Martin Maldovan, Ori Stein, and Edwin L. Thomas*

The engineering of optical and acoustic material functionalities via construction of ordered local and global architectures on various length scales commensurate with and well below the characteristic length scales of photons and phonons in the material is an indispensable and powerful means to develop novel materials. In the current mature status of photonics, polymers hold a pivotal role in various application areas such as light-emission, sensing, energy, and displays, with exclusive advantages despite their relatively low dielectric constants. Moreover, in the nascent field of phononics, polymers are expected to be a superior material platform due to the ability for readily fabricated complex polymer structures possessing a wide range of mechanical behaviors, complete phononic bandgaps, and resonant architectures. In this review, polymer-centric photonic and phononic crystals and metamaterials are highlighted, and basic concepts, fabrication techniques, selected functional polymers, applications, and emerging ideas are introduced.

other materials: (1) scalability; (2) wide tunability; (3) ease of functionalization; (4) mechanical flexibility; (5) compatibility with various patterning methods; (6) relatively low cost; (7) light-weight. Moreover, the artificially created non-linear photonic/phononic behavior of the periodic structures can be further diversified and enhanced by introduction of intrinsic non-linear behavior of additives to achieve state-of-the-art multifunctional properties (optical, electrical, mechanical, etc.) (Figure 1).

1.1. Current Trends

Research on photonic crystals (PhCs) has been explosive for nearly three decades since the concept of the 3D PhCs was proposed independently for inhibition of the spontaneous emission of atoms by Yablonovitch^[1] and for strong

1. Introduction to Wave Interaction with Periodic Structures

Compared to their behavior in unstructured, bulk materials, the propagation of photons and phonons in periodic micro- or nano-structures can be dramatically altered enabling the deliberate engineering of the photon or phonon interaction with matter. Although control via periodic structures has been demonstrated in a host of material systems, our review will focus on polymer-based structures and their associated applications. Polymer-based structures have several exclusive advantages over

Dr. J.-H. Lee, Dr. S.-J. Jeon,
Dr. O. Stein, Prof. E. L. Thomas
Department of Materials Science and Nanoengineering
Rice University
Houston, TX, 77005, USA
E-mail: leejh@rice.edu; elt@rice.edu

Dr. J. P. Singer, Dr. M. Maldovan
Department of Materials Science and Engineering, MIT
Cambridge, MA, 02139, USA

Dr. C. Y. Koh
DSO National Laboratories
Singapore, 118230, Singapore

This is an open access article under the terms of the Creative Commons Attribution-NonCommercial License, which permits use, distribution and reproduction in any medium, provided the original work is properly cited and is not used for commercial purposes.

DOI: 10.1002/adma.201303456

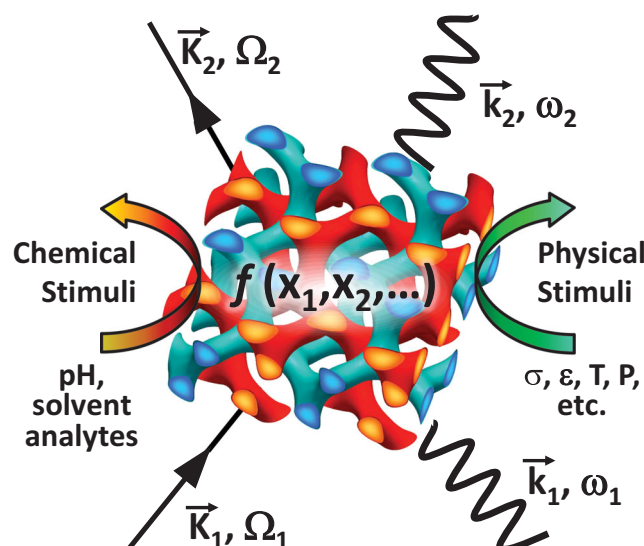


Figure 1. The versatility, flexibility, and multi-functionality of a periodic polymer/fluid structure is illustrated. The functional polymer represented by a double-gyroid structure (red, blue networks) is simultaneously interacting with phonon (Ω) and photon (ω) waves while the material's interaction parameters (periodicity, dielectric constant, impedance, etc.) continuously respond to a broad range of physical and chemical stimuli, resulting in tunable photonic and phononic behavior.

localization of photons by John^[2] in 1987. The capability to create artificial photonic dispersion and photonic bandgaps (PBGs) has led to the emergence of a major interdisciplinary field of science and technology as is evidenced by the publication rate shown in **Figure 2a**. Initially, PhC research was predominantly driven by physics; however much of the current research activity occurs in engineering disciplines, surpassing the output of physics. The contribution from biologically focused research is small, but rapidly growing. With regards to application areas, the main research focus has been laser applications due to the initial concepts of Yablonovitch and John, but now sensors and energy applications are fast-growing without any apparent slow-down in their growth rates compared to laser applications (Figure 2b). At this rate, interest in sensor applications is likely to surpass that of laser applications in a few years. Recently, the exotic properties promised by photonic metamaterials have added a new growth area. In the continued development of photonics, polymer structures will play an increasingly critical role, and it is therefore timely for a review of the recent progress in fabrication and applications of photonic polymer structures.

Phononic crystals (PnCs) are periodic structures comprised of materials having different mechanical impedances. These micro- and nano-composites can create artificial acoustic dispersion and phononic bandgaps (PnBGs) similar to PhCs. The annual number of publications on PnCs is relatively smaller than that of PhCs, but since 2000 the number has grown rapidly as can be seen in Figure 2c. Importantly, due to the speed of sound being several orders of magnitude slower than the speed of light as well as the absence of a fundamental speed of sound, phononic structures can be easily designed to have interesting dispersion relations in the deep sub-wavelength regime. This has led to burgeoning research in acoustic metamaterials to control the flow of acoustic waves below the diffraction limit. A number of non-conventional phenomena can arise from phononic metamaterials such as acoustic cloaking,^[3–5] negative acoustic refraction,^[6–8] and negative modulus.^[9] As the engineering of mechanical waves in solid/solid and fluid/solid structures has been demonstrated in the acoustic and ultrasonic regimes, polymer-based phononic metamaterials enable reconfigurable, adaptive, and active functionality.



Jae-Hwang Lee has been a research scientist in Materials Science at Rice University since 2011. He received his Ph.D. in Physics at Iowa State University in 2006 for his research on metallic wood-pile photonic crystals. As a postdoctoral researcher, he joined the Thomas group at MIT in 2007 and studied nonlinear mechanical behavior of nano-structured materials. His current research interest is focused on optical and mechanical metamaterials and micro-ballistic characterization of nanostructures.



Edwin “Ned” Thomas is Dean of Engineering at Rice University, with appointments in materials science, chemical engineering and chemistry. His research is focused on 2D and 3D lithography, direct-write and self-assembly techniques to create polymer based metamaterials with unprecedented optical, mechanical and thermal properties. He joined Rice in 2011 after a career at MIT and is a member of the National Academy of Engineering.

1.2. Basic Ideas of Band Diagrams

We next briefly introduce basic concepts and ideas related to the band structure of a periodic material. The group velocity governing the energy flow of both electromagnetic and elastic waves is defined by $v_g = d\omega/dk$, where ω and k are an angular

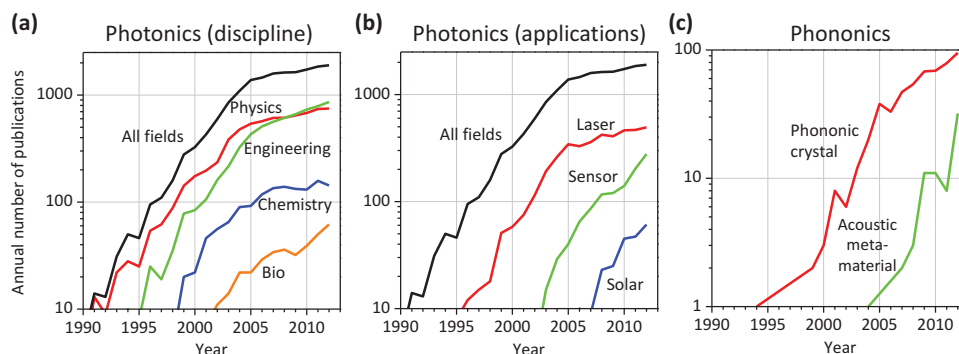


Figure 2. (a) Annual photonic crystal research papers produced by different disciplines. (b) Annual photonic crystal research papers featuring lasers, sensors, and solar applications. (c) Annual research papers on phononic crystals and acoustic metamaterials. Note the factor of 10 difference in scale compared to figures (a) and (b). Data from Web of Knowledge, ISI.

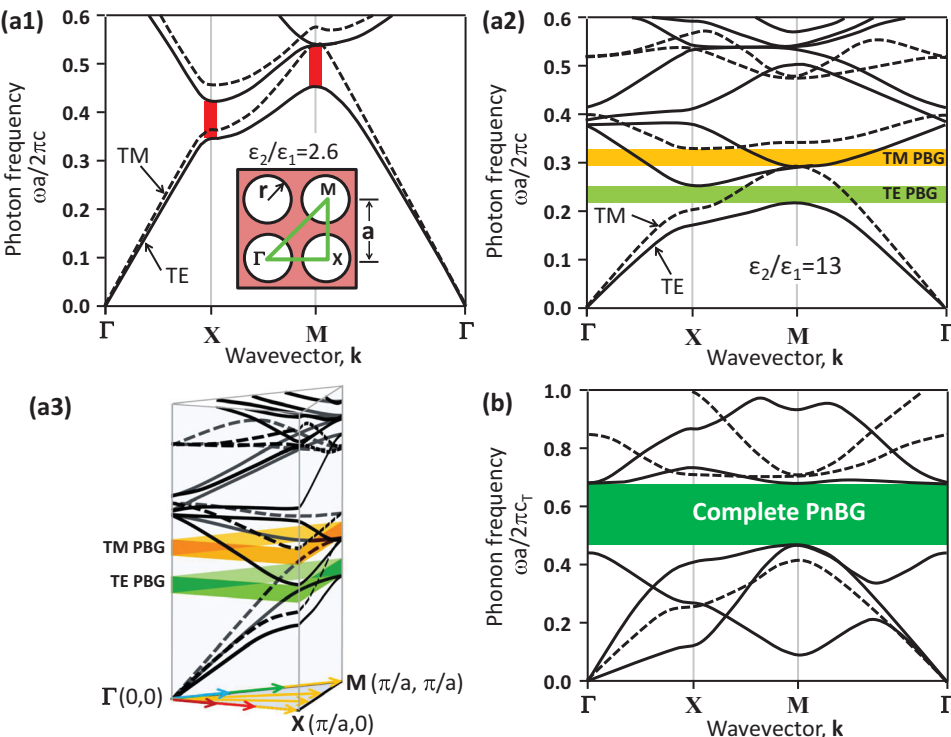


Figure 3. (a1) The 2D photonic band diagram of a typical polymeric solid having a permittivity of $\epsilon = 2.6\epsilon_0$ with embedded air cylinders in a square lattice. The air cylinders have a radius $r = 0.45a$, where a is the lattice constant of the structure (inset). The partial PBG for TE-polarization is shown in red for the Γ -X and the Γ -M directions, respectively. (a2) The 2D photonic band diagram of the same structure with a higher permittivity of $\epsilon = 13\epsilon_0$ exhibiting a PBG for TM-polarized waves and for TE-polarized waves. However, since the TE and TM gaps do not overlap, there is no polarization-independent complete gap. (a3) The 2D photonic band diagram in (a2) is folded along the boundary of the irreducible BZ. (b) The phononic band diagram of the same structure with typical polymer solid density of $\rho = 1190 \text{ kg m}^{-3}$, transverse sound speed $c_T = 1800 \text{ m/s}$, and longitudinal sound speed $c_L = 3100 \text{ m/s}$, respectively, for in-plane (solid lines) and out-of-plane (dashed lines) elastic waves.

frequency and a wavevector, respectively, and a plot of $\omega(\mathbf{k})$ vs. \mathbf{k} is known as the dispersion relation or the (photonic, phononic) band diagram. When the slope of dispersion curve approaches zero, for example, at the edge of a Brillouin zone (BZ), the propagation speed of the waves is significantly slowed or the modes become a standing wave ($v_g \sim 0$) which can result in the enhanced interaction of the photon/phonon with the material or the prohibition of energy flow. When a PhC or a PnC has a so called *complete* bandgap, no propagation mode exists within a range of frequencies (PBG or PnBG) regardless of directions and polarizations of photons or phonons. For a given propagation direction, the width of a bandgap, represented by a gap-to-midgap ratio, $\Delta\omega/\omega$ in frequency is generally proportional to the optical parameter contrast, $(\mu_2\epsilon_2)\mu_1\epsilon_1^{1/2}$ for PBGs, or the elastic parameter contrast, $(\rho_2K_2/\rho_1K_1)^{1/2}$ for PnBGs, where μ_i and ϵ_i are magnetic permeability and dielectric permittivity, and ρ_i and K_i are the mass density and bulk elastic modulus of at least two different constituent materials. In a 2D or 3D lattice, since these ratios depend on the propagation direction, a sufficiently large contrast is essential to open a complete PBG or a PnBG to prohibit the propagation of waves in all directions.

A band diagram showing the dispersion relation, $\omega(\mathbf{k})$ up to the boundary of the irreducible BZ is an effective means to view the overall characteristics of $\omega(\mathbf{k})$ of a 2D or 3D photonic or phononic crystal. For simplicity, we consider a 2D PhC with

a square symmetry to illustrate a 2D photonic band diagram for in-plane propagation with two different polarizations. Our chosen 2D PhC is made of air cylinders arranged on the square lattice (symmetry $p4mm$) in a polystyrene (PS) matrix with permittivity $\epsilon = 2.6\epsilon_0$ (Figure 3a1). The photonic band structure for the PhC is plotted against dimensionless frequency $\omega a/2\pi c$ and only needs to be considered as a function of the wave vector \mathbf{k} over one quadrant of the BZ (the irreducible BZ) due to rotational and mirror symmetries in this particular PhC.

For transverse electric (TE)-polarized light, the 1st PBG appears for dimensionless frequency between 0.35~0.42 (red gap) for propagation along the Γ -X direction while the PBG shifts to 0.45~0.54 (blue gap) for the Γ -M direction. Thus, there is no complete PBG for TE-polarization; this is also true for transverse magnetic (TM)-polarization. For relatively long wavelengths ($\lambda \gg a$), $\omega(\mathbf{k})$ always approaches a linear relationship with a slope of c/n_{eff} for all PhCs, where c and n_{eff} are the speed of light in vacuum and an effective refractive index for a given polarization. An effective index can be used because the PhC acts as a homogeneous medium for these long wavelengths. This does not mean, however, that the PhC is an effectively isotropic medium. Indeed, for normalized frequencies less than 0.3, the TM polarization mode (with the magnetic field oscillating along the z -axis) has a slope greater than that of TE polarization mode (with the electric field oscillating along

Table 1. Optical and mechanical characteristics at room temperature of selected materials affecting photonic and phononic behavior. The values of refractive index are defined at a specific wavelength (given in parentheses) and values for K and G are provided for quasi-static conditions. The longitudinal impedance contrast, Z/Z_{air} , is estimated using a density and a bulk modulus.

Material	n	ρ [g cm $^{-3}$]	K [GPa]	G [GPa]	c_L [km s $^{-1}$]	c_T [km s $^{-1}$]	Z/Z_{air}
Polydimethylsiloxane (PDMS)	1.43 (580 nm)	0.97	1	0.003	3.0	0.8	3100
Poly(methyl methacrylate) (PMMA)	1.49 (550 nm)	1.18	6.2	2.2	2.7	1.3	8600
Polystyrene (PS)	1.59 +10 $^{-4}$ i (500 nm)	1.05	3.6	1.5	2.3	1.2	6100
Polycarbonate (PC)	1.59 (550 nm)	1.20	2.4	1.9	2.8	1.3	5400
Silicon	3.50 (1.36 μ m)	2.33	98	65	9.0	5.4	47900
Aluminum	1.01 + 6.6i (550 nm)	2.70	69	26	6.4	3.1	43200
Steel	2.76 + 3.8i (633 nm)	7.80	160	79	5.8	3.1	111800
Diamond	2.42 (550 nm)	3.5	442	478	18.4	9.2	124400
water	1.33 (550 nm)	1.0	2.2	10 $^{-6}$	1.5	N/A	4700
Air	1.00 (550 nm)	10 $^{-3}$	10 $^{-4}$	N/A	0.34	N/A	1

z -axis), because the electric field of TE polarization can concentrate more within the high dielectric constant regions than can the TM polarization.

To see the influence at a much higher permittivity value, we replot the PBG diagram for silicon ($\epsilon = 13\epsilon_0$) (Figure 3a2). Since n_{eff} is also strongly increased, all modes are scaled down in frequency; for example, the slope of c_0/n_{eff} for long wavelengths ($\lambda \gg a$) decreases corresponding to the larger n_{eff} value. No TE propagation modes exist for the frequencies within the range 0.22–0.25 (green gap) regardless of propagation direction. Similarly, no TM propagation modes exist over a different frequency range 0.29–0.32 (yellow gap). As the two forbidden frequency ranges do not overlap, this particular square PhC does not have a complete PBG (simultaneous PBG for both polarizations). Note that $\omega(\mathbf{k})$ for all possible wavevectors \mathbf{k} in the BZ cannot be represented by lines but by curved surfaces as a function of k_x and k_y . For example, the photonic band diagram in Figure 3a2 shows the lines of intersection between the curved surfaces of $\omega(\mathbf{k})$ and the BZ planar boundaries of the BZ as seen in Figure 3a3. Despite this limited representation of $\omega(\mathbf{k})$, the band diagram in Figure 3a2 is still very useful for most cases because it shows propagation modes associated from zero to the maximum wavevectors along the zone boundaries as illustrated by the colored arrows on the wavevector plane in Figure 3a3.

A dielectric material is not only an optical material, but of course is also a mechanical material as well. For example, the previous 2D PhC is also a 2D PnC for elastic waves and exhibits the phononic band diagram shown in Figure 3b. In this case, we assign the y axis to the dimensionless phonon frequency given by $\omega a/2\pi c_T$, where c_T is the speed of transverse waves in the constituent material. In a homogeneous and isotropic solid, elastic waves can propagate through three different polarization modes, two transverse modes and one longitudinal mode, in contrast to only two transverse modes (TE and TM modes) for optical waves. However, in a PnC, these modes will in general be coupled depending on the symmetry of the particular PnC. In this 2D PnC, as the x - and y -displacements are coupled, elastic waves with displacement in the xy -plane (*in-plane* waves) are neither purely transverse nor purely longitudinal. Due to

the lack of discrete periodicity along the z -direction, elastic waves with displacements in the z -direction (*out-of-plane* waves) are independent from the in-plane waves. In particular, for very low frequencies (or equivalently $\lambda \gg a$), there are three modes, two in-plane modes and one out-of-plane mode. Similar to the photonic dispersion, the phononic dispersion, $\omega(\mathbf{k})$, is linear for $\lambda \gg a$, but in this case, we have three different slopes, representing three different speeds of sound for the PnC (Figure 3b). Although the two in-plane modes are coupled to each other, one mode has higher slope (or faster speed of sound) than the other. The speed of sound for longitudinal waves $c_L = (K/\rho)^{1/2}$ is faster than that of transverse waves $c_T = (G/\rho)^{1/2}$ in a homogeneous solid having a density ρ , bulk modulus K , and shear modulus G (since $K > G$). Thus, the higher propagation speed mode is more longitudinal-like (compression-dominant) mode and the other is transverse-like (shear-dominant) mode (see Table 1). In contrast to the incomplete PBG of the PhC, this PnC having realistic mechanical parameters of typical of an epoxy polymer exhibits a complete PnBG in which for a range of frequencies no elastic waves can propagate regardless of the elastic polarizations and 2D propagation directions. Moreover, the $\Delta\omega/\omega$ of the complete PnBG is even wider than those of the incomplete PBGs due to the larger contrast in the mechanical impedance, $Z_2/Z_1 = (\rho_2 K_2/\rho_1 K_1)^{1/2}$ for longitudinal waves. Note that the photonic and phononic band diagrams are plotted in two different dimensionless frequency scales, one is scaled by the speed of light (3.0×10^8 m/s) and the other by the speed of transverse sound in this specific background medium (e.g., 1.8×10^3 m/s). Thus, the real frequencies (or energies) of photons and phonons are different by four-to-five orders of magnitude. As a single periodic structure can be both a PhC and a PnC (see Figure 3), one can imagine novel opto-acoustic devices, called phoXonic crystals, enabled by engineering both the photonic and phononic dispersions together.^[10]

As materials generally exhibit intrinsic dispersion of optical as well as mechanical parameters with frequency (especially polymers), the material parameters should be considered at the particular desired working frequencies. Table 1 shows representative values of each material to emphasize the difference among the materials. The refractive indices of polymers are

Table 2. Characteristics of polymer fabrication techniques.

Techniques	Feature range	Remarks	Ref.
3D Printing	1 μm – 1 mm	Arbitrary layer-by-layer patterning	[16,17]
Interference Lithography	500 nm – 1 μm	Wide area (1 mm ² – 1 cm ²) patterning of large library of patterns, can be positioned and tuned by FLaSk	[18–36]
3D Direct Write	100 nm – 1 μm	Arbitrary interconnected patterning	[25,37–60]
Spin Coating and Layer-by-Layer	1 nm – 1 μm	Many sequential steps and limited to 1D structures	[61–67]
Block Copolymer Self-assembly	1 nm – 100 nm	Order can be influenced by structural or field templating	[68–97]
Fiber Drawing/Printing	100 nm – 100 mm	Restricted to fibers, electrospinning has minimal positioning control while printing has nearly arbitrary positioning	[43,79,98–109]
Colloidal Processing	10 nm – 10 μm	Wide area (1 mm ² – 1 cm ²) patterning of a limited set of 3D structures	[110–116]

reasonably constant in the visible and near IR regime; however, they show higher dispersion in the UV and anomalies in mid-IR due to intrinsic molecular group optical resonances. Thus, their refractive index becomes a complex function of frequency with a significantly increased imaginary part (or an extinction coefficient). Compared to the attainable mechanical contrasts, refractive index contrasts of polymers-based PhCs are limited due to low and small range of refractive indices of polymers range from 1.4 to 1.7 with a theoretical lower limit of ~1.29 for an amorphous fluoropolymer without pores.^[11] The effective refractive index can be increased by the addition of nanoscale high-index inorganic materials^[12] or decreased by creating nanopores^[13] but this often results in higher light scattering depending on the size, refractive index difference, and spatial distribution of the foreign materials.

The mechanical dispersion of a polymer at a given temperature can generally be expressed in terms of dynamic moduli, where the real and imaginary parts are related to in-phase and out-of-phase displacements with respect to the driving force. Polymers show strong dispersion at various temperatures and frequencies due to intrinsic molecular mechanical resonances. Since a modulus of a viscoelastic polymer tends to increase monotonically as a function of frequency while temperature softens the material (which leads to the time-temperature superposition principle), the dispersion of a modulus beyond a rheologically measurable frequency limit ~ 500 Hz can be predicted from its temperature dependent moduli using the Williams-Landel-Ferry (WLF) empirical model^[14,15] for viscoelastic linear chain polymers.

2. Periodic Patterning of Polymers

Key to controlling the waves inside a material is providing the requisite geometry (lattice, symmetries, topology, scale) as well as both the appropriate intrinsic component material parameters and the emergent properties expressed by the structural building blocks. In considering fabrication techniques for periodic polymeric materials, one general method for categorizing is the property of the polymer that is necessary to enable the patterning. For example, photopatterning is one of the most common forms of structural fabrication, but leads to some restrictions due to the need for photoactivity of the materials utilized. This can be problematic as many of

the stimulus-responsive materials in the studies considered in this review are utilized for unique optical properties, such as gain, polarization, or photomechanical effects. Even materials whose non-optical properties (*e.g.* mechanical or electronic) simply rely on their crystallinity are inherently scattering. At the same time, a major advantage of most polymeric materials is that they can be fluid-processed in some way, such as in a solvent or as a melt. We therefore approach our review of fabrication of ordered polymers by considering separately the work in (1) photopatterning methods and functional resists and (2) methods involving primarily the fluid processing of polymers (backfilling, extrusion, and colloidal or block copolymer (BCP) self-assembly). Table 2 summarizes the key features of each fabrication technique and some of the details that will be discussed.

2.1. Photopatterning Methods

Photolithographic methods are one of the most ubiquitous techniques for processing of polymeric materials, such as by the crosslinking of UV-sensitive coatings or conventional projection/contact nanolithography. It is therefore logical that many of the fabrication strategies employed for making periodic polymers are photolithographic. In these approaches, the selection of the resist is often a key component of the process design determined not only by the final desired structure and the intended environment for the device application, but also the necessary steps to execute the patterning. The first level this selection takes is in the use of a liquid or solid resist. Liquid resists generally consist of a monomeric or short-chain polymeric material that rely on a multifunctional polymerization to form a crosslinked network, with by far the most common chemistry employed, being acrylate free-radical polymerization. In these systems, the degree of crosslinking can be controlled by the composition of multifunctional groups and monitored by changes in refractive index due to the formation of the network. Clearly, the liquid resists possess considerable advantages in terms of the flexibility of processing; however, there are many applications where film-based patterning is more advantageous, necessitating the use of a solid resist. These solid resists have the added advantage of being able to be positive-tone (exposed regions removed), negative-tone (exposed regions fixed), the former not being an option for liquid resists. Ex post

laser ablation for example, can accomplish both a dual mode approach with positive tone patterning of a previously negative tone liquid resist.^[117] Solid resists are processed by deposition from solvent and most commonly consist of either positive-tone novolac chemistry or positive or negative-tone chemically amplified resists based on pendant group removal or epoxy chemistry, respectively. Taking the flowability of the resist as a first criterion, the optical properties are the next most critical consideration for a polymeric fabrication process.

3D Printing with Photopolymers: Optical 3D printing sets strong requirements on both the fluid and optical material properties. In these systems, either in their commercial forms or more recent lab scale demonstrations, such as microprojection stereolithography,^[16] a fluid resist is employed and the patterning is done in a layer-by-layer fashion. This is accomplished by using a mechanical platform that is gradually lowered along the z-axis into a liquid resist bath onto which the structure is patterned in a 2D fashion either by a rastering laser, or in the case of microprecision stereolithography, a single exposure by a digital mirror array. A key requirement for such a scheme is that the unexposed regions of a layer are not exposed by the patterning of subsequent layers. As a result, the polymeric materials employed for these techniques must possess extremely high optical absorption at the exposure wavelength, thus allowing the z resolution of the technique to be defined by a combination of this absorption and the thickness of the introduced liquid resist layers.

Interference Lithography (IL): At the opposite end of the exposure parameter space is IL. In this technique, a given 1D, 2D, or 3D pattern is generated in a single exposure (though multiple exposures may be used for the final structure). IL is based on the formation of non-uniform intensity fields by the interference of two or more light sources of different directions, polarizations, amplitudes, and/or phases. At the zone of coincidence of the sources, the interference patterns will be periodic or quasi-periodic with periodicity determined by the above parameters along with the wavelength(s) of the sources. 1D and 2D IL has been a common and powerful technique for the generation of patterns for some time;^[18] however, the more recent extension into 3D has greatly increased its capabilities. The sources for 3D IL are generated either by the typical multiple free space beams (multi-beam IL (MBIL))^[19,20] or by passing a single (generally coherent) source through a contacting diffracting optic (phase mask IL (PMIL)).^[27,118,119] The advantage of the former being a greater predictability of MBIL, as it is sometimes possible to solve the inverse problem. PMIL, as advanced by Rogers and colleagues, is a more relaxed optical system, where a 1D or 2D patterned (possibly in multiple layers)^[21] mask is used to produce multiple diffracted beams from a single incident beam. It is then the subsequent interference of these diffracted beams within the resist below the mask that creates the 3D pattern. Unlike the layer-by-layer process, material absorption limits the maximum uniform height of 3D IL, and therefore, the patterning is often commonly conducted on the tails of the absorption curve either in the UV-blue or green visible regimes or to enable thicker structures by using multiphoton absorption.^[22,23] The largest advantage of IL as a 3D fabrication technique is its ability to fabricate submicrometer lattice structures in a single (or small number) of exposures from a massive library

of possible symmetries including: face-centered-cubic (fcc)-like,^[24] tetragonal,^[25] simple cubic,^[26] woodpile (**Figure 4a**),^[27] and quasicrystalline.^[28,29] The last of these is exceptionally difficult to define by self-assembly (although ABC terpolymers have demonstrated several quasi-periodic tilings, as shown in **Figure 11a**)^[93–95] and complicated to generate in a top-down approach due to the lack of a repeating motif, while at the same time, quasicrystalline structures have demonstrated highly desirable phononic and photonic properties.^[120–122]

Direct Laser Writing: In between optical 3D printing and IL is 3D direct write (DW) optical lithography. DW lithography is in general the most intuitive form of lithography and also provides the greatest degree of arbitrary control, as patterns are not restricted to a specific periodicity or characteristic length scale. In this way, it is very similar to optical 3D printing; however, the distinction here is that the patterning is conducted on a monolithic sample of solid or liquid resist with the patterning performed by 3D rastering. In this fashion the resolution can be set by the optical limit of the focal spot, which with high numerical aperture generally >0.5, but including oil immersion objectives >1, can be as small as hundreds of nm in the radial direction and on the order of a micrometer in the axial direction. More recently, the need for oil has been eliminated by utilization of the resist itself as the immersion fluid, enabling extremely tall structures (hundreds of micrometers) to be written (**Figure 4b**).^[37,38] 3D-DW also requires low optical absorption at the exposure wavelength, with the earliest demonstrations utilizing single photon absorption at the edges of the UV absorption band.^[39] To both overcome the effects of even this absorption and improve the resolution, multi-photon lithography (MPL)^[40–45] or other non-linear effects^[46–48] is now utilized for creating arbitrary 3D structures. MPL is typically performed as a UV excitation driven by double adsorption of visible or near-infrared (NIR) light; however, three photon MPL has recently been demonstrated.^[41] This multiple absorption serves to also improve optical contrast: for typical high numerical aperture systems (~1.4), the optical limit of multiphoton absorption is around $\lambda/2$; however, feature sizes of $\lambda/4$ – $\lambda/8$ are regularly achieved in MPL DW due to other chemical effects, such as oxygen quenching.^[44,49] Another very interesting technique for making smaller features is through stimulated emission depletion (STED), a technique that, much like MPL, was inspired by fluorescence microscopy. In this technique,^[40,50,51,52] a second, shaped pulse or continuous-wave source is used coincidentally to deactivate by stimulated emission excited initiators before they can complete the initiation step (generation of radical, etc.). The overlapping area between the two focal spots is then deactivated leading to a smaller net excitation area. A most interesting aspect is that while each beam is optically limited, their overlap is not, with reported resolutions down to $\lambda/20$. As 3D-DW is essentially performed on a microscope, it possesses the added advantage of being able to be used in conjunction with other patterning techniques, either by consecutive writing in a resist patterned by IL (**Figure 4c**)^[25,53,54] or by infiltration of liquid resist into structures created by direct ink writing,^[55] imprint,^[56] or colloidal self-assembly.^[57–59]

Dynamic Patterning Techniques: The techniques introduced above rely on static optical properties of the resist materials;

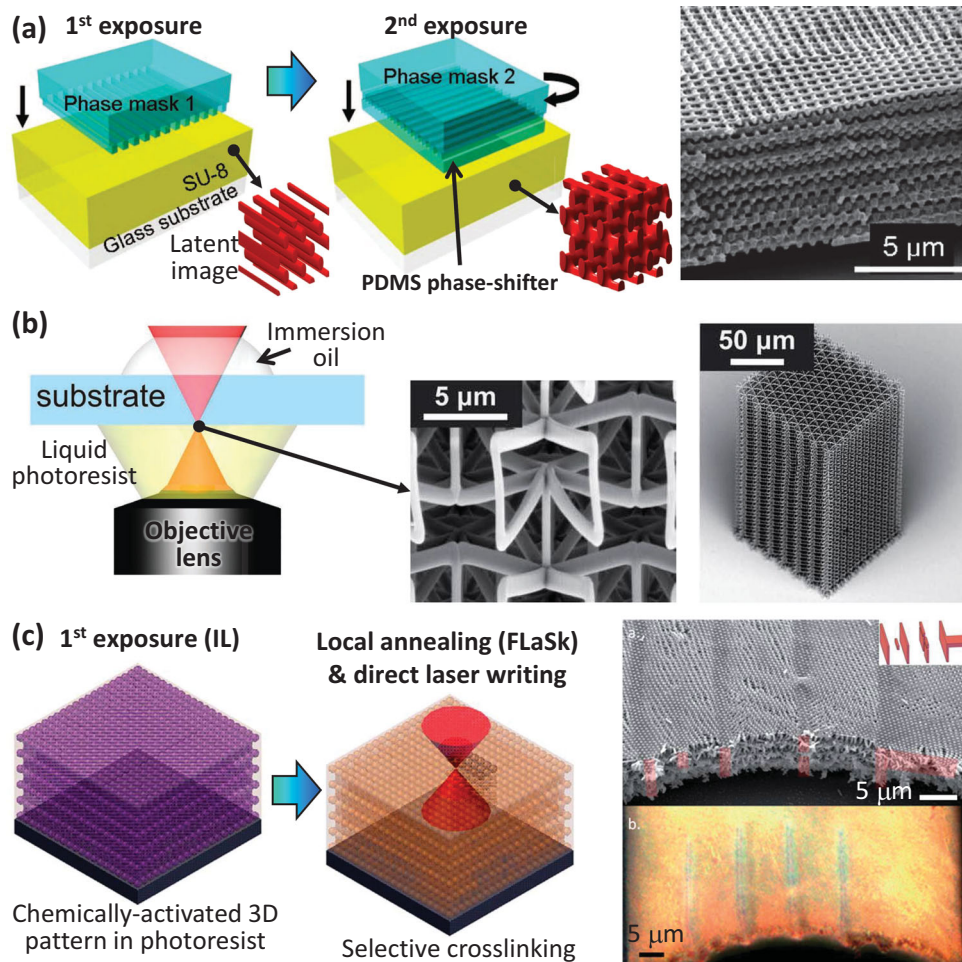


Figure 4. (a) Schematic of double exposure PMIL and a scanning electron microscope (SEM) image of a fabricated woodpile structure. Reproduced with permission.^[27] Copyright 2010, American Vacuum Society. (b) Schematic of dip-in 3D-DW and SEM images of patterned 200 μm tall negative Poisson ratio structure. Reproduced with permission.^[37] (c) Schematic of a combinatory approach (IL + FLaSk DW). SEM (top) and optical (bottom) images of a fabricated hierarchical photonic structure containing 3D-DW designer waveguide defects. Reproduced with permission.^[25] Copyright 2011, The Royal Society of Chemistry.

however, dynamic properties of the resist can also be manipulated to initiate unique patterning mechanisms. A simple example is self-propagating polymer waveguides (SPPWs).^[123–125] In SPPW, a physical mask is placed on top of a liquid polymer photoresist which is exposed to angled collimated UV light. The resist is selected to exhibit a significant increase in index upon polymerization and crosslinking such that the exposing light is waveguided through the resist, including through intersections (or nodes) of two waveguided beams. The net result is the highly robust fabrication of 3D polymeric truss structures down to the micrometer scale with high aspect ratios. Other dynamic patterning methods include focused laser spike (FLaSk) annealing of chemically amplified resists (Figure 4c). This technique exploits the autocatalytic process of a chemically amplified resist, where crosslinking/deprotection is induced by photoacid groups introduced during the exposure. By utilizing the kinetically limited nature of thermal heating by the laser beam, FLaSk enables a highly localized post-exposure bake using a direct write laser to create hierarchical periodic

structures from the latent photoacid pattern generated by IL exposure.^[25]

Functional Resist Systems: The material properties thus far discussed have influenced the patterning processes, but have no direct effect on the properties of the final fabrication beyond the structure. The majority of photoresists possess properties of typical crosslinked thermosets or (in the case of positive tone resists) properties characteristic of thermoplastics. Their properties are optimized for the patterning process, but there is frequently less attention paid to other material functionalities. This requires design of resists that are both photoactive and also have other desirable properties. A simple example of this is hydrogel resists, which can be achieved by incorporation of a large fraction of bifunctional monomers into a fluid resist with or without solvent. In this way, solvent tunability of mechanical properties has been obtained in 3D printing^[126] and DW.^[56,127,128] Fillers, such as nanoparticles^[129–131] or liquid crystalline polymers,^[132] may also be incorporated to impart functionality, such as optical or mechanical properties. Another key

example is the utilization of BCPs as resists, which has been utilized to generate hierarchical structures by both photolithography,^[133] electron beam (e-beam) lithography,^[68,133,134] and, most recently, simultaneous orientation control and annealing by DW FLaSk zone annealing.^[135] In this way, patterns containing the nanoscale structure of the BCP via self assembly occur within the larger structures defined by the second photopatterning technique.

Beyond photostructured media, photopatterning may also be utilized to change other properties of polymers. One example is the already discussed variation of optical properties during crosslinking. This can be enhanced by the inclusion of other optically active media, such as the modification of optical properties of dye-doped polymers, as has been advanced for 3D data recording. Optomechanical polymers, such as liquid crystals (LCs), can also have transient structure induced in them by optical exposure. This has been utilized to introduce quasi 2D structures into thin films of azopolymers and also to tune previously patterned azopolymer 1D and 2D grating structures. In this way, the diffractive behavior of these films could be tuned.^[136] Moreover, photo-mechanical activation can be induced in a LC film (see Figure 7).

2.2. Fluid Processing Methods

Despite great improvements in photopatterning techniques and materials, there are still some systems that are not optically processable or applications where composites of periodic polymers and other materials, so as to provide higher modulus or thermal or electrical conductivity, are necessary. In these cases, the fluid processability of polymers, either by dissolution in solvent or by melt processing, is exploited to achieve the desired composite structure.

Film Processing: Other than in the case of liquid based 3D writing, polymers are most frequently processed as films or coatings. For applications where a uniform polymer layer is required, such as in solid resist photolithography, techniques that impart good control over the deposited thickness is necessary. For photolithography, spin coating (or blade coating for larger scale reel-to-reel setups) from solvent is the most common method to position thin films for patterning, and is also used to deposit liquid BCP-solvent films for self-assembly. Spin coating can also be used as a technique for generating 1D periodic polymer (and polymer-nanoparticle) structures by sequential deposition from orthogonal solvents or sequential underlayer-crosslinking with layer dimensions selected by choice of the solution concentration and spin parameters.^[61–65] Similar 1D periodic structures can be made using electrostatic layer-by-layer deposition of cationic – anionic polymers by sequential dipping into polyelectrolyte solutions of controlled pH to achieve target layer thickness.^[66,67,137] Such 1D films have more recently been processed by a more scalable spraying^[138] or inkjet printing^[139] processes. While these methods require many more process steps than a self-assembly process to generate periodic structures, they allow for simplified manipulation of the individual layers during fabrication to introduce contrast or functionality by, for example, the control of porosity^[66] or incorporation of inorganic layers.^[64]

Backfilling/Infiltration and Extrusion: A simple process to create a bi-composite is via backfilling, where the fluid polymer is infiltrated into a previously patterned solid template. For example, templates of crosslinked polymers or inorganic materials can be employed without removal of the template to enable solid/solid composites, for applications such as PnBG tuning. Often, however, it is desirable to be able to remove the template and access the infiltrated, now periodic polymer. In 2D, this is exactly what is accomplished by micro/nanoimprint,^[140,141] which can be used to pattern fluid polymer, even those materials which would be difficult to process optically (such as LCs) by employing high temperature infilling of a patterned contact mask followed by solidification of the polymer material (by cooling below the glass transition or the crystallization temperature) and removal of the mask.^[136] Further, as nanoimprint can induce phase-mask-like features, sequential microimprint and nanoimprint of a thermally softened polymer followed by consecutive PMIL has been demonstrated for the fabrication of hierarchical structures.^[25,54,119] Another method for transient templates that can achieve 3D structuring is inversion of a different 3D structure, such as by acid etching of a silica colloidal or anodized aluminum oxide template (see Figure 25c).^[142] Another example is the production of 3D elastomeric structures for phonon engineering by infiltration and crosslinking within a template produced by IL of a positive tone resist.^[143,144] The template can be then removed by flood exposure and development (see Figure 25b), enabling a 3D elastomeric PhC.

When the polymeric systems themselves possess some molecular or supermolecular level order, introduction of the material into a template can exert substantial additional influence on the alignment and organization of these components. This is analogous to the mechanical rubbing of substrate and superstrate to induce nematic order in LC displays. A similar effect occurs in LCs infiltrated into nanoimprint templates which results in the alignment of the LC domains for future patterning effects.^[145] More complex LC textures have also been demonstrated for conical smectic LC phase within arrays of various shaped micropillars.^[146,147]

Template ordering also is the case for BCPs, as has been extensively explored in 2D via graphoepitaxy.^[68–70] Here, the periodic microdomain structured polymers are restricted by either a surrounding (produced by IL^[148] or transiently by nanoimprint)^[71] or embedded geometry (due to resolution requirements, produced exclusively by e-beam)^[72] and the polymers are forced to adopt some lowest energy morphology commensurate to the template. This latter technique allows for preprogramming of the individual domains by deliberate positioning of the embedded template, even allowing the potential for determining through simulations the optimal surrogate post arrangement to arrive at a specified target structure.^[73] While two layer templated BCP from a 2D embedded template has been demonstrated (Figure 5a),^[74] full 3D graphoepitaxy has only been demonstrated in a limited sense for BCP within ordered and disordered^[75,76] interstitial pores. For example, lamellar BCP have been previously backfilled into colloidal or inverted colloidal structures.^[77,78] The polymer microdomains assembled with symmetries commensurate to the pore structure, for example, the self-assembly lead to concentric onion-like structures. The self-assembly of cylindrical BCP in anodic

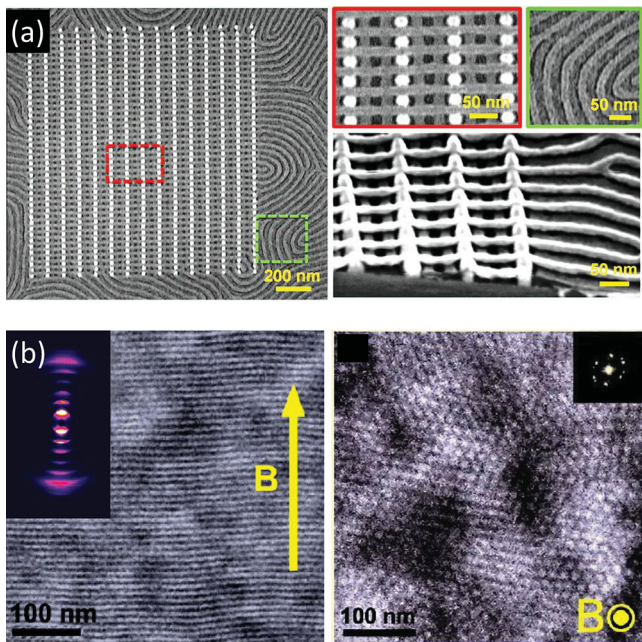


Figure 5. (a) SEM images of two-layer graphoepitaxy structure of a cylindrical BCP thin film revealed by etching. Order is controlled in both layers independently by the positioning of photoresist pillars (visible as bright dots) previously patterned by e-beam DW. Reproduced with permission.^[74] Copyright 2012, American Association for the Advancement of Science (AAAS). (b) Transmission electron microscope (TEM) image of a section of a thick film (>1 mm) of lamellar BCP perpendicular to an applied in-plane external magnetic field is shown with small-angle X-ray scattering data (left). Hexagonally-packed cylindrical BCP aligned along the magnetic field directed normal to the film with fast Fourier transform (FFT) data (inset right). Reproduced with permission.^[85] Copyright 2011, American Chemical Society.

aluminum oxide (AAO) nanopores generated quite regular helical nanostructures with pitch and structure of the helix determined by a combination of the pore diameter and the normal cylinder domain diameter and inter-domain spacing in the bulk BCP.^[79,80] Hierarchical assembly of BCPs has yet to be incorporated into devices, but the possibilities for multiscale periodicity present a large opportunity for future work where control of wave interaction with the hierarchical structure on multiple scales can be exploited.

For BCP, these physically constraining templates can be extended to other, effective templates using other types of forces. Closest to graphoepitaxy is chemical epitaxy,^[81,82] where patterning of the chemical functionality of the substrate to preferentially favor one of the blocks in the BCP or to be equally favorable, resulting in preferential domain orientations and arrangements. Other unstructured, field driven methods of BCP alignment, such as crystallization,^[83] magnetic (Figure 5b),^[84,85] electronic,^[86] mechanical,^[87] thermal,^[88–90] or solvent evaporation^[91] or epitaxial crystallization^[92,149] driven alignment have also been investigated.

Fiber Generation and Printing: Extrusion drawing is a ubiquitous method for the production of polymer and glass filaments where a preform of homogenous or assembled set of materials is passed as a melt through a reducing die and further stretched to obtain a fine diameter fiber. A huge advantage of

fiber drawing for the production of periodic systems for optical and acoustic applications is that, by proper selection of the set of material properties in the preform (viscosity, interfacial energy, Poisson ratio, etc.), both the morphology and the relative dimensions of the preform components can be maintained in the greatly size-reduced fiber, allowing for the macroscale ordered structure to be translated to the micro/nanoscale. In this way, concentric 1D (Figure 6a)^[98] or 2D^[99–101] periodic structures can be created at optically and acoustically relevant length-scales. Analogously, to a more limited extend, 1D optically active multilayers have been produced^[150,151] by 2D coextrusion of layered polymers and polymer melts. Electrospinning is a related technique to fiber drawing where a polymer solution is rapidly accelerated by a strong electrostatic field while removing solvent to form nanoscale to microscale diameter fibers.^[79] This has also been demonstrated as an effective means to generate cylindrical confinement for the ordering of BCP microdomains (Figure 6b).^[43,102,103] A disadvantage of electrospinning is a relative lack of control over the positioning of the electrospun fibers, as well as precise control of fiber diameters. Current work using concentric two fluid spinning allows more elaborate designs.

Commercial nozzle based printing techniques using molten polymers serve to translate fiber drawing into a direct write process. Features on the sub-mm scale are possible and this technique is becoming a favored “additive manufacturing” technique for affordable rapid prototyping. Recently, a variation of this technique uses functional sol-gel inks.^[104–108] By utilizing shear thinning colloidal solutions, the ink can flow easily during the high pressure extrusion writing process and then rapidly solidify after writing. In this way structures of various materials, including polymers^[106] can be rapidly patterned on multiple length scales, down to single micrometer features as applied to PhC templates.^[105] Further, by completely immersing the nozzle in a crosslinkable fluid medium, this technique has demonstrated arbitrary patterning of vascular networks unconstrained by the usual self-supporting requirements of 3D writing processes.^[109]

Colloidal Processing: Self-assembly is a versatile set of techniques for the fabrication of functional polymeric structures. In these bottom-up processes, the natural arrangement of a particular structure is built into the chemical and physical parameters of one or more building blocks. As has already been introduced, certain polymeric systems, by virtue of their molecular composition, possess inherent means of ordering; however, different organizational methods of polymeric materials can be induced by, for example, the formation of colloidal polymer particles which themselves form assemblies out of solution via secondary interactions. By utilizing slow evaporation or various other techniques such as electrophoresis,^[110] crystals of very high quality over a large area (up to cm scale) can be obtained. The most ubiquitous colloidal assembly system, that of monodisperse spheres, results in a fcc arrangement of the particles, advantageous for phononic and photonic properties due to its relatively high symmetry ($Fm\bar{3}m$) and the existence of good optical and mechanical contrast from the two distinct phases (air and polymer). The inverse structure; however, possesses superior photonic band properties and is therefore often the final structural target through a “lost-wax” inversion by backfilling

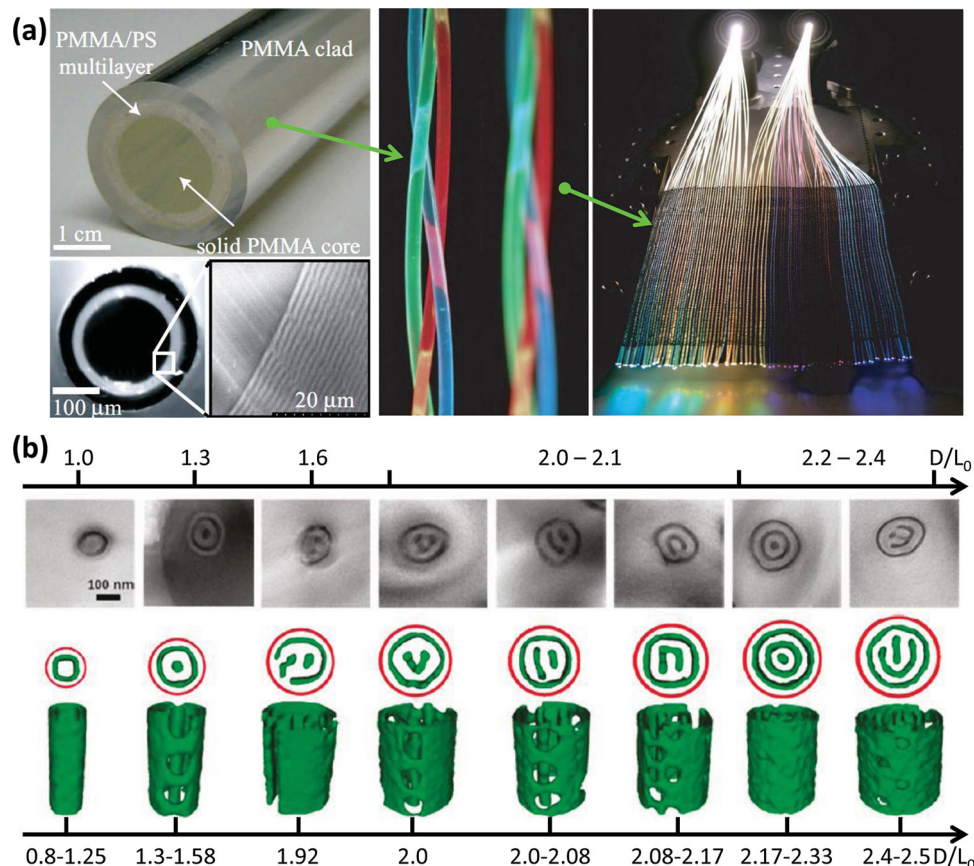


Figure 6. (a) Solid core polymer fiber preform and a resultant PhC fiber showing different colors of leaky light. Reproduced with permission.^[98] Copyright 2008, Optical Society of America. (b) Electrosynthesized fiber of bulk double gyroid BCP microdomains demonstrating through both simulations and TEM images the ability for the cylindrical confinement to induce new microphase morphologies. Reproduced with permission.^[102] Copyright 2010, American Chemical Society.

and removal of the (different material) colloidal system. Colloids themselves may be used as removable backfilling media, as has been demonstrated for colloids within conventional lithographic or IL templates.^[111–113] Much as with BCP, the topography serves to both position and induce order in the confined colloidal particles.

2.3. Selected Functional Polymer Applications

The use of various chemically functionalized polymers can make the optical properties and physical structures of PhCs responsive to various stimuli such as electric field, ionic charge, temperature, and stress. We next introduce several polymer systems potentially useful for tunable, responsive photonic structures.

Liquid Crystal Polymers (LCPs): Liquid crystals are a popular class of materials to achieve tunable and active PhCs^[152,153] due to several advantages: (1) transparency over a wide range of wavelength from 400 nm to 5 μm, (2) large optical birefringence ($\Delta n = n_{||} - n_{\perp} \approx 0.2$) throughout the whole optical regime, (3) very high optical non-linearity,^[154] (4) easy infiltration,^[155,156] (5) gain doping capability for active devices,^[157,158] (6) response to diverse stimuli, for example, electrically tunable^[159,160] and

thermally tunable metamaterials^[161] and PhCs,^[162] and photo-tunable PhCs.^[163,164] Since the majority of LCs are low molar mass organics and LCs have been recently well reviewed as an important photonic material,^[165] we focus on polymeric LCs.

Linear LCPs can have flexible main chain, flexible side chain or rod-like main chain architectures. The strong optical anisotropy of the liquid crystalline mesogens affords complex properties. For example, the strong temperature dependence of the index of refraction in LCP BCPs can provide thermochromic sensors (see section 3.4). A polymer actuator was demonstrated by de Haan et al.^[166] using polymerizable LCs combined with optically defined alignment layers. In their approach, a planar alignment cell whose inner surfaces were coated with linearly-polymerizable polymer was exposed to linearly polarized UV light through a photomask using relative motion between the photomask and the substrate during exposure in order to create either radial or tangential alignment. A polymerizable LC monomer was then inserted into the cell whereupon the director adopted the local alignment direction and was subsequently cross-linked to permanently fix the alignment. By removing the alignment cell, a crosslinked LC polymer film was achieved with the prescribed tangential-or radial-alignment (Figure 7a). When an IR absorbing dye was doped into the polymerizable LC, the polymer film could then be 3D-deformed under IR irradiation

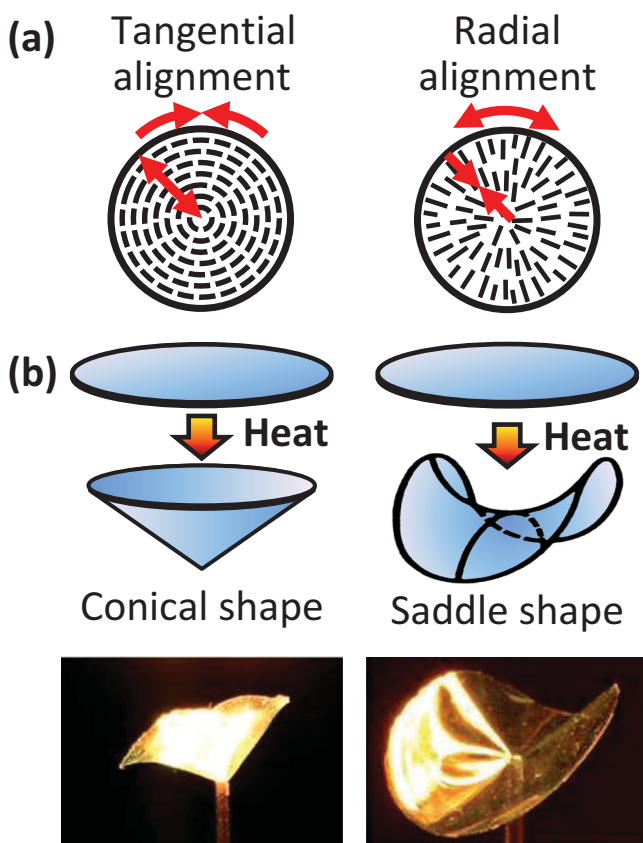


Figure 7. (a) Schematic of the director patterns in LC-polymer films fabricated with tangential and radial alignments. The red arrows show heat-induced deformation directions. (b) Heating of the film by IR absorption causes reversible out of plane deformation dependent on the mesogen alignment. Photographs show actual LC-polymer films deformed under IR irradiation. Reproduced with permission.^[166]

due to anisotropic thermal expansion and mechanical instabilities (Figure 7b).^[166] Polymers with designed molecular functional groups, like LC mesogens are important for various switchable PhC and PnCs via mechanical instability as seen in Figure 25a and discussed in section 4.3 on switchable phononic crystals.

Shape-Memory Polymers (SMPs): An SMP is deformable to a pre-designed shape driven by various stimuli and is reversibly recoverable to its original shape. Such materials could lead to various active photonic and phononic applications. Compared to shape-memory metallic alloys, SMPs have many advantages including 100× larger extent of deformation (up to 800% strain), several fold lighter weight (density ~ 1.0 g cm⁻³), significantly lower cost (~25×), and easier processing conditions.^[167]

Recently Liu et al. created interesting 2D periodic patterns using SMPs. In their approach, an initially flat SMP plate was heated and then evenly compressed and cooled to a temporary shape. Then by local heating using a focused pulsed laser beam, they could form a protrusion array. Alternatively, heating of a SMP plate followed by local indentation, cooling and then polishing to a flat surface, can form an array of uniform spherical caps upon heating due to shape recovery.^[168] Although SMPs have not

been used for photonic applications yet, the combination of the SMPs and PhCs such as a flexible PhC on a SMP substrate or a PhC made of a SMP is expected to enable multifunctional opto-mechanical photonic devices.

Polyelectrolytes (PEs): PEs are polymers carrying ionic charges along the polymer chain backbone, which usually makes the polymer water-soluble, and such PE materials are essential components for water purification, oil recovery, paper-making, and various types of mineral processing.^[169] Besides the traditional industrial applications, PEs have attracted attention for photonic materials. Layer-by-layer (LBL) electrostatic assembly of PEs was used to synthesize PhCs^[170] and to enable dynamic tunability of PhCs.^[171,172] As the 1D assemblies are built up by alternating a polycation layer with a polyanion layer by sequential adsorption from aqueous solutions, precise control over layer thicknesses is possible by appropriate choice of charge density and molecular weight.

BCPs with a PE block (BCP-PE) can self assemble into chemically-tunable PhCs for colorimetric sensors^[97,173] and electrically-tunable PhCs for display applications.^[174,175] For BCPs with a total molecular weight ~100 kg mol⁻¹, the periodicity of the dry self-assembled BCPs (~100 nm) is insufficient to provide a PBG in the visible regime. However, for example, by quaternization of the pyridine groups in the poly(2-vinyl pyridine) (P2VP) block in a lamellar PS-*b*-QP2VP BCP, solvents can swell the period up to 600%. Additionally, the selective swelling of the PE block by the typically lower index solvents increases the refractive index difference with respect to the glassy PS block and the glassy PS block forces essentially 1D swelling normal to the layers, giving a larger layer thickness change than for 3D swelling as takes place in colloidal PhCs.

3. Polymer-Based Photonic Structures

In this section, we review polymer-based PhC structures for sensors, energy, and display applications as well as highlight some emerging ideas. Several simple polymer-based PhCs are now commercial products due to their unique visual effects created by structural colors. For example, films for decorative packaging are made by multilayer polymer extrusion and provide a unique appearance distinguished by multiple colors dependent upon the viewing angle (Figure 8a). As these dramatic visual effects can be created without any additives, such films could safely be used in food packaging and bio-applications. The reflectivity of the conventional multilayer film made of isotropic materials is generally decreased at high incidence angles especially near the Brewster angle for TM-polarization. Since certain polymers like polyester and PMMA can exhibit large birefringence if oriented, the introduction of well aligned PMMA and polyester layers to the multilayer polymer film can provide high reflectivity of multilayer dielectric mirrors over all angles (Figure 8b),^[176] particularly useful for applications related to broad-band and unpolarized light sources such as for sunlight and general lighting. LCs having self-assembled periodic structures have been recently introduced for temperature- and stretch-responsive fabrics and have attracted a great deal of attention from the textile and fashion industry.^[177] Polymer-based PhCs can help produce advanced textile applications in combination

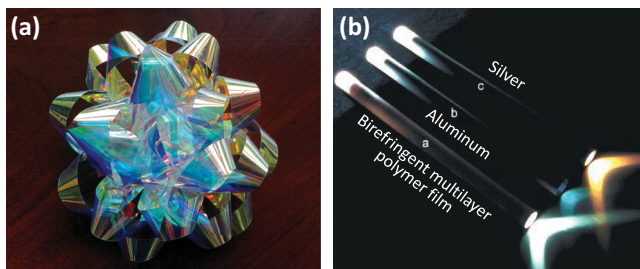


Figure 8. Structural colors from PhCs made of polymeric materials. (a) A decorative bow made of multilayer polymer film. (b) Light transport tubes made of giant birefringent multilayer polymer film are superior to those made of aluminum and silver mirrors. Reproduced with permission.^[176] Copyright 2000, American Association for the Advancement of Science.

with traditional synthetic fiber materials. Moreover, in the cosmetics industry, companies such as L'Oréal employ 3D periodically structured microparticles, such as micelles comprising ordered polymer or ordered metal oxide nano-spheres, with other ingredients to create unique visual effects.^[178] These applications of periodic polymer structures are just beginning and the potential of periodic structures based on polymers are enormous by virtue of the many advantages of polymers especially in cost and manufacturing.

3.1. Photonic Crystals

In PhC design, the physical structure together with optical parameters of constituent materials determines the optical characteristics of a PhC. Moreover, in many applications, because the structures can also affect electrochemistry as well as charge and mass transport, the structural design is very significant. This section will highlight various functionalities arising from structural characteristics.

Periodic Structures: The simplest PhC structure is a 1D multilayer reflector, a stack of two alternating materials having different optical parameters. For instance, a 1D PhC or a dielectric mirror consisting of two different dielectrics each with a quarter wave optical thickness is an indispensable optical component especially for laser applications due to the very high reflectivity without absorption. The applications of 1D PhCs have recently been extended to sensors, tunable optics, and displays primarily by the use of soft matter, particularly polymers. Since 1D polymer PhCs can readily respond to various external stimuli as generally depicted in Figure 1, the dynamics of 1D polymer PhCs are still open for research and advancement.^[97,179]

For static optical properties of 1D PhCs for normal incidence, simple formulae to

predict the center position and width of the lowest PBG, and the maximum reflectivity are available.^[179–181] For light entering a 1D PhC at off-normal incident angle, the wave vector is expressed as $\mathbf{k} = \mathbf{k}_{\parallel} + k_z \mathbf{z}$, where \mathbf{k}_{\parallel} is the tangential component of \mathbf{k} , parallel to the dielectric layers and k_z is the component perpendicular to the layers. A PBG diagram of a 1D PhC in which the frequency of light is plotted as a function of \mathbf{k}_{\parallel} is useful to demonstrate the optical response of a 1D PhC for an arbitrary angle of incidence (Figure 9a). Since \mathbf{k}_{\parallel} must be conserved inside and outside of the PhC, the light lines (red) represent the wavevectors corresponding to the largest \mathbf{k}_{\parallel} of photons entering the PhC from air. For frequencies within the green areas, the band diagram shows no modes within the light lines. This means that this particular 1D PhC having a large refractive contrast can completely prohibit the transmission of two frequency bands for light incoming from air regardless of the incident angle and polarization. Because of the existence of propagation modes outside of the light lines, however, the propagation of light inside the PhC is still allowed if the light source is inside of the PhC or the refractive index of the incident medium becomes significantly close to the average index of the PhC. Although most band diagrams are calculated under

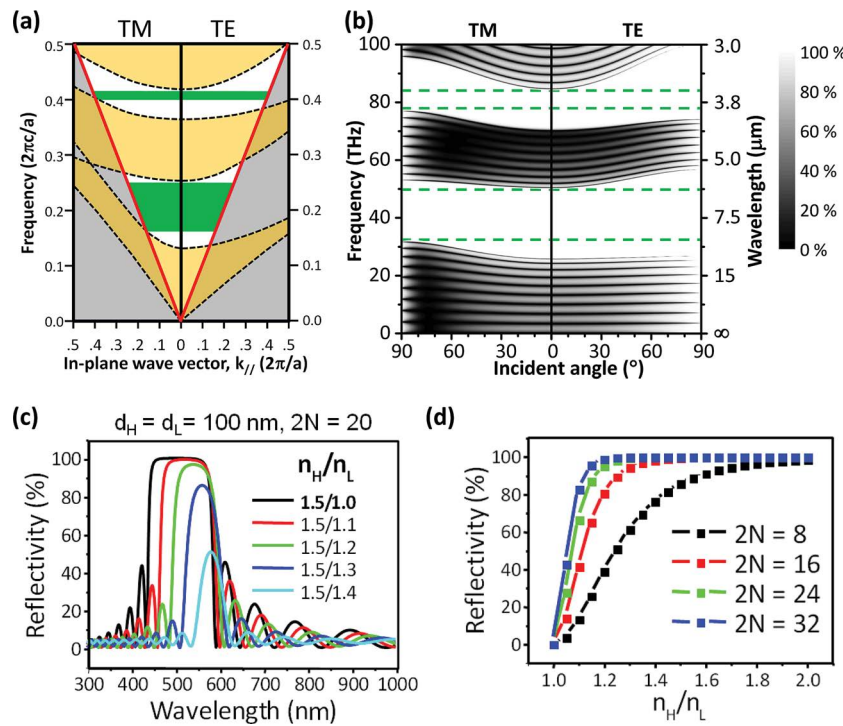


Figure 9. (a) Projected photonic band structure of a 1D PhC made of PS ($n_1 = 1.6$) and tellurium ($n_2 = 4.6$) layers with a thicknesses ratio of $d_1/d_2 = 2$. The red lines are the light lines having a slope corresponding to the speed of light in air. Reproduced with permission.^[183] Copyright 1998, American Association for the Advancement of Science. (b) 2D plot of calculated reflectance spectra of a PhC consisting of 10 pairs of PS and tellurium layers with thicknesses of 1.0 μm and 0.5 μm , respectively for TE- and TM-polarizations as a function of the incident angle from air. The grey scale indicates the value of the reflectivity (white = 100% reflection). The relatively low reflectivity of TM-polarized light for incident angles ranging from 60 to 80° is due to the Brewster angle effect. (c) Reflectance spectra of 20 pairs of dielectric layers calculated by transfer matrix method as a function of refractive index ratios with a fixed thickness of 100 nm for each layer. (d) The peak reflectivity vs. the ratio between high and low refractive indices is plotted for several different numbers of pairs of high and low refractive index layers.

periodic boundary conditions, corresponding to a PhC having an infinite number of dielectric layers, the angle-dependent reflectivity spectra of a 1D PhC with a finite number of layers (Figure 9b) shows how the actual finite (<100%) reflectivity is related to the photonic band diagram, where a higher incident angle corresponds to larger k_{\parallel} within the light lines of the band diagram. Due to the finite number of unit cells in real-world PhCs, the maximum reflectivity and the width of the PBG are strongly influenced by the number of unit cells and the contrast in refractive index between the layers. In Figure 9c, reflectance spectra of a 1D PhC comprised of 20 pairs of two dielectric materials having refractive indices, n_H and n_L are calculated by the transfer matrix method.^[182] With increasing n_L , the resulting smaller ratio between n_H and n_L causes a lower reflection peak value and a narrower reflection band. In this specific example for increasing n_L , the peak position also shifts toward longer wavelengths because an average refractive index of n_H and n_L is increasing. Generally polymer based PhCs have a limitation in the attainable contrast of the refractive indices because most polymers have refractive index between 1.4 and 1.6 in the visible regime while the lowest refractive index is fixed to 1.0 for air (vacuum) (see Table 1). Figure 9d shows that the low reflectivity originating from the limited index contrast can be relieved by using a larger number of layers. In contrast to the conventional dielectric mirror fabrication approaches which use vapor deposition, polymer-based PhCs made by self-assembly and IL can achieve a sufficiently large number of layers at very low cost.

Any 1D or 2D PhCs tends to show a complete PBG originating from Bragg diffraction near $\omega a / 2\pi c \sim 0.5$ (which is also called the fundamental PBG) when sufficiently high refractive

index materials are introduced (see Figure 9a and Figure 3a2) due to stronger light scattering by interfaces with the higher refractive contrast. However, complete bandgaps for 3D PhCs are more difficult to obtain. For example, a close-packed fcc PhC (e.g., an opal PhC) (Figure 10a) and its inverse structure (e.g., an inverse opal PhC), both of which belong to space group $Fm\bar{3}m$ (Figure 10c), do not have a complete low frequency PBG arising from Bragg diffraction for any combination of optical materials because the 2nd and 3rd photonic bands cross each other at the symmetric points, U and W regardless of refractive index contrast.^[184–186] This band crossing of the fcc PhC can be lifted to open a fundamental PBG by changing to diamond symmetry with space group $Fd\bar{3}m$,^[184] with the structure based on connected cylinders on the diamond lattice currently exhibiting the best (largest) complete gap of any fabricated 3D PhC. As seen in Figure 10e, the inverse-opal PhC does have a complete PBG between 8th and 9th bands ($\omega a / 2\pi c \sim 0.8$)^[185,186] for sufficiently high refractive index materials ($n \geq 3.0$),^[186] however, this high-energy PBG is less favorable due to its very narrow band width and therefore high susceptibility to structural imperfection.^[187] Despite these limitations, the opal-based PhCs have been very attractive for various applications that will be discussed later because these PhCs can be fabricated by colloidal self-assembly, and exhibit a strong PBG effect along the [111] direction (along the surface normal) arising from a partial gap at the symmetric point, L by Bragg diffraction (see Figure 10d and 10e). From various examples in the following sections, we will see that 1D-like applications of 3D PhCs are very effective for various sensing and structural color applications. Moreover, as new fabrication approaches, such as shear-induced ordering^[188,189] have been introduced, non-traditional

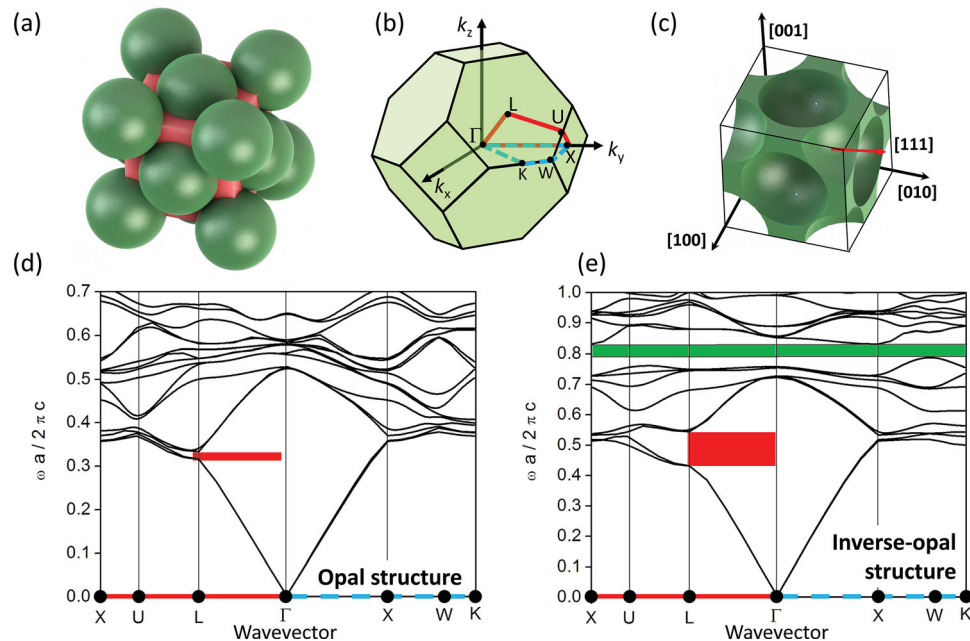


Figure 10. (a) A 3D PhC comprised of close packed spheres (the opal structure). A cubic lattice is represented by a red box. (b) Wigner-Seitz cell of the fcc lattice showing the BZ boundaries. Two paths of wavevectors are represented in red and blue lines for the 3D band diagrams. (c) A 3D PhC made by inversion of the close packed fcc structure (the inverse opal structure). (d) A 3D photonic band diagram of the opal structure made of silicon ($n = 3.5$). The partial gap along [111] direction (Γ -L) is represented in a red gap. (e) A 3D photonic band diagram of the inverse opal structure made of silicon ($n = 3.5$). A wider partial gap (a red gap) along [111] direction (Γ -L) and a complete gap (a green gap) between 8th and 9th bands are shown.

PhCs departing from the opal-based PhCs have been demonstrated and corresponding theoretical studies have been presented for these new PhCs.^[190]

Aperiodically Ordered Structures: The origin of a PBG is usually explained by the Bragg scattering of photons by a periodic optical potential given by the spatially varying refractive index. This results in flat photonic band at the BZ boundary as in Figure 3a2, and it is widely believed that the creation of a PBG requires a periodic lattice structure. Interestingly, however, various aperiodic structures including quasicrystals^[191,192] and nearly amorphous structures having only short range order^[193,194] have demonstrated PBGs as well.

A quasicrystal has long-range orientational order but lacks the translational lattice order characteristic of a crystal and was first observed in an Al-Mn alloy by Shechtman et al.^[195]

For photonic applications, because a quasicrystal can have a higher point group than in ordinary PhCs, it is possible to more closely approximate spherical symmetry of the BZ, which is advantageous to the opening of complete PBGs especially at low refractive index contrast. Due to the intermediate nature of quasicrystals between ordered and random, they can have multiple PBGs originating from different short-range (or amorphous-like) and long-range (or crystalline-like) interactions.^[196]

Some 1D aperiodic PhCs including 1D Fibonacci quasi-crystalline PhCs demonstrate PBGs which originate from short-range interactions created by a localized resonance state which decay via a power law relation, while the long range interaction decays linearly.^[197,198] Quasicrystals have been realized in several soft matter systems, such as organic dendrimers^[199] and self-assembled terpolymers (Figure 11a),^[93] as well as PS colloidal particles directed by a 2D optical lattice,^[200] photo-crosslinkable polymers by 3D stereo lithography,^[17] IL,^[28,29] and 3D DW.^[60] For example, quasi-crystalline PhCs having the Penrose lattice structure have demonstrated a wide variety of lasing modes^[201] and low lasing threshold.^[202] Moreover, a potentially more important application area can be quasicrystalline photovoltaic devices due to their more isotropic optical response, since conventional PhC structures work only for specific wavelength, angle, and polarization, and are therefore limited and inefficient for the broad, unpolarized solar spectrum.^[203] Despite challenges in understanding the aperiodic photonic systems, due to their complexity in numerical simulations, their rich underlying physics and complementary

functionalities to their periodic counterparts will enable novel opportunities in future photonic devices.

A non-crystalline structure, consisting of a continuous-random-network of diamond-like tetrahedral-bonded silicon rods in air numerically exhibits a reasonably wide complete PBG.^[206] The origin of this PBG is strong light confinement at defects,^[194,204,206] which is an analog of Anderson localization in an electronic system.^[207] It is still challenging, however to understand the exact mechanism of the PBG in the non-crystalline system as well as extract out structural design principles.^[208] Since the above non-crystalline structure is based on silicon and air, a polymer-based non-crystalline structure is not expected to exhibit such a wide complete PBG due to a much smaller refractive index contrast as discussed earlier. In nature, some non-crystalline structures made of proteins exhibit strong structural colors with only short-range-ordering^[204,209,210] despite the low refractive indices of the proteins ($n = 1.35\sim1.60$)^[211,212] similar to those of synthetic polymers. For example, the spongy keratin structure with only short-range-order in the macaw feather creates a vivid blue structural color (Figure 11b). The spongy structure exhibits an isotropic pseudo-PBG having low but non-zero photon density of states as shown by finite-difference time domain simulations.^[204] Therefore, polymer-based non-crystalline structures should also suffice to create “isotropic” structural colors. Building blocks such as tetrahedrally-connected rods can be packed in arbitrary orientation or can be dispersed in a matrix without losing the omni-directional structural color. Especially since the non-crystalline keratin structure is a result of self assembly induced phase separation of β -keratin from the cellular cytoplasm,^[209] researchers are trying to create interconnected amorphous photonic structures via self-assembly based on the phase-separation of polymers.^[213] Other systems include an aqueous solution of aggregated gel particles^[214] and disordered arrays of PS microspheres with interstitial air.^[215] The PS/air system displays structural colors with a very low angle dependence. IL can be used to fabricate photonic particles similar to the tetrahedral motif as demonstrated for multivalent micrometer-sized polymer particles (Figure 11c).^[205] Such non-crystalline photonic structures are attractive for structural coloring for cosmetics (Figure 8c) or angle-independent reflective displays.^[216]

Biological Polymer Photonic Structures: Many creatures have body parts that exhibit vibrant visual effects often resulting

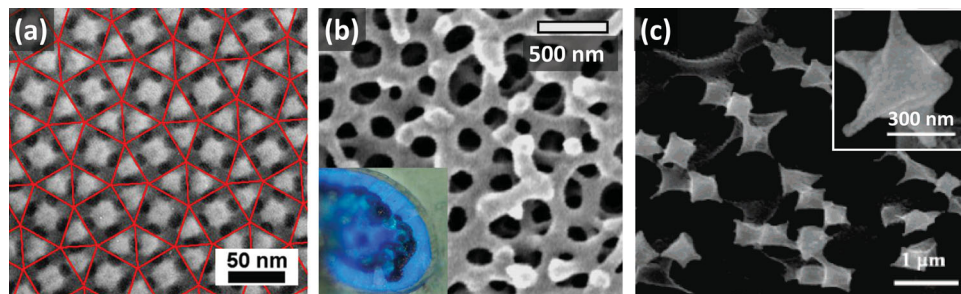


Figure 11. (a) Bright-field TEM image of a phase-separated blend of polyisoprene (PI)-PS-P2VP star terpolymer and a PS homopolymer showing a 2D quasi-crystalline structure. The red lines show the structure is comprised of a packing of equilateral triangles and squares. Reproduced with permission.^[93] Copyright 2007, American Physical Society (b) SEM image of the spongy keratin structure of a scarlet macaw blue feather (inset). Reproduced with permission.^[204] Copyright 2012, National Academy of Science of the USA. (c) 6-valent polymer particles created by IL and UV/ozone analysis. Reproduced with permission.^[205] Copyright 2007, American Chemical Society.

from extremely complex and hierarchical geometries including the double gyroid,^[217,218] as well as relatively simple structures such has fcc packing of micellar spheres,^[219] hexagonally packed cylinders,^[220] and lamellae.^[221,222] Coloration of biological structures is generally a combined result of interference, diffraction, absorption and incoherent scattering.^[222,223] Among many examples of structural colors, some aquatic species like cephalopods exhibit actively-tunable structural colors by controlling reflection and absorption as well as variation of their body surface texture.^[221,222] For example, the squid species *Loligo pealeii* uses protein-based multilayer reflectors. The optical response of the periodic protein structure of the squid is controlled through secretion of chemical signals from the sympathetic nervous system to change the layer spacing and refractive index (Figure 12a). Such behavior inspired an electrically tunable self-assembled block copolymer system, which can mimic the tailored reflectivity of cephalopods.^[175] Biophysical^[224] and self-assembling properties^[212] associated with the evolutionarily selected reflectin protein have also been studied in many insects. Single gyroid structures found in certain butterfly species inspired the design of 3D periodic chiral structure made of silicon having strong circular dichroism based on the large circular polarization PBG with a gap width exceeding 30% and suggested design principles for chiral photonic devices (Figure 12b).^[225]

The finely spaced free-standing horizontal lamellae on more widely spaced vertical stems (Figure 12c) create optical effects in butterfly wings by both multilayer interference and diffraction. Because air serves as low refractive index medium, higher refractive index contrast is possible than for other structures consisting of two different polymers. Additionally, the hierarchical solid/air structure facilitates rapid vapor phase mass transport and selective optical response to various vapors^[227] or a superhydrophobic surface.^[228] Research on optical biological structures^[229] based on natural occurring polymers continues to create new ideas for photonic structures made from synthetic polymers.

3.2. Light Emission

Dye-doped polymers are an attractive gain medium for laser applications due to the usual advantages of polymers discussed in the introduction. For example, a 2D PhC laser in Figure 13a can be simply fabricated by nanoimprinting of an organic dye (Pyrromethene 597) doped thermoplastic polymer film on a glass substrate. Such thin film lasers can be integrated into lab-on-a-chip applications as their fabrication processes are compatible with various soft lithography techniques. Although optical pumping from the top of devices is simple and convenient for lasing, the pumping process is quite inefficient due to the limited interaction distance of the thin gain medium along the film normal direction. While mirrorless lasing occurs at the PBG edge arising from the lattice constant a , the other lattice constant b can be optimized (Figure 13a) in order to scatter some of the vertically oriented pumping light along the in-plane direction to maximize the optical interaction length. By this clever design, the lasing threshold drops over 10x.^[230]

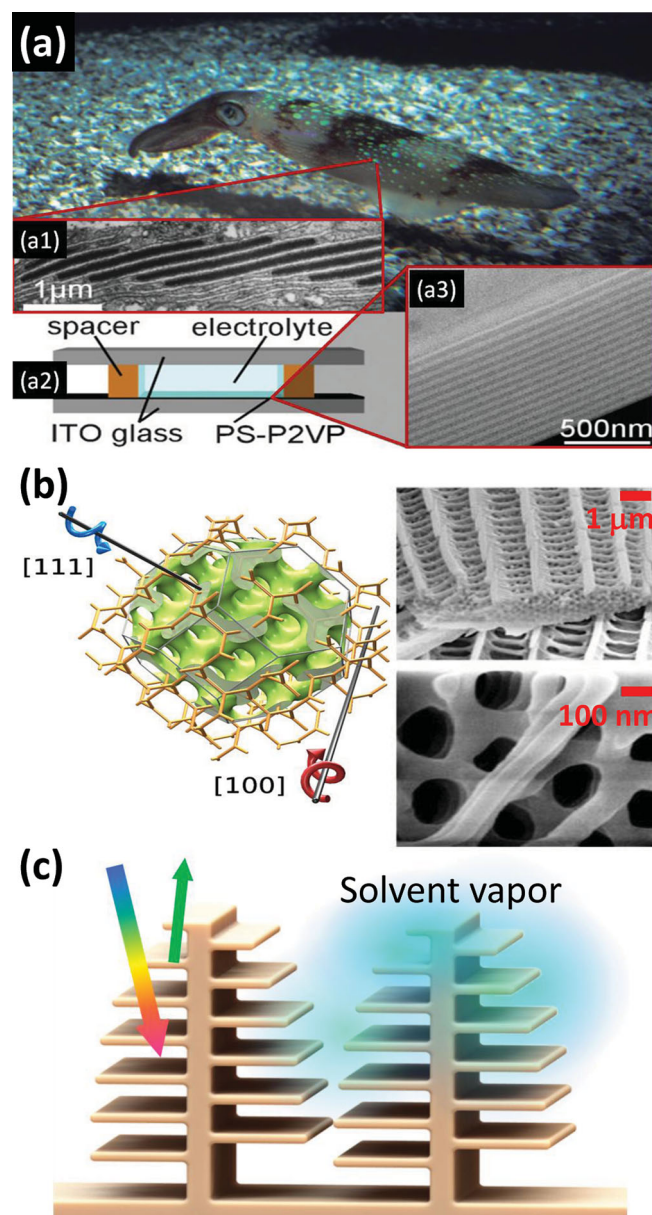


Figure 12. (a) Protein-based multilayer reflector of *Loligo pealeii* squid and the corresponding electrochemically tunable BCP lamellar structure using a voltage to create H^+ in a PS-*b*-P2VP system that triggers large swelling of the P2VP domains. Inset a1) TEM cross section of a squid iridophore showing periodic layers, a2) electrically tunable BCP, a3) TEM of 1D lamellar BCP layer.^[175] (b) Single gyroid chitin network and a model constant mean curvature surface clipped to a truncated octahedron shape and SEM images of a wing scale of *Callophrys rubi* butterfly. The network's single type of 3-coordinated vertices are at Wyckoff sites 8a in space group $I\bar{4},32$ (no. 214 in ref.^[226]) Reproduced with permission.^[225] Copyright 2011, American Physical Society (c) Schematic of hierarchical photonic structure of butterfly wing scales and their tunable reflectivity corresponding to uptake of vapor.

A laser cavity structure was demonstrated with a gain medium sandwiched by two 1D PhC fabricated by layer-by-layer (LBL) alternating deposition of PMMA and TiO_2 nanoparticles.^[234] Contrast this top-down, multistep LBL fabrication of

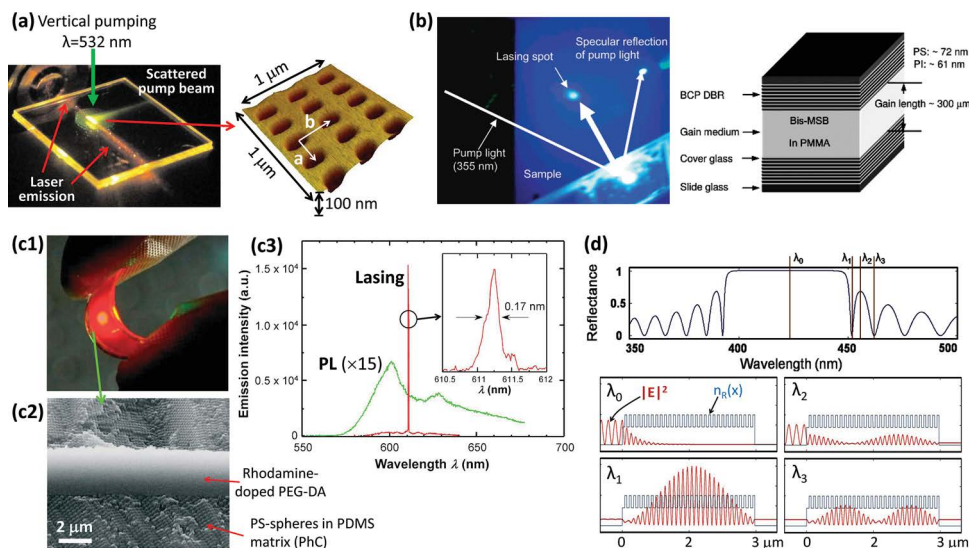


Figure 13. (a) Photograph of an operating PhC laser shown with the atomic force microscope (AFM) image of a surface of the PhC structure with lattice constants, a and b . Reproduced with permission.^[230] Copyright 2008, American Institute of Physics. (b) Photograph of the 410 nm lasing from the BCP-based laser is shown with a schematic of its structure. A highly directional lasing output in the backward direction was observed. Reproduced with permission.^[231] Copyright 2006, American Chemical Society. (c1) A photograph of the laser action of the all polymer film laser shows excellent mechanical flexibility. (c2) A cross sectional SEM image shows the gain medium cavity confined by colloidal 3D PhCs. (c3) The emission spectra below and above the lasing threshold. The inset represents the high-resolution spectrum of the laser emission. Reproduced with permission.^[232] (d) Reflectance spectrum of a 1D PhC comprised of 30 unit cells showing the electric field intensity profiles for four selected wavelengths within and outside the PBG. Reproduced with permission.^[233] Copyright 2012, Optical Society of America.

the 1D PhC mirrors surrounding the cavity layer, to the single step bottom-up self-assembly approach using high-molecular-weight ($\sim 6 \times 10^5$ g mol $^{-1}$) PS-*b*-PI (Figure 13b).^[231] The 1D BCP PhC consists of alternate layers of PS ($n_{PS} = 1.59$, $d_{PS} = 72$ nm) and PI ($n_{PI} = 1.51$, $d_{PI} = 61$ nm) to form mirrors surrounding the organic chromophore doped PMMA cavity layer. Moreover, since many laser dyes can be dissolved into most BCPs, it is straightforward to create distributed feedback lasers where the lasing medium is distributed within the photonic crystal (mirror). A similar lasing device was demonstrated using the [111] feedback of a fcc self-assembled PS spheres in a PDMS matrix and although the refractive index contrast n_{PS}/n_{PDMS} was only $\sim 1.59/1.43$, it was still sufficient to exhibit Bragg feedback for pulsed lasing.^[232] Since the layered materials (PS and PDMS), the gain medium (dye-doped poly(ethylene glycol) diacrylate), and the substrate (poly(ethylene terephthalate) (PET)) are all polymeric materials, a flexible laser is possible (Figure 13c). Fine tuning of the PBG could also be achieved via swelling of the PDMS matrix by adding PDMS oligomer. The very narrow spectral width (full width at half maximum ~ 0.17 nm) shows the possibility for single mode lasing (Figure 13c). Thus, the use of both colloidal and BCP self-assembly in addition to the multiple spin coating technique^[62,63] allows facile creation of low cost, all-organic, flexible laser devices. Furthermore, other highly tunable PhC lasers responsive to various stimuli including solvent,^[97] temperature (thermochromic),^[235] mechanical strain (mechanochromic),^[236] and electric field (electrochromic)^[175] can be envisioned.

In contrast to lasing using an optical cavity, since the photon group velocity decreases significantly due to band flattening near a PBG (see the band diagrams in Figure 3a2),^[237]

band-edge lasing (or cavity-less lasing) is also possible.^[238,239] In recent numerical simulations, a phosphor-embedded 1D PhC is expected to boost fluorescence efficiency up to 7 times because of the slow group velocity at the edge of a PBG resulting in high electric field intensity (λ_1 in Figure 13d).^[233] Taking into account that a PBG of lamellar BCP PhC can be tuned via addition of homopolymer(s) to cover the entire visible regime,^[240] self-assembly of phosphor-loaded BCPs and/or dye-doped BCPs can be also considered for visible lasers.

Most white inorganic light-emitting diode (LED) solid-state lighting typically uses only blue LED modules as the light source with phosphors added to generate green and red hues instead of using three primary color LEDs due to cost. Because the photoluminescence (PL) efficiency of the phosphors directly relates to the overall energy efficiency, enhanced PL is practically very important. In line with the recent trend to replace inorganic phosphors with organic dyes due to cost and toxicity issues, PL enhancement in periodic polymers will be very attractive to reduce the amount of active material. Dye-doped LC blue phases^[241,242] could be useful for this application, however, the approaches using periodic polymers such as BCP would be advantageous for LED applications considering the unfavorably large temperature dependency of the optical characteristics of LCs.^[243]

3.3. Photovoltaic Applications

Polymer photovoltaic (PV) cells have been intensively investigated due to their low cost and flexible mechanical properties compared to inorganic (mostly silicon-based) PV cells. Since

recent progress has improved power-conversion efficiencies up to 9% and solution process fabrication reduces production costs, the future of polymer PV cells is quite promising.^[244]

Due to the spectral broadness, time-varying incident angle, and directional/diffusive nature of solar radiation, various strategies have been developed to enhance the power-conversion efficiency of PV cells. Some examples of the different aspects of the PV device are illustrated in **Figure 14**. Since most PV cells can work at a much higher photon flux without saturation (due to a number density of atoms in a PV cell being significantly larger than the number of photons falling on it), the introduction of solar concentrators (Figure 14a) enables one to reduce the size of PV cells without a loss of power generation. Moreover, the luminescent concentrators such as PL dye/quantum dots within a transparent polymer matrix can make PV cells much less sensitive to the solar illumination angle. The periodic patterning of the air/anode interface can provide a self-cleaning antireflection layer^[245,246] for long-lasting higher efficiency by virtue of structural hydrophobicity and TiO₂ based degradation of deposited organic contamination. Moreover, the periodic structure at the anode/p-type interface can enhance light-trapping via diffraction^[247,248] or plasmonic scattering^[249,250] (if it is made of metals) (Figure 14b). The active interface between the p- and n-type transport polymers can be engineered to have a bi-continuous, bulk hetero-junction (BHJ) morphology,^[244] at the scale of the exciton diffusion length (~10 nm),^[251,252] for enhanced exciton collection^[253,254] or to have a PhC structure to recycle light for improved photon absorption.^[255] (Figure 14c). Since such patterning of the active interface also affects the electrical properties, numerical

designs of periodic active layers in organic PV cells have been carried out to enhance light harvesting to achieve broadband and wide-angle range absorption enhancement without sacrificing electrical performance.^[256] The surface of the metallic cathode can also be patterned to increase photon absorption via surface plasmons^[257] and photon trapping^[258] (Figure 14d).

Besides these approaches, multi-junction PV cells have been demonstrated to utilize low-energy photons below an energy gap of a single-junction PV cell. For example, tandem polymer PV cells having multiple junctions have demonstrated a higher power-conversion efficiency (without using any photonic dispersion engineering).^[259] Thus, the introduction of PhCs is expected to create additional efficiency. Indeed, multi-fold enhancement in photon absorption was demonstrated by slow light at the PBG edge arising from the periodic patterning of an photoactive polymer layer having bicontinuous donor (deprotectable polythiophene derivative (TDPTD)) and acceptor ([6,6]-phenyl-C61-butyric acid methyl ester (PCBM)) phase (TDPTD:PCBM)^[255,260] (**Figure 15a**). Moreover, the PhC topography generates more favorable free carrier transport for TDPTD:PCBM by virtue of the 45% larger interfacial area and a modified static internal electric field distribution in the photoactive region, which induces the field-dependent dissociation of excitons at the active region. Instead of directly patterning the active materials, PET substrates have been 2D patterned using IL, such that the subsequently solution coated PV cells had improved light absorption via trapping and guiding, and demonstrated up to 21% higher efficiency (Figure 15b).^[36] Such photonic substrates are also possible via standard photolithography, for example, SU8 pillars on a PET substrate, were top coated with a transparent conductive polymer (Orgacon) to form the anodic component.^[261]

Periodic structures are both angle-dependent and wavelength-dependent and this is generally disadvantageous for PV cells due to the broad solar spectrum and the time-varying illumination directions (Figure 15). As previously discussed, isotropic non-crystalline and near-isotropic quasicrystalline structures (see Section 3.1) can help provide angle independent performance. Recent calculations show that the PV cells

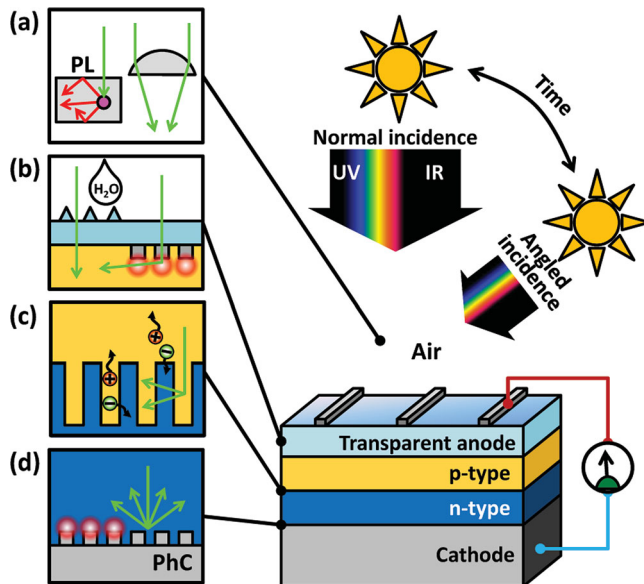


Figure 14. Schematic illustration of various strategies to enhance the power-conversion efficiency of a single-junction PV cell. (a) Concentrators (luminescent and geometric) (b) Anode patterning for antireflection and self-cleaning and introduction of (metallic) gratings for enhanced light trapping. (c) *pn*-junction interface engineering for efficient exciton harvesting and for enhanced photon absorption via a PhC interface. (d) Cathode patterning.

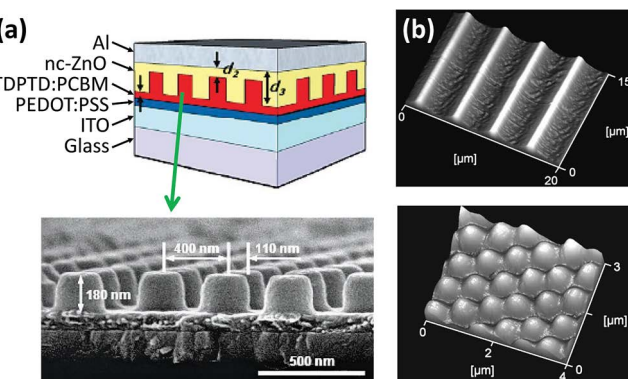


Figure 15. (a) Cross sectional schematic of 2D PhC and SEM image of hexagonal array of active polymer columns prior to backfilling with nanocrystalline-ZnO. Reproduced with permission.^[255] Copyright 2009, American Chemical Society. (b) AFM images of linearly and hexagonally patterned PET substrate. Reproduced with permission.^[36]

employing quasicrystalline plasmonic structures demonstrate constant light absorption efficiency during the course of a day as well as over the course of a year.^[262] Therefore, quasicrystalline patterning of substrates and active polymers using various techniques including IL^[29,263] are attractive to explore.

A bicontinuous BHJ design has attracted great attention because the two component interpenetrating network of electron and hole transport materials enables efficient collection of the optically excited electron-hole pairs at low-cost.^[253,254] Recently Park et al. employing a blend of copolymer and fullerene derivative, demonstrated an internal quantum efficiency close to 100%, implying that all incoming photons create electron-hole pairs.^[264] Therefore, self-assembled bicontinuous interpenetrating hole transport/electron transport BCP morphologies such as the double gyroid can be very attractive for PV applications^[265,266] since their continuously connected microphase-separated domains with widths on the order of 10 nm can allow the efficient dissociation and transport of photo-generated excitons to the respective electrodes.^[267] Compared to other PhCs in PV cells,^[268] however, the structural scale of the micro-phase separation in BCP materials will be too small to achieve a PhC effect. In this direction, Zavala-Rivera et al. demonstrated a novel hierarchical BCP structure via collective osmotic shock of a PS-*b*-PMMA BCP that can be applied to improve PV efficiency via photonic dispersion engineering.^[269]

3.4. Sensors

Sensor applications of PhCs are growing exponentially as seen in Figure 2b and polymer PhCs have shown great potential including the pioneering works in chemical sensing by Asher and his students.^[114] Generally accurate and precise sensing requires both specificity and sensitivity, reversibility (reproducibility), rapid to near-equilibrium response (low equilibration time once the sensor is exposed to the analyte) as well as valid calibration over the range for which the response occurs. Since the basic idea of sensing is to induce a noticeable change in the optical parameters of PhCs, mostly refractive index and periodicity, detectable stimuli are not limited to just chemical stimuli since polymer PhCs respond to a set of physical stimuli as summarized in Table 3. PhCs can also be used to improve the sensitivity of sensors via their PBG effects. For example, a vapor sensor using the PL quenching by trinitrotoluene (TNT) vapor of an emissive conjugated polymer can have much better sensitivity if a PhC is used for PL amplification^[270] or dispersive PL quenching.^[271] Moreover, molecular IR absorption signals of various gases can be amplified by the slow group velocity at the edge of a PBG.^[272]

An 1D PhC having an initial maximum reflectance (R_{MAX}) of 89% at $\lambda_{peak} = 600$ nm is selected as an example. To illustrate the trend of the optical response caused by various cases of solvent swelling, a small fixed change is applied to each refractive index and layer thickness. Figure 16 demonstrates the complexity in the optical responses of a 1D polymer PhC corresponding to the swelling of one or both types of polymer layers. While the solvent swelling of a polymer always increases the physical thickness, the refractive index of the swollen polymer depends on the refractive index of the solvent (n_s) and

Table 3. Periodic polymer systems developed for sensing various types of analytes.

Analytes	Structure Materials	Ref.
Humidity	1D lamellae TiO ₂ , PHEMA	[273]
	2D cylinders poly(styrenesulfonate)- <i>b</i> -poly(methyl butylene)	[96]
	3D inverse opal PAAm	[274]
pH	1D etalon PNIPAm-PAAc microgel	[275]
	3D opal Hydrolyzed PAAm, PS spheres	[276,277]
Ion	1D lamellae PS- <i>b</i> -P2VP	[97]
	3D inverse opal PNIPAm-crown ether	[278]
Sugar	3D opal PAAm, PNIPAm-flavin, PS spheres	[114,279]
	1D lamellae PBA functionalized PS- <i>b</i> -P2VP	[280]
Strain	1D lamellae PS- <i>b</i> -P2VP	[236]
	3D opal PS-polybutadiene	[281]
Blast Wave	3D diamond-like SU8	[30,31]
Temperature	1D lamellae PS- <i>b</i> -PI	[235]
	1D lamellae PS- <i>b</i> -MMA/LC	[282]
	3D inverse opal PNIPAm	[283]
	3D opal (PNIPAm- <i>co</i> -PAAc)-ETPTA core-shell	[284]

the relative selectivity of the solvent for each type of layer. For example, when the solvent has its index between that of the high and low index polymers, $n_L < n_s < n_H$, the refractive index contrast is substantially reduced when a degree of swelling is large, which always results in deterioration of R_{MAX} (#5, #6, and #7) and the deterioration becomes greatest for a neutral solvent (swells both layers equally well) (#7). For the two other possible solvent conditions, ($n_s < n_L < n_H$) and ($n_L < n_H < n_s$), either solvent preferentially swelling of the n_L layer (#1) or of n_H layer (#3) are advantageous for colorimetric sensing as this condition increases the refractive index contrast and hence the reflectivity. To induce a large wavelength shift in the peak position ($\Delta\lambda_{peak}$) to enable high sensitivity, the use of a neutral solvent that swells both polymers is advantageous (#2 and #4) but one or both of the blocks may need to be crosslinked to avoid structural deterioration at high degrees of swelling. Since the refractive index of water ($n \sim 1.33$) is lower than that of most polymers ($n_s < n_L < n_H$), either swelling the n_L layer (#1) or swelling both layers (#2) can be more favorable than swelling the n_H layer (#5). Case #4 shows the best performance in the sensitivity without loss of reflectivity, but requires a solvent with a high refractive index. Note that as this simplified demonstration does not reflect any specific interaction parameters between polymers and solvent, even for the co-swelling cases (#2, #4, and #7), since the same amount of refractive index change is assumed for both types of layer.

Humidity Sensing: Relative humidity (RH) sensing schemes are mostly based on intrinsic swelling behavior of hydrogel materials. Certainly any vapors of good solvents for polymer constituents of PhCs should be detectable. The well-known hydrogels, polyacrylamide (PAAm) and poly(2-hydroxyethyl methacrylate) (PHEMA), have been introduced into PhC structures and their RH-responsive behaviors have been studied for

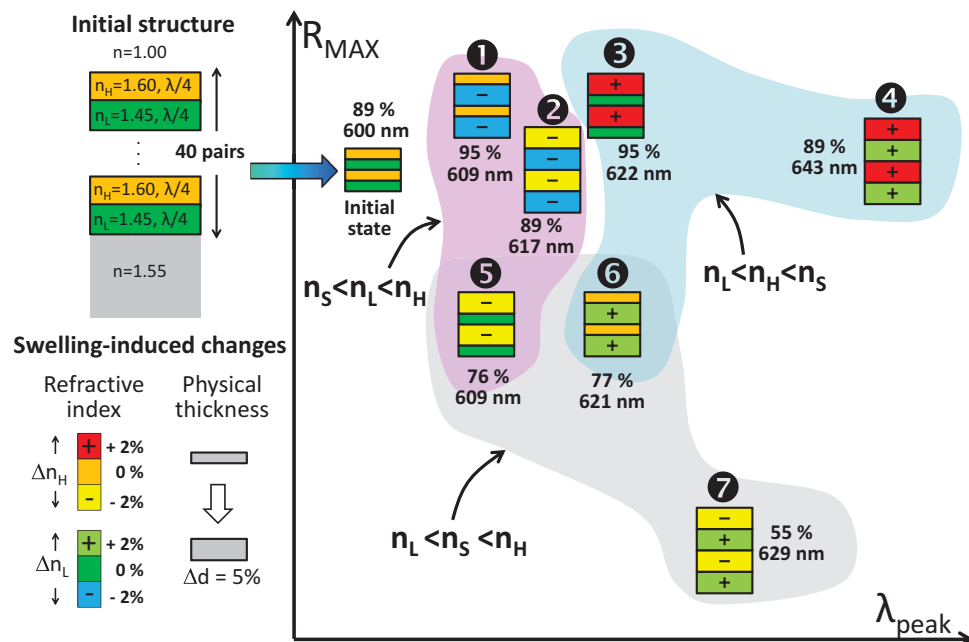


Figure 16. The simplified seven cases of solvent swelling for a 1D bilayer stack. Changes of reflectance peak wavelength, λ_{peak} , and maximum reflectance, R_{max} , of a lamellar PhC structure corresponding to small variations of refractive index ($\pm 2\%$), and thickness ($\pm 5\%$). The initial lamellar PhC consists of 40 pairs with high ($n_H = 1.60$) and low ($n_L = 1.45$) indices and with the layer thickness equal to a quarter-wave optical thickness ($d = \lambda/4n$). Depending on the refractive index of the solvent (n_s) and the preference of the solvent for each type of polymer layer, a wide range of responses can occur.

a decade.^[273,274,285,286] For example, a 1D PhC RH sensor consisting of alternating layers of TiO₂ and PHEMA-*co*-PGMA was fabricated by sequential spin coating.^[286] Although the $\Delta\lambda_{peak}$ varied approximately 70 nm for viewing angle differences between 30° and 60°, the PhC sensor exhibited several advantages including a good repeatability over 100 times, a large $\Delta\lambda_{peak}$ of 150 nm for a change in water volumetric ratio of only 0.01 due to the highly non-linear coil to globule collapse transition that leads to a substantial change in layer thickness with a relatively fast response time (<150 s). A different approach using a cylinder forming PSS-*b*-PMB BCP^[96] provided RH sensing (Figure 17a) due to the hygroscopic nature of the PSS matrix. The range of the reflectivity peak shift could be controlled by the PSS sulfonation level. For example, at a sulfonation level of 76%, the sensor exhibited a shift $\Delta\lambda_{peak}$ of ~200 nm for a change of RH from 20 to 90% with a response time less than 5 s. Since these electrolytic RH sensors also exhibit several orders of magnitude changes in electrical impedance depending on the RH, these BCP PhCs can also be used as opto-electrochemically responsive sensors.

pH Sensing: An example of the usefulness of pH sensing is to monitor food product quality because pH is directly correlated with elevated CO₂ gas levels, the prime indicator of bacterial activities causing food spoilage in packed foods.^[287] pH changes are basically detectable by the ability of the PE block to immobilize counter ions with different hydration affinities, resulting in osmotic swelling.^[275–277,288–293] For example, a poly(acrylic acid) (PAAc) hydrogel PhC structure is highly sensitive to pH. PAAc can be made by hydrolysis of PAAm or copolymerized with PAAm. An opal PhC of PS spheres surrounded by a PAAc

hydrogel showed nearly 200 nm shift in reflective wavelength for a pH change from 2 to 5.5.^[292] A broader detection range of pH was enabled by hydrolyzing PAAm copolymer^[276] covering the visible regime from 550 nm to 800 nm, for pH from 2 to 10.

Sensing Ions: For ionic sensing, designing a polymer backbone with analyte-selective binding molecular recognition groups (MRGs) is desirable. Some exemplary MRGs developed are 8-hydroxyquinoline for Cu²⁺,^[294] an aptamer for Hg²⁺,^[295] and crown ether for Pb²⁺.^[114,277–279,296–298] Hg²⁺ ion sensing occurs due to binding to aptamer units crosslinked with PAAm which results in shrinkage of the hydrogel-colloidal PhC.^[299,300] The structure showed a wavelength shift of 150 nm for a change in Hg²⁺ concentration from 0 to 1 μM. Opal hydrogels of PS-*co*-PDMAA spheres could detect SCN⁻ ions in the concentration range from 10–10⁴ nmol/g.^[301] Modified methods using the opal hydrogel PhCs were developed for the detection of Hg²⁺^[302] and ionic strength.^[303] Quaternized PS-*b*-P2VP (denoted PS-*b*-QP2VP) gels (Figure 17b)^[97] have pyridinium rings, which makes the film water swellable and ion exchangeable. The stronger the hydration energy of an exchanged ion, the greater the degree of swelling by water. For example, a low hydration energy ion SCN⁻ showed a reflective peak at near 400 nm and a high hydration energy ion, CH₃COO⁻, showed a reflective peak near 650 nm (Figure 17b).

Sugar Sensing: Real-time non-invasive, painless sensing motifs that can monitor the glucose concentration in blood or in a bodily fluid are of obvious importance and have been extensively studied.^[114,279,280,304–309] Asher's group suggested two sensing motifs, glucose oxidase based sensing^[114,279] and

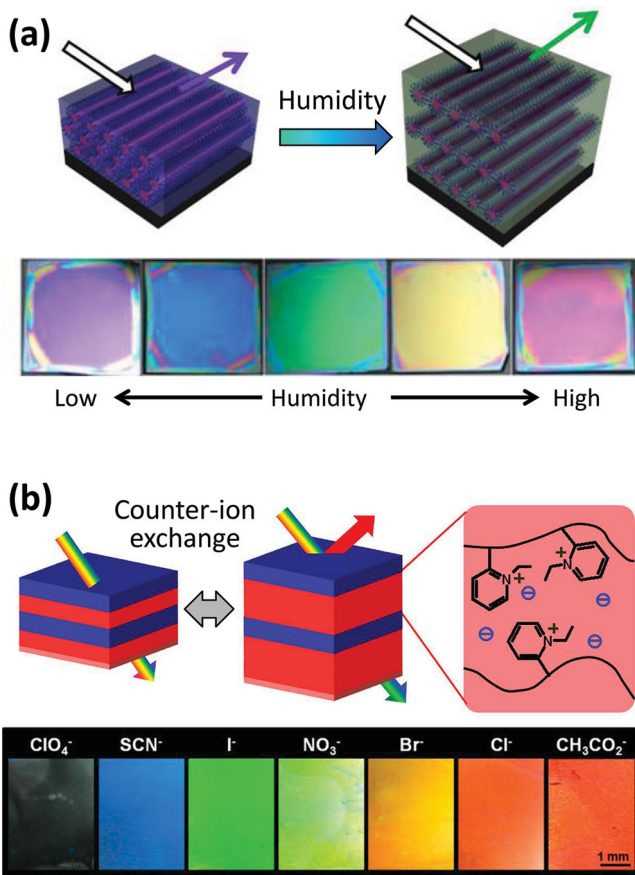


Figure 17. (a) Schematic illustration of the PSS-*b*-PMB BCP humidity sensor at low and high RH and photographs of sensors at different RH. Reproduced with permission.^[96] Copyright 2012, American Chemical Society. (b) Schematic representation of the mechanism for color change in the PS-*b*-QP2VP photonic lamellar gels by a direct exchange of counter-ions in the QP2VP layers and photographs of the films showing different colors with increasing hydration energy of the counter-anions. Reproduced with permission.^[97] Copyright 2012, American Chemical Society.

boronic acid based sensing.^[304–307] The reduced state of glucose oxidase causes sensor swelling, whereas boronic acid forms bis-bidentate complexes that shrink the hydrogel volume and produce reflective peak blue-shifts. Other physiologically important sugars, such as fructose, galactose, and mannose, form only mono-bidentate complexes to boronic acids, which are unable to form crosslinks with boronic acids, resulting in differences in swelling behavior according to the molecular structure of the physiological sugars.

For fructose sensing, Ayyub et al. fabricated PS-*b*-P2VP PhC films modified with BMPBA.^[280] Selective binding between fructose and the boronic acid converts boronic acid to negatively charged boronate and the induced charge swells the P2VP layers. 1,3 diols of fructose have a stronger affinity to boronic acid over 1,2 diols of other sugars, which is the origin of the selectivity. Sucrose, a di-saccharide, has 1,3 diols, but the affinity is much weaker than fructose, a monosaccharide, due to steric hindrance. The structure showed a reflective red

shift of almost 200 nm for the change in fructose concentration from 500 μM to 50 mM.

Strain Sensing: Given the easy and extensive deformability of polymer based materials, using polymers as strain or stress sensors is straightforward. A useful recent review overviews mechanochromic photonic gels.^[310] After the first report on the tunability of the optical response of an elastic polymer opal PhC by Yoshino et al.,^[281] many research groups have intensively investigated mechanochromic materials based on the inverse opal structures of hydrogel^[311,312] and on layered elastomers.^[313–315] For example, the static and dynamic PBG tuning characteristics by coupling their hydrogel inverse opal PhC structure to a piezoelectric actuator were investigated.^[312] The device exhibited a 172 nm total PBG tuning range and could be modulated at frequencies up to 200 Hz. Hard core (PS)-soft shell (PEA) particles were utilized to study the strain-responsive behavior of an opal PhC^[316,317] while PS/PEA particles were used to fabricate polymer opal PhC fibers by extrusion. Stretching the fiber alters the sphere to sphere distances inducing a shift in the peak position of the PBG.^[188] A 1D lamellar BCP PhC is well suited for colorimetric detection of the degree of compressive strain.^[236] Since BCP lamellar films can be conformally coated onto non-planar and patterned substrates, these mechanochromic films act like a “strain paint.” The strain induced peak shifts are summarized in Table 4. The largest value for peak shift/strain was achieved by the 1D lamellar system.

Blast and Shockwave Sensing: The structural colors of a glassy or semicrystalline PhC can be permanently altered by plastic deformation of a polymer/air structure due to shock waves, including blast. Cullen et al. created a colorimetric blast injury dosimeter utilizing 3D polymeric PhCs fabricated by multi-beam IL and investigated blast-induced color change as shown in Figure 18a.^[30] A mixture of hydrogen and oxygen gases was exploded in a cylindrical shocktube and the blast was transferred along the tube to impact the sample. Sample color before and after exposure to the blast at peak overpressures of 655 kPa and 1090 kPa are shown in Figure 18a. The microstructure undergoes various deformation modes resulting in a complex deformation pattern with strong gradients. The prototype blast injury dosimeter arrays were also affixed to animals and a correspondence found between the blast injury dosimeter color changes and brain pathologies, including neuronal degeneration and reactive astrocytosis.^[31] The power-free colorimetric sensing motif may allow this type of blast injury dosimeter to be deployed for use by warfighters.

Temperature Sensing: Thermal changes, the most ubiquitous stimulus, affects almost all materials properties, including material dimensions, solubility and phase behavior. In particular for polymers, the temperature dependence of the Flory-Huggins interaction parameter reflects the temperature-induced changes in monomer-solvent, monomer-monomer and solvent-solvent interactions, which can lead to chain expansion or contraction and subsequent differences in average index of refraction of each type of domain as well as domain thickness. Investigations of temperature-responsive optical behavior of polymeric based PhCs date from the study of Takeoka et al.^[283] using the strong thermal response of poly(*N*-isopropylacrylamide) (PNIPAm) in aqueous solutions. In this case, the detectable range of temperature was limited because PNIPAm does not form a gel in

Table 4. Summary of characteristics of polymer-based PhC systems for strain sensing. (Note: a negative sign in the sensitivity is because an applied stress direction is perpendicular to a light propagation direction and these responses show relatively less sensitivity due to the Poisson's ratio effect.)

PhC system	Max. strain, $\Delta\epsilon_{MAX}$	Peak shift [nm]	Sensitivity $\Delta\lambda/\Delta\epsilon_{MAX}$ [nm/%]	Ref.
PMMA/air (3D inverse opal)	+57% Tensile	545 → 475	-2.2	[313]
Silica spheres/ poly(acrylamide) (3D opal)	-45% Compression	800 → 450	7.8	[311]
PS spheres/poly(2-methoxyethyl acrylate) (3D opal)	-15% Compression	610 → 517	6.2	[312]
PS spheres/PDMS (3D opal)	+20% Tensile	590 → 560	-1.5	[315]
PS core/PMMA, PEA shells (3D opal)	+13% Tensile	636 → 603	-2.5	[316]
PS spheres/PEA (3D opal)	+30% Tensile	600 → 540	-2.0	[188]
PS- <i>b</i> -P2VP (1D lamellar)	-20% Compression	760 → 520	12.0	[236]
PU/Pebax (1D lamellar)	+125% Tensile	600 → 410	-1.5	[151]
PSPI/PDMS (1D concentric)	+120% Tensile	800 → 550	-2.1	[318]
Poly(dodecylglycerol itaconate)/PAAm (1D lamellar)	-64% Compression	600 → 415	2.9	[319]

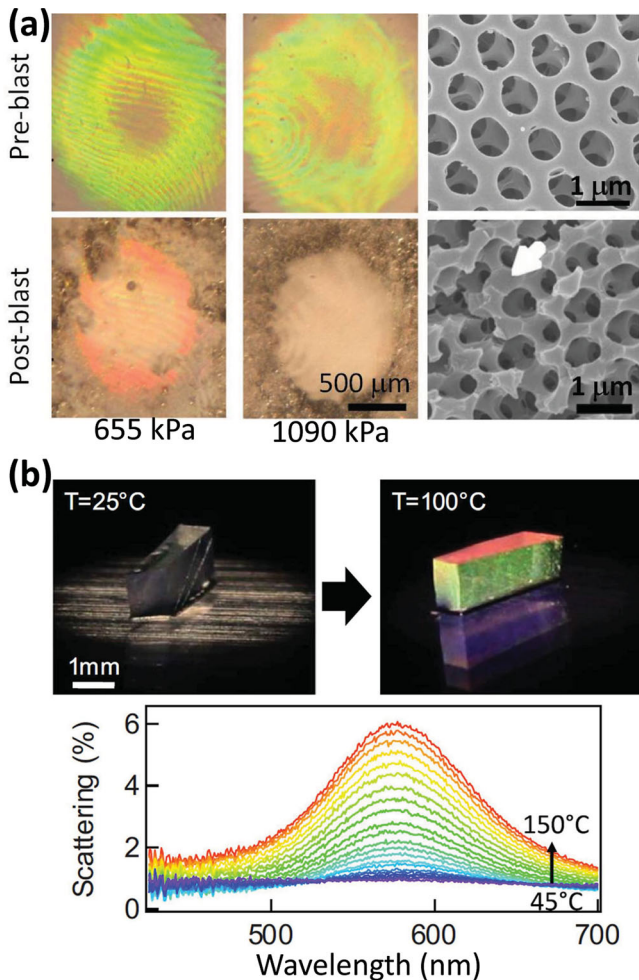


Figure 18. (a) Photographs of blast injury dosimeters using 3D PhCs made by IL before and after exposure to blast waves having peak overpressures of 655 and 1,090 kPa. The SEM images allow identification of changes in the structural features of the blast injury dosimeter after the shock. Reproduced with permission.^[30] Copyright 2010, Elsevier Inc. (b) Photograph of a transparent PhC shows colors at elevated temperature and its temperature-dependent optical scattering spectra. Depending on a viewing angle, different colors are observed from the PhC at 100 °C, as shown by the spectra below. Reproduced with permission.^[320] Copyright 2009, American Institute of Physics.

water below its lower critical solution temperature of 32 °C. For a wider temperature range, alternating stacks of crosslinked poly(*para*-methyl styrene) (PpMS) and PNIPAm-*co*-PAAC were introduced.^[321] Covalent cross-linking of the PNIPAm contributed structural stability and a wider detection range from 20 to 50 °C with good sensitivity of $\Delta\lambda/\Delta T \sim 10 \text{ nm}/^\circ\text{C}$. A PHEMA based 3D PhC fabricated from a template created by IL was reported by Kang et al.^[322] The PHEMA-*co*-PMMA hydrogel, swollen by humid air, showed a tunable PBG with $\Delta\lambda/\Delta T \sim 12 \text{ nm}/^\circ\text{C}$ from 25 to 50 °C.

Though the peak shift with temperature change is sufficiently high for the above system, the practical detectable range of temperature is limited to near room temperature. Thermochromic polymer opal PhCs were fabricated that could operate up to 150 °C,^[320] with refractive index matched polymers by assembly of core/shell spheres comprised of a PMMA core and a composite shell of 70% PEA and 30% PBzMA (Figure 18b). Due to the index matching at room temperature, the thermochromic behavior was caused entirely by the isotropic lattice expansion, $\Delta d(T)$ and the difference in temperature-dependent refractive indices, $\Delta n(T)$ of the spheres and the polymer matrix. Although the device demonstrated relatively small increase in scattering intensity (from 0 to 6%), the transparency of the material at room temperature is very attractive for visual applications like residential windows. In contrast to other thermochromic spectra, the reflectivity peak is essentially fixed due to the offsetting behavior of $n(T)$ of each polymer (decreased) and $\Delta d(T)$ (increased) on the optical path.

On the other hand, thermochromic BCP gels can operate over a much broader range of temperature with reasonable equilibration times (~10 min). For PS-*b*-PI, thermal expansion and variation in refractive index play a minor role while the temperature dependent segregation strength (reflected through the Flory-Huggins χ parameter) is chiefly responsible for the change in thickness of the gel layers and a reflective peak shift of 60 nm for a temperature change of 30 to 140 °C.^[235] For PS-*b*-P2VP, the P2VP domains become more hydrophobic as temperature increases because the fraction of protonated pyridine groups decreases as temperature increases with $\Delta\lambda/\Delta T \sim -1.5 \text{ nm}/^\circ\text{C}$ for temperatures from 0 to 80 °C.

A drawback of most of the temperature sensors discussed up to this point is that they inherently rely on liquid transport to

expand and contract the system, principally due to the temperature dependent solvent-polymer interactions. Thus, continuous contact with a liquid reservoir is necessary to avoid drying and allow solvent adjustment as necessary.

Liquid Crystalline and Semicrystalline Polymer Temperature Sensors: The development of dry (neat polymer) efficient temperature sensors may be possible using liquid crystalline or crystalline BCPs. Osuji et al.^[282] used a PS-methacrylic acid (PS-*b*-MAA) BCP blended with H-bonding LC mesogens to effectively increase the molecular weight and thus the scale of the lamellar microdomains, resulting in a green reflector. By increasing the temperature above the isotropic transition temperature of the LC domains, the peak reflectivity shifted 40 nm to produce an orange color. Dow Chemical Company^[323] developed self-assembled films of semicrystalline diblock copolymer based on linear low density PE and ultra low density PE. These films display a blue reflective color, but the color disappears when the film is heated up to the melting temperature (~100 °C). The color quickly returns as the films cool and crystallization again drives microphase separation between the blocks.

3.5. Imaging and Display Applications

As the previous sections have shown, polymer PhCs are highly responsive to a wide variety of stimuli. Thus, it is possible to select an easily controlled stimulus and then be able to address local regions of a PhC to create a specific reflective color, to store that color state and then, by reversing the stimulus, to reset to the original state/color. Depending on the form of the actual device, the potential applications range from photonic paper to video displays. Tunability for full color in a single pixel will increase resolution and brightness, and decrease processing/fabrication costs of displays. The choice of stimulus is quite broad, but needs to be able to be applied locally to induce the reflection change in a single pixel without crosstalk – thus, heat, or light or electric or mechanical fields are all possible but vary greatly in their practicality. If after the stimulus is stopped, the system relaxes, clearing the pixel, the stimulus must be continually applied so as to maintain the “on” state. For example, a thermal stimulus, while reversible, will need to continuously use energy to stay in the on state, thus, a bi-stable (hysteretic) system is desirable. Also if upon application of the stimulus, the system is permanently changed, then there is no ability to rewrite.

While a host of liquid containing photonic crystal systems can be stimulated over the visible spectrum by changing temperature, ionic strength, pH, solvent quality etc., in order for future integration of polymer based PhC pixels into display devices, a more direct driving stimulus and a faster response time will be necessary. The current best opportunities for polymer based PhC pixels appear to be for slower switching and non-volatile, reflective color devices. The first realization of a polymer PhC based multi-color pixel was accomplished by Honda et al.^[324] employing an inverse opal matrix of PHEMA-*co*-PAAc with PNIPAm spheres fabricated by double-templatting. This system could express four reflective colors at certain combinations of pH and temperature, expressed as (pH, temp): 700 nm at (7, 15 °C), 650 nm at (7, 40 °C), 560 nm at (2,

15 °C), and 540 nm at (2, 40 °C). However, as pointed out above, it is far from convenient to alter both the pH and temperature conditions for a single pixel. Conventional display technology uses indium-tin-oxide patterned transparent electrodes. By placing a responsive polymer PhC between two electrodes, the application of an electric field can either induce electrochemical changes or if a soft polymer is employed, the resultant capacitive forces can mechanically compress the PhC. Voltage tunable pixels of PS-*b*-P2VP^[173] were made by using an electrochemically switchable molecule as the swelling solvent. The solvent, trifluoroethanol ($\text{CF}_3\text{CH}_2\text{OH}$) is oxidized to trifluoroethoxide ($\text{CF}_3\text{CH}_2\text{O}^-$) under an applied field, which causes reduction in the degree of swelling.^[175] By applying voltages of up to 10 V, the film could be adjusted from its initial red color to blue with a response time of seconds and good repeatability over multiple cycles. Kang’s group has made further progress using a voltage induced pH gradient for gel swelling and deswelling.^[174,325] They also obtained a non-volatile pixel (negligible deterioration in 25 hrs) by taking advantage of pH hysteresis and optimized the pH trigger of the hysteresis loop by pairing of appropriate anions and PS-*b*-QP2VP. Lu et al.^[326] also showed a tunable behavior of PS-*b*-P2VP photonic gels in a water/ethanol 1:1 mixture. In their approach, the pyridine groups in the P2VP layers became charged depending on the applied electric potential and resulted in different degrees of swelling. The full range of visible wavelengths was expressed at low driving voltage (under 2.5 V) and repeatability was also demonstrated in multiple cycles. Response time, however, was very slow (~ 20 min) due to low conductivity of the water/ethanol mixture.

Ozin et al. fabricated multipixel electrochemical cells of a silica-polyferrocenylsilane (PFS) PhC composite between electrodes and controlled color by electrochemical swelling of the PFS using an electrolyte solution^[115] as illustrated in Figure 19a. They named their structure, “P-ink”, which combines a silica bead PhC structure with an electrically active polymer matrix. Under an oxidative potential, electrons are drawn out of iron atoms in PFS and the resultant increased osmotic pressure drives the influx of both ions and solvent into the polymer, causing the polymer matrix to swell and increasing the spacing between the silica beads. Applying a reducing potential runs the system in reverse. The composite system showed a $\Delta\lambda_{\text{peak}} \sim 110$ nm, repeatability over 100 cycles, a response time below 15 s, and non-volatility due to hysteresis over 80 min. By etching out the silica spheres to form an inverse opal PFS gel film, a much broader tuning range ($\Delta\lambda_{\text{peak}} \sim 300$ nm), faster response (~10 s), and an enhanced stability at low driving voltage (under 3V) due to the increased index contrast and enlarged contact area between the electrolyte solution and the PFS was obtained.^[327] Further commercial development of this system has improved the color range and speed (subsecond).

Xia et al. motivated by the capacitive actuation of elastomers, fabricated a PhC of poly(2-methoxyethyl acrylate) (P2MEA) with silica spheres.^[329] To enhance the electric-field-induced responsiveness, the permittivity was increased by in bandgap reduction of silver nitrate to metallic silver inside the films producing a small 20 nm shift in the stop-band peak position for an applied field of 25 V μm^{-1} . For faster response of tunable pixels, Shim et al. suggested utilizing the electrophoretic movement of

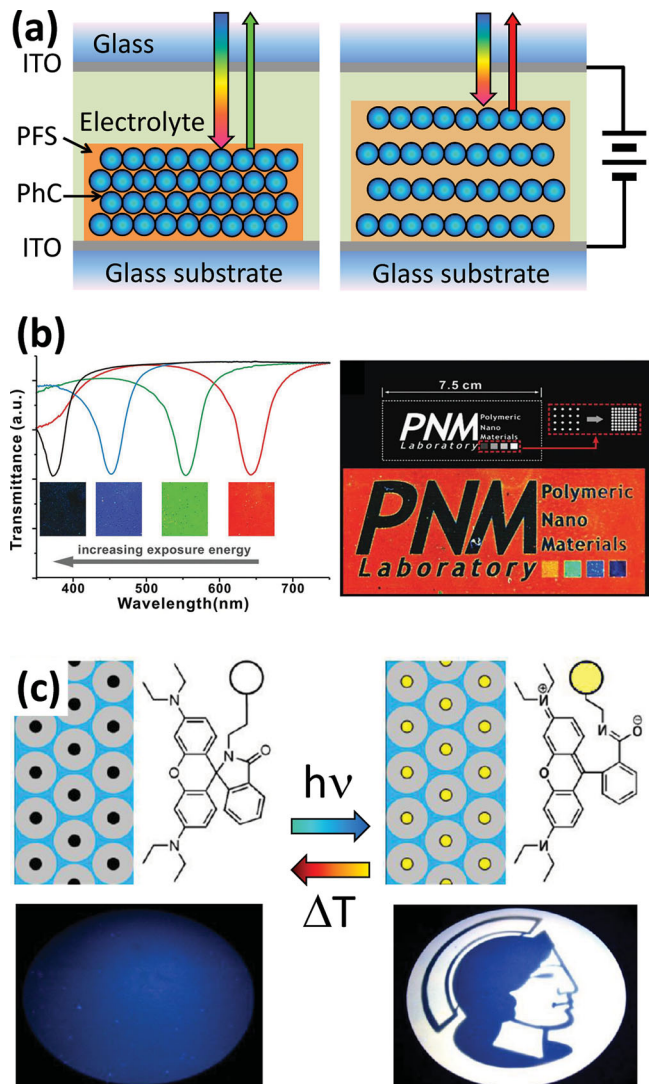


Figure 19. (a) Schematic of the electric field driven swelling of a silica-PFS PhC composite. (b) Optical responses of the PS-*b*-QP2VP photonic gel film (left) depending on UV irradiation dose and multicolor patterns created using a photomask having gradient pattern density to control local crosslink density (right). Reproduced with permission.^[328] (c) Schematic of writing and erasing of opal photonic paper by UV induced ring-opening and temperature induced ring-closing reaction of RhBMA dye 3 (top) and optical images of a patterned elastomeric opal film after activation of RhBMA-labeled beads (right) and temperature-induced reversible erasing (left). Reproduced with permission.^[317] Copyright 2013, American Chemical Society.

highly charged PS particles.^[330] The particles form a non-closed packed fcc structure due to the high surface charge of the particles and the entire system of particles moves to the oppositely charged electrode with a gradient by Coulombic attraction, which also results in reflective peak blue shift. They showed a $\Delta\lambda_{\text{peak}} \sim 110$ nm, a response time of 10 ms and demonstrated stable color switching behavior for 40 min using 1.2 V, 5 Hz AC field.

A lithographic scheme utilizing photocrosslinking of ion-exchanged PS-*b*-P2VP film was developed (Figure 19b) using the strength of UV exposure energy control the degree of blue

shift in color of the photonic gels (a more densely crosslinked gel leads to less swelling). The sensitivity of the polymer to UV crosslinking can be retarded by radical-inhibiting anions with the inhibition power proportional to the size of halogen anions. It is possible to tailor the color of specific areas by ion-exchange before photomasking and UV exposure leading to a periodic pattern of red, green, and blue regions similar to a color filter for emissive display devices.^[328] Jiang et al. photopatterned a polymerized opal PhC of PHEMA-*co*-PMOEA with PS spheres by swelling with monomer followed by UV exposure and observed color differences between the patterned and unpatterned areas due to differential uptake of solvent vapor.^[331]

For rewritable photonic paper, one scheme is to add a solvent to locally swell the structure, followed by removal of the solvent in order to return the structure to its initial state. This approach suffers from low resolution due to slow diffusion of the solvent beyond the contact area as well as degradation due to evaporative loss of volatile solvents. An opal PhC with cross-linked PS spheres in a PDMS matrix demonstrated changes color by contact with ink^[332–334] such as silicone based volatile fluids ($M_w \sim 200$ g mol⁻¹) that swell the PDMS. The shift in the reflective peak was dependent on the molecular weight of ink, with the maximum peak shift of 130 nm for the lowest molecular weight ink. The writing process took place in 2 sec and the peak position recovered in about 10 sec after removal of the ink via evaporation. A different rewritable photonic paper was made of an opal PhC of hard core-soft shell particles: crosslinked PS-(EA-iBMA-HEMA) core-shell with a UV responsive fluorescent dye (rhodamine B methacrylamide (RhBMA) 3) inside the cores.^[317] The opal PhC initially reflects blue light, but when exposed to UV at 366 nm, the RhBMA 3 in the exposed regions provides a strong yellow fluorescence emission due to the ring-opening reaction and the complementary blue structural reflectivity and yellow dye emission give a white appearance. However, to erase, the temperature must increased up to 130 °C for 5 min and the exposed region goes back to the initial dark (blue) state by ring-closing of RhBMA 3 as shown in Figure 19c.

3.6. Metamaterials

We next describe recent developments in the hot area of “metamaterials.” Meta – literally Greek for beyond – holds the promise for entirely new material behavior and properties quite unlike those in any conventional materials in nature. Much of the activities in metamaterials concern optical and acoustic applications ranging from negative index materials to materials that can cloak an object. The popularization of metamaterials may be traced back to the seminal paper by Pendry,^[335] who introduced the concept of artificial magnetic resonance leading to the creation of a negative index optical material; this led to the birth of a vigorous field of work in electromagnetic, and more recently, elastic and acoustic metamaterials. We next present a section on optical metamaterials and acoustic metamaterials are treated in section 4.4.

Optical Metamaterials: In contrast to PhC where the period is commensurate with the target range of wavelengths of light, optical metamaterials are based on sub-wavelength scale structures, ranging from several times to several orders smaller than

the targeted wavelength. The novel optical responses of metamaterials are often achieved by sub-wavelength resonators, so called “*artificial atoms*” comprised of metallic and dielectric materials that induce collective motion of electrons in a specific mode. Moreover, with nanostructural engineering, the local permittivity $\epsilon(\mathbf{r})$ and permeability $\mu(\mathbf{r})$ of the artificial material can be independently and nearly arbitrarily designed and this unprecedented control enables material constructs that can control the flow of light via what is known as “transformation optics”.^[336,337] For example, using transformation optics, one can distort the normal straight trajectory of light passing through a certain region of free space in a desired manner to effectively “hide” an object (Figure 20a). Any object within the inner spherical region does not interact with external optical waves and is thus, essentially invisible.^[336] Due to the conceptual similarity with the motion of light in a distorted space-time induced by a heavy celestial object, light trajectories in metamaterials can be related to light dynamics in curved space through the invariance of Maxwell’s equations under coordinate transformation.^[338] Thus, the “black hole concept” of astronomy can be practically applied as an omnidirectional light absorber^[339] (Figure 20b).

Since the refractive index is given by $n^2 = \epsilon\mu$ from Maxwell’s equations, a material can have a real value of n enabling a non-decaying propagation of light when ϵ and μ are simultaneously either positive or negative. Since a medium having all negative ϵ and μ results in a negative angle of refraction, the sign of n is determined to be negative. Such negative refractive index

materials (NIMs) are one of the most intensively studied class of optical metamaterials where the counterintuitive negative refractive index arises as a result of the metamaterial artificial molecules.^[342] In contrast to a negative ϵ arising from an electric resonance in typical materials such as metals, a magnetic resonance creating a negative μ is comparatively more difficult to achieve. In the NIMs, sub-wavelength metallic structures having inductive and capacitive components are employed to create the magnetic resonance at the frequencies where ϵ is negative. There are two main challenges to the realization of NIMs at optical frequencies. One is fabrication of very high resolution constructs, as sub-100 nm features are required. The other is the inherent optical losses caused by metallic constituents, especially in the visible and near infrared regimes. The losses dampen the electron oscillation that couples with the light and limit optical NIM to applications requiring short propagation paths. PhCs made of dielectrics (negligible optical absorption) can also be used for the negative refraction^[343,344] because some of photonic bands can make the phase and group velocities anti-parallel, leading to the same effect as the metallic resonators but with much reduced loss. As the photonic band engineering for NIMs could require less stringent refractive index contrast than that required for a complete PBG, a polymer-based PhC can be utilized for NIMs,^[345] as well as for sacrificial fabrication templates discussed below.

Fabrication of metamaterials for optical applications has mostly employed top-down lithography using extremely high resolution patterning techniques such as e-beam lithography,^[346] focused ion beam milling,^[347] nano-imprint lithography,^[348] and laser DW.^[349] For the rapid expansion of metamaterials research, low cost nano-scale fabrication is necessary. Self-assembly or directed self-assembly of BCP is a very attractive approach due to the inherently small length scales well below 50 nm and low cost. The double-gyroid phase of BCP is distinguishable from the other microdomain structures by its 3D self-supporting, bicontinuous topology. NIMs based on a double-gyroid BCP have been theoretically investigated. Figure 20c shows the computed energy flux distribution in the structure creating a NIM.^[340] This type of structure was experimentally obtained by etching one phase of a double-gyroid BCP followed by inversion via electrodeposition of gold (Figure 20d). This successful demonstration of a 30 nm gyroid-structured gold network exhibited very promising characteristics with a relatively high optical transmission of 20% for a 300 nm thick structure, indicating efficient energy transport by plasmonic resonances.^[341]

One of the many advantages of polymers is their ability to accommodate additives such as gain-media. For example, a dye dispersed in an epoxy matrix can help overcome the inherent losses in the metallic components by providing additional photons. An extremely low-loss and active optical NIM was thus demonstrated using Rhodamine 800 in the visible wavelength range between 722 and 738 nm.^[350]

Parity-Time Symmetric Materials: Most photonic structures made of dielectrics are based on spatial modulation of a real part of a complex refractive index, $N(x) = n_R(x) + i n_I(x)$, with the choice of material made to maximize the periodic variation in the real part of the index while minimizing the imaginary part $n_I(x)$ over the wavelength regime of interest to afford negligibly small loss. A new idea is to create a periodic imaginary index

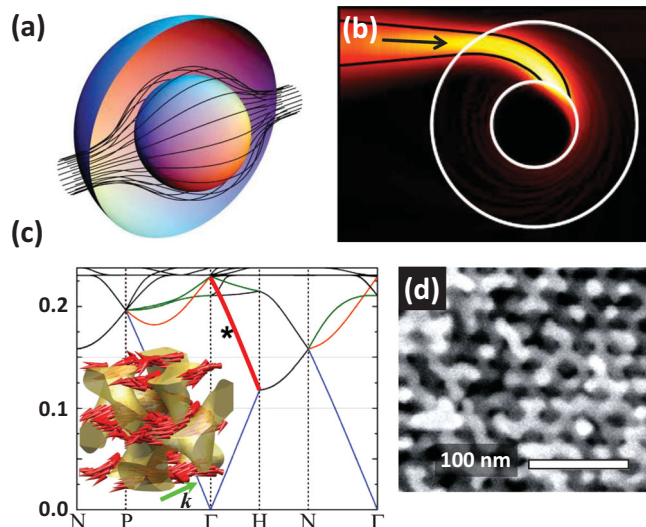


Figure 20. (a) Ray trajectory of light entering the spherical transformation space is guided smoothly around any object within the inner spherical region. Reproduced with permission.^[336] Copyright 2006, American Association for the Advancement of Science. (b) Calculated photon trapping by a photon black hole created by designing a spatial varying silicon-silica composite. Reproduced with permission.^[339] Copyright 2009, American Institute of Physics. (c) The photonic band diagram of a metallic double gyroid structure enabling negative refraction of light. The local energy flux vectors (the inset) of the negative refraction mode (thick red line in the band diagram) is in the opposite direction to the wavevector. Reproduced with permission.^[340] (d) SEM image of BCP derived gold gyroid network with $a = 35$ nm and filling fraction of 30%. Reproduced with permission.^[341]

profile, $n_l(x)$, with alternating loss and gain regions. These artificially structured materials are termed “*PT*-symmetric materials,” due to parity (*P*) and time (*T*)-reversal symmetry and have been theoretically and experimentally studied and various novel optical phenomena revealed. In contrast to a conventional PhC incorporating a gain medium, the modulation amplitude of $n_R(x)$ is required to be comparable to that of $n_l(x)$ for the *PT*-symmetric materials. Since the magnitude of optical gain is the practically most limiting factor, the modulation space for *PT*-symmetric materials occupies a relatively small region in the index modulation diagram, while plasmonic and metadielectric metamaterials occupy the widest region in the n_R vs. n_l modulation space (Figure 21a).

The idea of *PT*-symmetric optical system is an analogue of a *PT*-symmetric system in quantum mechanics. In the Schrödinger equation (Equation 1, the Hamiltonian $p^2/2m + V(x)$ is generally a Hermitian operator, which ensures real eigenvalues (or observable energies) and probability conservation because the potential $V(x)$ is real,

$$i\hbar \frac{\partial \Psi(x, t)}{\partial t} = \left[-\frac{\hbar^2}{2m} \frac{\partial^2}{\partial x^2} + V(x) \right] \Psi(x, t) \quad (1)$$

where p and m are momentum operator and mass. Interestingly, a class of non-Hermitian Hamiltonians having a

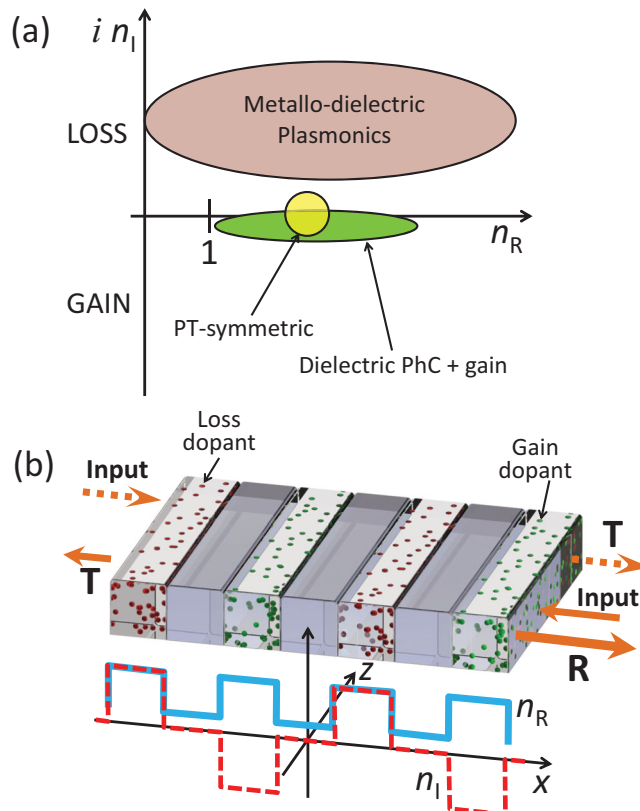


Figure 21. (a) Diagram of the modulation space of real index vs. imaginary index for various photonic systems. (b) Schematic of a 1D periodic material having *PT*-symmetry requiring even and odd functions of n_R and n_l , respectively. The non-reciprocal behavior of the *PT*-symmetric system for the two different input beams (solid and dashed arrows) is illustrated.

complex potential can still have real eigenvalues if the potential obeys *PT*-symmetry.^[351] This requires the complex potential, $V(x) = V_R(x) + iV_l(x) = V^*(-x)$, where space and time reversal operators, *P* and *T* are defined as $x \rightarrow -x$ and $t \rightarrow -t$. By this requirement, the real part of the complex potential $V_R(x)$ needs to be an even function of position x and the imaginary part $V_l(x)$ has to be an odd function. When the amplitude of $V_l(x)$ exceeds a certain threshold, the real values of the non-Hermitian Hamiltonian become complex. A similar transition also exists in the *PT*-symmetric optical system and results in the disappearance of the stable propagation mode (without decay or divergence of the light intensity), therefore the optical feedback between gain and loss medium must be carefully balanced.^[352]

PT-symmetry can be created in an optical system because some optical processes are formally identical to the Schrödinger equation (Equation 1). For example, in the paraxial equation of diffraction,^[353] the complex refractive index, $N(x) = n_R(x) + i n_l(x)$ corresponds to the complex potential, $V(x)$, so the real part $n_R(x)$ needs to be an even function of position x and the imaginary part $n_l(x)$ has to be an odd function. The schematic in Figure 21b shows two dielectric media having different refractive index $n_R(x)$ periodically arranged with gain and loss molecules alternatively doped to the low (or high) refractive index medium to additionally modulate the imaginary refractive index $n_l(x)$ to be an odd function. Optical systems satisfying such *PT*-symmetric conditions with balanced modulation in both n_R and n_l have demonstrated unique and intriguing optical characteristics such as unidirectional invisibility.^[354,355] For example, the antisymmetric gain/loss grating in Figure 21b exhibits negligible reflection of light entering from the left (100% transmission) rendering it invisible, whereas for light incoming from the right side, which encounters gain medium first, strongly enhanced reflection is observed with the reflected optical power exceeding unity due to the stimulated emission from the optically-excited gain medium. Thus, in contrast to PhCs where many applications require high dielectric contrast, rendering it difficult/impossible for polymers to provide the required optical properties, for *PT*-symmetric materials on the other hand, polymers have a good advantage since it is easily possible to provide the requisite gain/loss modulation amplitudes that will enable further novel optical functionalities. For this reason, while not yet demonstrated in a polymeric system, we believe *PT*-symmetric materials to be an exciting future frontier for the application of optically active periodic polymers. *PT*-symmetry ideas may also be extended to other areas such as plasmonics and metamaterials to provide future routes to overcome the loss issue discussed earlier.

4. Polymer-Based Phononic Structures

Phonons are quasi-particles representing quantized mechanical vibrations that propagate through solids, liquids, or gases. Phonons exist across a very wide range of technologically relevant frequencies, ranging from seismic waves for detection of underground oil deposits (sub Hz), to audible sound (Hz-kHz) to ultrasound (MHz) (e.g., medical sonograms) to very

high frequency thermal phonons (THz). It is hence not surprising that the ability to control and manipulate the flow of phonons has captured the interest of the scientific community. In recent years,^[5,8,32,116,356–382] it has been shown that the propagation of acoustic energy may be efficiently and even precisely controlled by novel sonic devices, bringing exciting and promising opportunities for sound management. Initially coined as PnCs, recent work aimed at manipulating acoustic propagation with structures having key components on the sub-wavelength scale has led to the development of acoustic metamaterials.

Phononic crystals typically have their properties attributed to the effects of Bragg-type scattering, hence the PnBG and bands exhibiting negative refractive behavior tend to lie at frequencies ($\omega a / 2\pi c_{\text{eff}} \sim 0.5$), where c_{eff} is a speed of sound for the effective medium corresponding to the particular PnC. Acoustic metamaterials commonly have their behavior attributed to artificial mechanical resonances present within the unit cell design with the corresponding negative index flat bands and bandgaps occurring in the sub-wavelength or low frequency ($\omega a / \pi c_{\text{eff}} < 0.1$ regime).

4.1. Phononic Crystals

Nelson^[360] first suggested considering a binary composite as an artificial acoustic material, made using two constituent building blocks. Given a particular periodic arrangement of these constituents, wave interference and/or resonant effects occur to give rise to strong coherent back-scattering, resulting in sound waves of certain frequencies not being allowed to propagate within the periodic structure (Figure 22a1) while waves with frequencies outside these gap regions are transmitted (Figure 22a2). As previously noted, this range of forbidden frequencies is thus called the PnBG. This property offers an efficient mechanism to manipulate the propagation of sound waves,^[357,361–367] such as to suppress various mechanical vibrations to sensitive equipment or to reduce transmitted noise. Additionally, a purposefully introduced defect placed into the periodic structure can lead to useful PnC devices such as sound waveguides, resonant acoustic cavities, or sonic filters just as in the case of designed-in defects in PhCs.

Analogous to the PhC, the midgap frequency of the fundamental (the lowest) PnBG is inversely proportional to the periodicity (Bragg scattering) or structural size (resonant scattering). Initially, theoretical and experimental PnCs were primarily studied at low frequencies ($f < 1 \text{ MHz}$) where the required periodicities ($a > 1 \text{ mm}$) can be easily obtained through manual

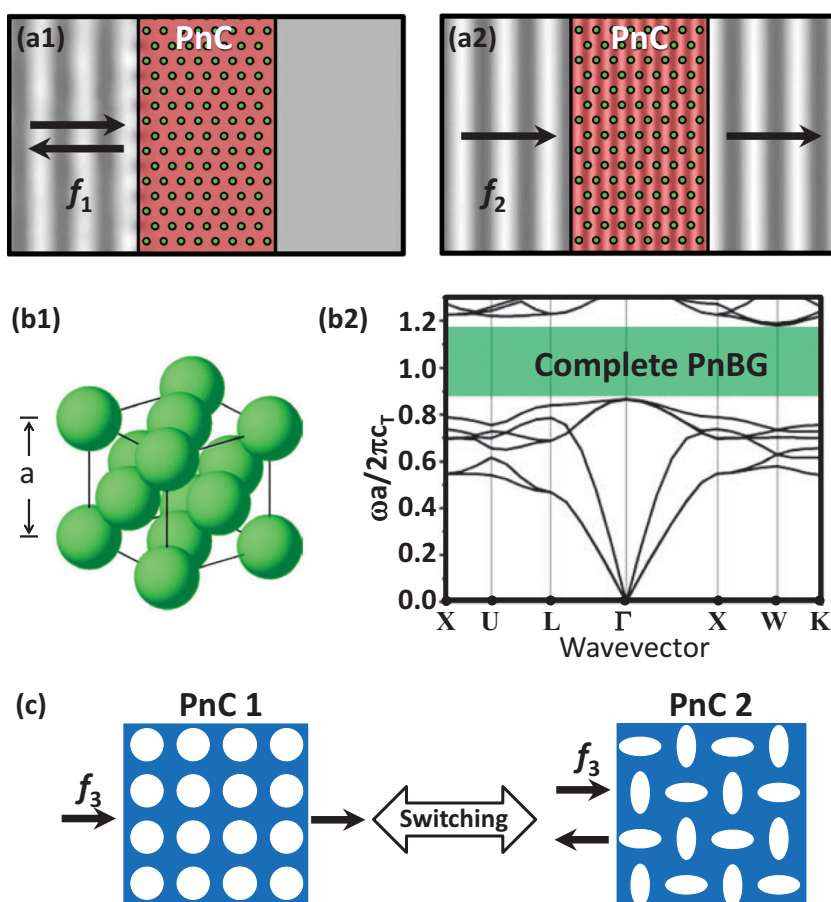


Figure 22. Behavior of PnBGs (a1) Transverse plane wave of a frequency (f_1) inside the PnBG propagates through a solid and is completely reflected by a solid/solid 2D PnC made of cylinders arranged in a triangular lattice embedded in a matrix. (a2) The sound wave of a frequency (f_2) outside the PnBG is transmitted through the PnC to the other side solid. Adapted from.^[370] (b1) An illustration of a 3D PnC consisting of lead spheres ($r = 0.25a$) arranged on a fcc lattice embedded in epoxy matrix. (b2) A phononic band diagram of the 3D PnC shows a large complete PnBG. Adapted with permission.^[1182] (c) A mechanically switchable phononic device. The PnBG shifts due to the dramatic change in symmetry.

fabrication of the structures.^[361–369] Thus, low-frequency PnC structures were mostly fabricated from metal or semiconductor material platforms. More recently, however, several different fabrication technologies have allowed for the significant reduction in the feature size of the structures, providing new means for an effective control of high frequency ($f > 1 \text{ MHz}$) phonons in small-form-factor PnCs.^[32,116,370–377] In particular, polymer-based PnCs with fine feature sizes have demonstrated successful control of very high frequency ($f \sim 1 \text{ GHz}$) hypersonic phonons.^[32,116,370,375–377]

Hypersonic phonons in periodic structures were first experimentally observed in a self-assembled lamellar phase PS-PI BCP with sub-200nm period.^[383] Despite the relatively low mechanical contrast between the two solvent swollen micro-phases, non-acoustic modes corresponding to the band-folding characteristic of periodic structures were observed utilizing Brillouin light scattering (BLS). Subsequently, hypersonic polymer-based 2D PnCs, made of an array of air holes in an epoxy background material, were fabricated via IL^[32,33] and a

directional PnBG utilizing BLS was experimentally observed. The 2D PnCs can of course be extended to 3D PnCs exhibiting complete 3D PnBGs. For example, a 3D PnC consisting of lead spheres in the fcc lattice in an epoxy matrix (Figure 22b1) demonstrates a large complete PnBG prohibiting the propagation of all elastic waves. Analogous to the 3D PhC band diagram (Figure 10d,e), the 3D phononic band diagram (Figure 22b2) clearly shows a complete 3D PnBG. A hypersonic version of spheres on a fcc lattice was made using PS nanospheres fabricated by colloidal self-assembly and provided the first experimental observation of a GHz hypersonic PnBG using BLS.^[116] More recently, experimental BLS observations of PnBGs were also reported in one-dimensional periodic (SiO₂/PMMA) multi-layer films at GHz frequencies.^[375,384]

In addition, one-dimensional all polymer (PS/PI)^[383] and (poly(vinyl pyrrolidone)/PS)^[377] PnCs have also been shown to modify the propagation of GHz phonons, as elastic modes injected through a picosecond laser pulse and detected via an optical probe beam show typical folded dispersion curves. These studies clearly demonstrate that polymer-based PnCs constitute an attractive material platform for the development of high-frequency sonic devices, given by the multitude of suitable fabrication techniques of polymers, such as self-assembly, spin-casting, IL, etc. (see Section 2), which can be utilized for creating a wide range of 1D, 2D, and 3D periodic sub-micrometer structures. Polymer-based systems may also further enhance the richness of possible acoustic propagation behavior, by virtue of their inherently time-dependent dynamical behavior, such as their viscoelasticity corresponding to very strong temperature and strain-rate sensitivity of their mechanical properties. Polymeric acoustic metamaterials thus have properties dependent on both the geometric structure and the material constitutive relations; the latter impacts the time-scale of their response, the non-linearity of the response in terms of amplitude dependence, etc. Propagating modes in phononic structures offer interesting opportunities to probe the dynamics of confined polymeric systems^[375,376] through the generation and study of interface and spatially confined modes. Importantly, this interplay between the time-scale response (hence frequency dependence) of the constituent materials and the structural design has led to structures that demonstrate unique switching behavior^[34,385–390] (see Figure 22c) driven by strain induced phase-transition^[35] suggesting further development of active devices for controlling acoustic energy flow at the nanoscale.^[385]

To explore how the detailed structure can influence the band diagram, we now revisit the 2D square lattice with circular features having *p4mm* plane symmetry (see Figure 3a1) and vary the structure of the inclusions. In the case of hard-cylinders embedded in a softer polymer matrix (Figure 23a1), we obtain the dispersion relation (Figure 23a2), with a PnBG at about $\omega a / 2\pi c_T \sim 0.6$. In this design, the cylinder lattice structure serves as a Bragg scatterer that gives rise to the fundamental PnBG in a phononic crystal. The displacement eigenmodes along Γ -X at the X point (BZ boundary) (A and B in Figure 23a2), show the characteristic field localization in the scatterer and the matrix respectively. Now to enable an acoustic metamaterial, we add an additional layer, softer than the polymer matrix around the hard cylinder (Figure 23b1). This layer allows the hard cylinder to become a mechanical resonator within each unit cell with

the softest material acting as a weak coupling layer between the internal cylinder and the outer matrix. This is the crucial design component that gives the additional degree of freedom required for a mechanical resonance. We see that the corresponding dispersion relation becomes significantly different (Figure 23b2) – a distinctive feature being the flat low-frequency band located at $\omega a / 2\pi c_T \sim 0.15$ above which the PnBG now appears. The displacement fields of the eigenmode C (Figure 23b2), show a more distinctive localized nature characteristic of resonant type behavior. Mode D (Figure 23b2), exhibits displacement fields that propagate throughout the entire polymer matrix, with no indication of scattering.

These two simple examples serve to point out the rich behavior afforded using polymeric materials. Moreover, given the large range of constitutive mechanical behavior available for polymer rubbers, glasses, and semicrystalline materials, a wealth of possibilities exist for controlling the propagation of elastic waves in macro-, micro-, and nanostructured polymers.

4.2. Broadband Super Absorption

There have been numerous attempts to develop compact, deep sub-wavelength acoustic metamaterials for the efficient absorption of low frequency sound and vibrations. As the wavelength of audible sound, for example, is in the order of meters, conventional Bragg based PnCs having a periodicity similar to the wavelength are highly impractical. Hence, sub-wavelength devices need to be designed in order to realize absorbers with practical form factors for low frequency acoustic waves. Central to this research is the desire to surpass the so-called “mass density law”,^[357] which is a scaling law based on an effective medium approach of estimating the transmission attenuation of an effectively “homogeneous” material. The transmission may be estimated by $T \sim 1/\omega h$, ω being the frequency of the acoustic wave or vibration, and h the thickness of the material. As this gives rise to the limitation of the absorption efficiency of a conventional material, attempts to surpass this mass density limit have focused on acoustic metamaterials. This development was sparked by the conceptualization of the locally resonant sonic crystal,^[357] and the experimental demonstration of a ~ 20 dB improvement in transmission attenuation beyond the mass density law by realization of a 3D construct similar to the 2D structure shown in Figure 23b1. The underlying mechanism is the introduction of an artificial resonance that is matched to the targeted incident acoustic frequencies. This mechanical resonance arises by using a dense, stiff metallic sphere surrounded by a “soft” polymer layer within a stiffer epoxy-based matrix (Figure 24a). By tailoring the impedance contrast, one is able to design and tune the resonant frequency to control the transmission attenuation (Figure 24b). It is readily apparent that the wide range of polymeric material platforms with widely different mechanical impedances will enable the facile design of simple mechanical resonators and a locally-resonant acoustic metamaterial with super absorption.

A simple variation of the resonant sphere concept was demonstrated in an all polymeric-metascreen based on the classic acoustic “bubbly” resonance,^[393] known as the Minneart resonance.^[392–394] The resonant frequency of a gas “bubble” in a

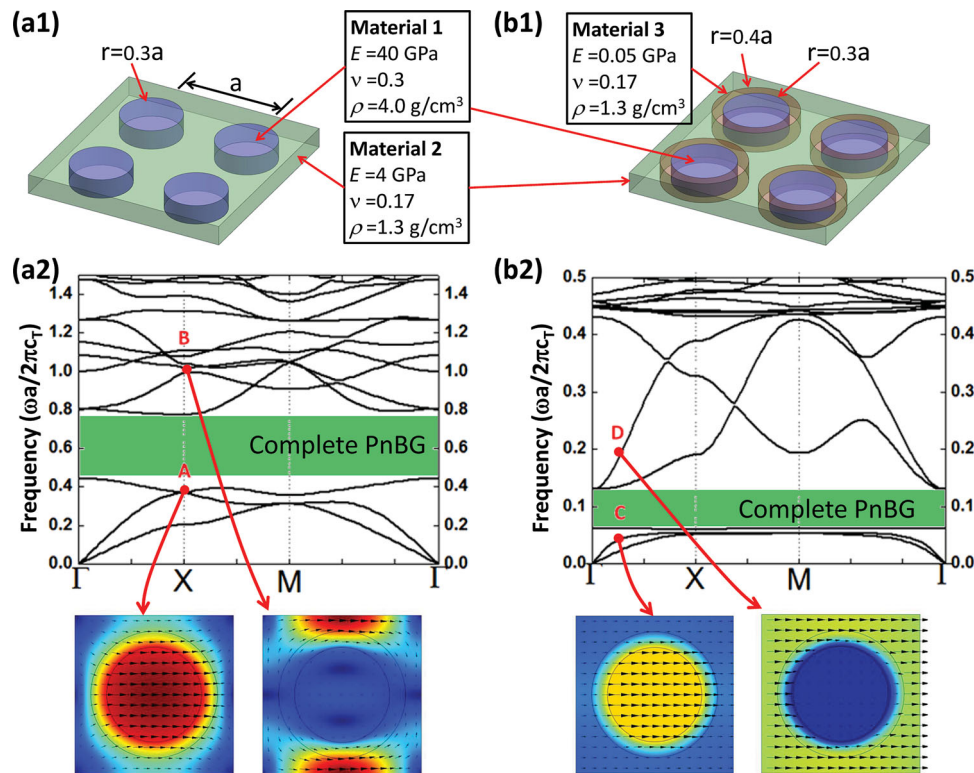


Figure 23. (a1) Two-component PnC comprised of a square lattice of hard cylinders embedded in a softer polymer matrix and (a2) its phononic band structure with displacement fields corresponding to the two eigenmodes, A and B. A PnBG ($\Delta\omega/\omega = 0.53$) is created from Bragg scattering of the impedance contrast Z_1/Z_2 of 6. (b1) Three-component PnC having an additional concentric very soft layer that serves to weakly couple the cylinders and the matrix and (b2) its band structure with displacement fields corresponding to the eigenmodes, C and D. A low frequency resonant PnBG ($\Delta\omega/\omega = 0.7$) is created by using a soft shell (Z_3) with impedance contrasts of Z_1/Z_3 of 50 and Z_2/Z_3 of 9. Adapted from.^[391] The color map for each mode indicates zero (blue) to a maximum displacement amplitude (red) with local directions and magnitudes of the displacements given by the arrows.

fluid medium is interestingly low, given by $\omega = \sqrt{3\beta_{\text{gas}}/\rho}/R$, where β_{gas} is the longitudinal modulus of the gas, ρ the mass density of the liquid, and R the radius of the bubble. In this work, by utilizing spherical air-void cavities as resonance elements within a soft PDMS matrix (Figure 24c), Leroy et al.^[392] were able to obtain very efficient vibration isolation in the ultrasonic regime (0.7 MHz) for waves incident from air onto a bubble meta-screen with only four-layers. This isolation may be further controlled by tuning the crosslink density and thereby the visco-elastic properties of the PDMS matrix. In this way the required impedance matching between the surrounding medium and the polymer matrix and the scattering cross section for the “bubbly” resonance may be optimized, so as to achieve very efficient absorption of incident acoustic waves (Figure 24d).

While the notion of impedance contrast is quite well-known from transmission line concepts,^[395] the details of the impedance (mis-) matching depend strongly on the interaction at the interface between the ambient medium and the designed metamaterial. This fact was exploited in developing ultra-thin low frequency (~200 Hz) absorbers consisting of “floppy” polymeric membranes.^[356] In this work, thin (~200 μm thick) rubber membranes ($E = 1.9 \text{ MPa}$, $\nu = 0.48$) were loaded with asymmetric iron platelets and designed to be resonant at ~200 Hz. The choice of a thin membrane provides good impedance matching to the incident acoustic wave; the presence of

the rigid iron platelets in the flexible membrane presents an efficient absorption or dissipative mechanism *vis-a-vis* the “flapping” of the membrane and the subsequent localization of strains at the interfaces between the rigid platelets and the flexible membrane. This gives rise to a dark, or non-radiative mode at the frequency range of interest. The absorber is deeply sub-wavelength (thickness $< \lambda/1,000$) and highly tunable through varying the mechanical properties of the polymer membrane and the additive rigid platelet geometries.

4.3. Tunable Phononic Structures and Tunable Materials

As mentioned, one advantage in utilizing polymeric platforms for PnCs is in their dynamic tunability. Given that polymeric materials can provide sufficient impedance contrast (see Table 1) to serve as the matrix material for solid-air based PnC architectures, the ability to utilize the interplay between the mechanical symmetry of the patterned polymeric nanostructure, which determines its phononic properties, and the boundary constraints to alter the phononic properties of the polymeric structure,^[35,386,387,390,395,396] affords unique opportunities for dynamic geometry phononic systems, such as for switching applications. For example, stresses caused by swelling of a patterned polymer constrained to a rigid substrate were able to

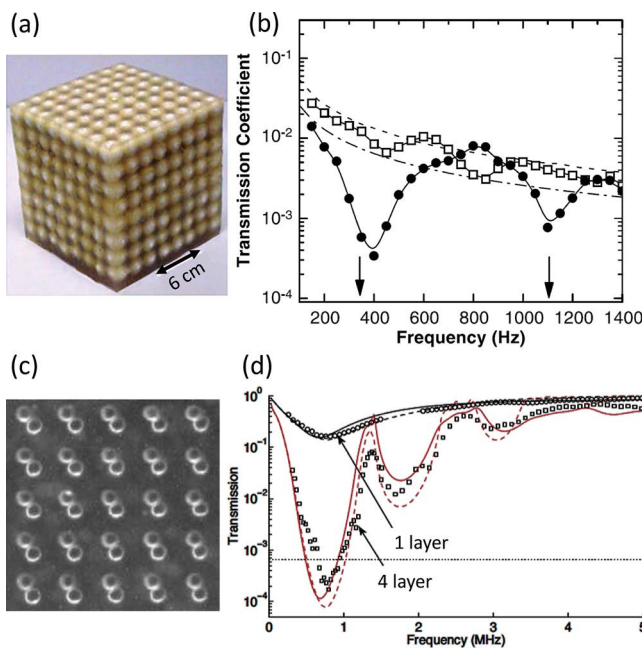


Figure 24. Polymer based acoustic “super absorbers” and reflectors. (a) Locally resonant 3D PnC comprised of rubber-coated lead spheres on a simple cubic lattice in an epoxy matrix and (b) its measured transmission spectra with (solid circles) and without (open square) resonators. Reproduced with permission.^[357] Copyright 2000, American Association for the Advancement of Science. (c) Bubble meta-screen made of air voids ($R = 39 \mu\text{m}$) in a PDMS matrix and (d) transmission spectra of a one-layer (circles) and four-layer crystals (squares) with lines of theoretical predictions. Reproduced with permission.^[392] Copyright 2009, American Institute of Physics.

induce an elastic instability in a PnC (Figure 25a).^[35] This recoverable instability actuated a discrete change in the polymer PnC, from the original *p6mm* hexagonal symmetry of the cylinders (Figure 25a left) to a herring-bone type pattern with elliptical inclusions, a *p2gg* plane symmetry (Figure 25a right). This led to the opening of a high-frequency PnBG, by virtue of this discrete symmetry breaking associated with the displacement

fields (Figure 25a bottom). The ability for tuning the boundary conditions as well as the utilization of solvent fields, pH, mechanical forces, or other stimuli to induce an elastic instability offer many possibilities of tunable phonon engineering and acoustic steering. This instability-driven switching of PnCs was further developed by Bertoldi and co-workers (recall Figure 22c) to achieve negative Poisson’s ratio behavior initiated by instability in silicone-based elastomeric cellular foams.^[390] Other approaches of tuning the phononic behavior include the utilization of magnetic as well as electro-rheological elements in an otherwise connected polymeric matrix to tune the PnBGs utilizing the respective magnetic and electric fields to alter the mechanical impedance of the elements.^[388,389] In addition, piezoelectric response has been demonstrated as an effective way to tune the acoustic band structure by opening and manipulating bands at electronically driven resonances.^[397,398]

The concept of utilizing external fields to trigger a change in the phononic behavior was also applied to a 3D PDMS micro-truss.^[34] The PDMS micro-frame having an *R3m*-like symmetry was fabricated by IL and subsequently strained by up to 30% in a uniaxial fashion along the [10̄10] direction (Figure 25b). BLS measurements were done to track the evolution of the phononic behavior, which showed a clear monotonic change in the propagation modes as a function of the applied strain (Figure 25b). By further tuning of the mechanical properties of the PDMS PnC, the strain-dependence of the propagation velocity can be tuned as needed.^[34]

Solid-fluid PnCs offer yet another route of dynamic tunability by tuning the material properties. In particular, Fytas and co-workers have demonstrated utilizing self-assembled microspheres^[116] as well as AAO nano-templates,^[385,398,399] that one can tune the PnBG and propagation behavior through a change of the characteristics of the solvent/fluid. Changing the colloid dimensions and the fluid type affected both frequency shifts and PnBG sizes. Thus, one may utilize an ambient solvent environment to tune the phononic properties of the PnC. A variant of this was demonstrated by tuning the viscosity of the polymer fluid as the disconnected cylinder phase in AAO-based nanotemplates^[385] to create hybridized PnBGs in the

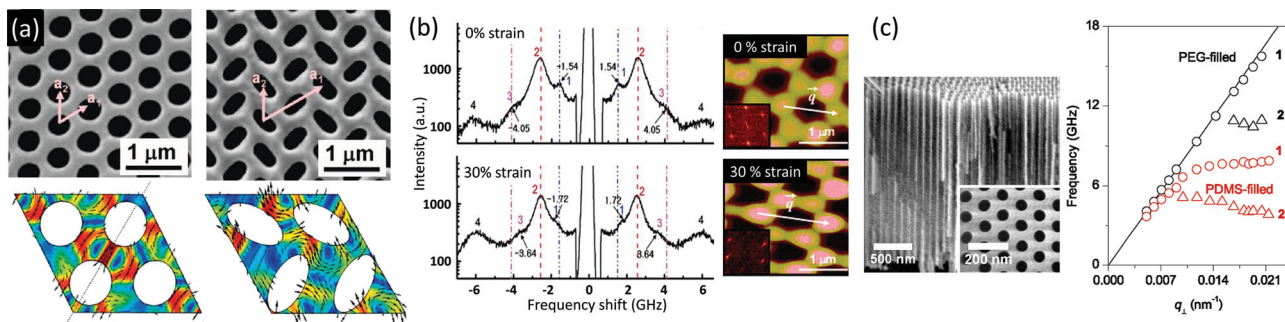


Figure 25. Tunable PnCs with polymer-based systems. (a) SEM images show the instability induced pattern transformation in hexagonal SU8 based photo-patterned polymer with displacement fields for the modes near the tunable PnBG. Reproduced with permission.^[35] Copyright 2009, American Chemical Society. (b) BLS spectra of PDMS microframe undergoing large strains (30%) along the [10̄10] direction, showing clear shifts in the peaks of modes 1 and 3, indicating a change in the propagation modes. The corresponding AFM images and Fourier transformed images (insets) indicate the breaking of the hexagonal symmetry due to the stretching. Reproduced with permission.^[34] Copyright 2006, American Chemical Society. (c) Tilted SEM image of AAO template without polymers (inset: top view). Experimental in-plane phononic dispersion relations of polyethylene glycol (PEG)-filled AAO (black symbols) and PDMS-filled AAO (red symbols) for the longitudinal acoustic branch 1 (open circles) and the weak flat branch 2 (open triangles). Reproduced with permission.^[385] Copyright 2010, American Chemical Society.

dispersion relation (Figure 25c), while leaving the rest of the low frequency behavior unaffected, since these modes are dominated by the solid AAO template.

4.4. Phononic Metamaterials

As mentioned in section 3.6, metamaterial concepts can be applied to both electromagnetic and elastic waves, the heart of the concept is the artificial building block, or “meta-atom”, resonant at frequencies much lower than those accessible from natural materials and strongly influencing the dispersion relation at low frequencies. Acoustic metamaterials can manipulate and control acoustic energy in surprising and non-intuitive ways. Some of these already mentioned include low frequency sound absorbers consisting of “floppy” membranes,^[356] as well as locally resonant elastic materials^[357] that greatly surpass the conventional mass density limit, realizing deep subwavelength (hence thin) yet very efficient absorbers of low frequency sound. Instead of using an elastic solids as resonating entities, the concept of an acoustic Helmholtz resonator utilizing the elasticity of a compressive fluid, typically enclosed in a rigid cavity with a small opening port,^[395] has also been employed in an underwater environment for negative refraction of acoustic waves^[8] and fabrication of broadband acoustic cloaks.^[5] Moreover, 2D composite structures made of

solid/liquid^[380] or solid/solid phases^[381] can also demonstrate acoustic cloaking.

As was the case for electromagnetic waves in optical metamaterials, cloaks can be designed for sound waves in mechanical metamaterials. Such “acoustic cloaks” can render arbitrary objects essentially invisible to sound waves by guiding the incoming sound wave around the object to be concealed (Figure 26a). This is done by extending the concept of electromagnetic cloaking through the electromagnetic conformal transformations^[336,400,401] to sound waves using the acoustic scalar wave equation instead of Maxwell's equations. By following the coordinate transformation approach, 2D and 3D theoretical acoustic cloaking shells were designed to hide objects from sound waves in fluids.^[3,4,378,379,402] The shells surrounding the objects were designed to have anisotropic and inhomogeneous effective elastic properties. Due to the difficulty associated with obtaining fluid based metamaterial shells, cloaking effects were subsequently obtained using solid/fluid metamaterial shells,^[5,380] which are experimentally easily accessible. One prominent example was an underwater acoustic cloak made of an aluminum plate having an array of cavities and channels designed and fabricated to operate for ultrasound (40–80 kHz) waves in water.^[5]

An important point is that, contrary to electromagnetic/optical cloaks, acoustic cloaks can inherently be made broadband by virtue of the range and tunability of the constitutive

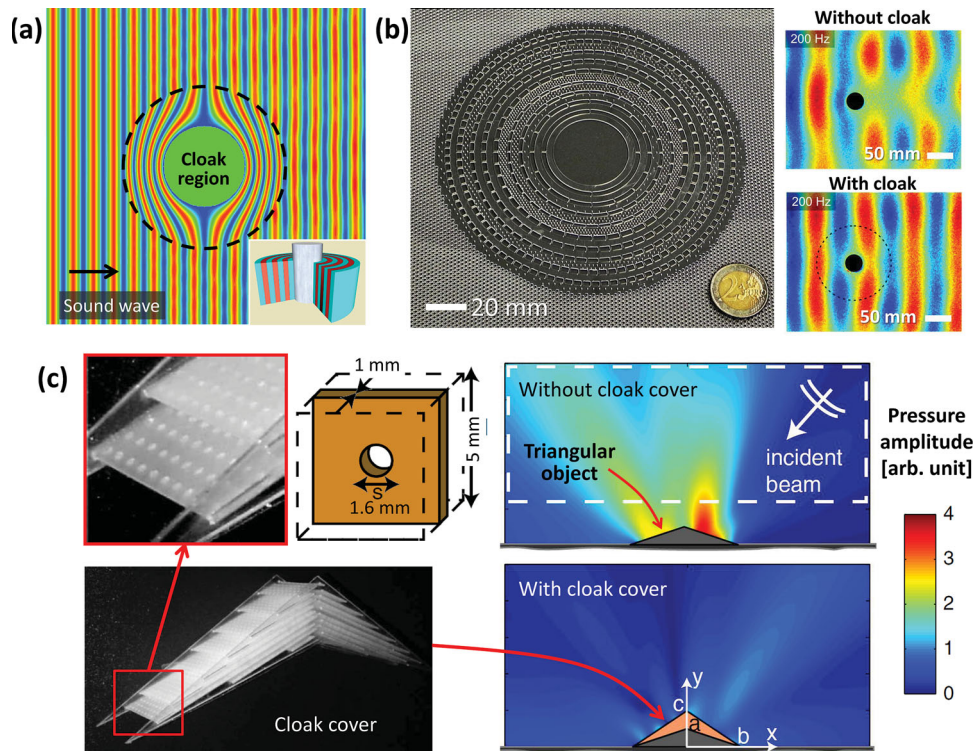


Figure 26. (a) Calculated pressure map for a planar longitudinal wave incident on a rigid cylindrical scatterer surrounded by a multilayered acoustic shell made up of 200 layers (see inset). Reproduced with permission.^[378] Copyright 2008, IOP Publishing Ltd. (b) Oblique-view photograph of a cloaking device made of PVC before filling with PDMS and experimentally measured displacement fields passing by a solid disk with and without the cloak device at 200 Hz. Reproduced with permission.^[381] Copyright 2012, American Physical Society. (c) Photographs of a ground cloaking cover consisting of perforated plates are shown with the unit cell and simulated acoustic signatures of a triangular object with and without the cloaking cover. Reproduced with permission.^[382] Copyright 2011, American Physical Society.

material parameters of the materials available. In the above case of the underwater acoustic cloak, the broadband response was enabled by the fact that the phase velocities of the propagating fluid modes could be manipulated by the cavities and channels fashioned out of the aluminum plate. However, it is also possible to fabricate this cloak out of a stiff polymer platform, as provided the impedance contrast in the scalar acoustic field (see Table 1) of glassy polymers and air or even water is large enough ($Z_{\text{polymer}}/Z_{\text{water}} \sim 2$). In this case, the key concept lies in tuning the effective phases of the acoustic waves as they propagate through the structured medium, which can be met with a very wide range of material choices making polymers attractive *vis-a-vis* their low density, easy fabrication, good environmental resistance, and sufficient mechanical impedance.

As mentioned earlier, the coordinate transformation methods work for scalar acoustic waves analogously to electromagnetic waves. However, it is not generally possible to design an exact cloak for bulk elastic waves due to the tensorial mechanical properties of solids. But, the situation is better for plate waves.^[4,402] Plate waves are also known as Lamb waves and propagate in materials having a thicknesses of a few wavelengths, leading to confined propagation of the out-of-plane mode. The displacement field has components along the normal to the plate and along the direction of propagation. Recently, the design, fabrication, and characterization of a thin polymer metamaterial elastic cloak for plate waves was demonstrated at acoustic frequencies (Figure 26b).^[381] The plate itself consists of 20 homogeneous and locally isotropic concentric rings made of glassy poly(vinyl chloride) (PVC) and rubbery PDMS – materials that possess a three order of magnitude difference between their Young's modulus ($E_{\text{PVC}} = 2.4 \text{ GPa}$, $E_{\text{PDMS}} = 2.0 \text{ MPa}$), providing sufficient mechanical impedance contrast for broad band cloaking operation. The metamaterial cloak was fabricated by drilling slots in a 1 mm thick PVC plate and the slots were then subsequently filled with PDMS. Elastic plane waves ($f \sim 200\text{--}400 \text{ Hz}$) were directed toward the polymer plate and the displacement fields from interactions among the incoming elastic wave, the polymer plate, and the object (26 mm diameter) were experimentally measured (Figure 26b). As evident for frequencies $f \sim 200 \text{ Hz}$, the shell directs the elastic waves around the object with negligible reflections, rendering the object nearly invisible.

Acoustic metamaterial theory and concepts have also been recently applied to develop a new class of acoustic cloaking devices known as “carpet cloaks” or “ground cloaks” to hide objects located on reflecting surfaces,^[353,403,404] an extension of the idea of electromagnetic ground cloaks to acoustic waves.^[382] The basic principle behind a ground cloak is that the cloak redirects incoming acoustic waves such that reflections from the flat surface by itself and the surface with the cloaked object are basically the same.

One of the first acoustic ground cloaks was built to hide objects from audible waves (frequencies $f \sim 2\text{--}4 \text{ kHz}$ in air) and was fabricated using an acrylic polymer.^[382] A triangular object (to be concealed) is placed on a ground plane and the object is then covered with a triangular shaped metamaterial whose effective material properties are derived by the coordinate transformation acoustic theory. The particular metamaterial system is made of regularly perforated planar plastic plates (Figure 26c).

The size and shape of the perforations in the plastic sheets, as well as the specific separation between the sheets, result in the required mechanical response of the structure to the incoming sound waves. Simulated scattering field patterns for the object by itself and the object covered with the metamaterial cloak are shown in Figure 26c. Theoretical and experimental results show that acoustic scattering from the object is significantly reduced by the presence of the cloaking device, providing a novel mechanism to hide objects on flat surfaces from sound waves in air.

These recent demonstrations of metamaterials and cloaking devices offer enormous opportunities to manage acoustic waves in ways inconceivable with common natural materials. Potential applications include making ships invisible to sonar, improved designs of concert halls, and soundproof rooms.

5. Outlook and Summary

This review focused on ordered photonic and phononic structures made primarily from polymers. We presented the basic ideas of band structures, design principles, selected fabrication techniques, research trends as well as promising material systems for experimentally accessing the many emerging ideas in these rapidly growing fields. The further elaboration of polymeric materials for PhC/PnC will enable progress in engineering of photons and phonons in both fundamental and applied aspects by virtue of a number of advantages of polymers including their wide range of mechanical properties, ease of functionalization, ability to host optical and mechanical additives and to be relatively inexpensively fabricated into nano- and micro-structure materials. In particular, polymeric based PhC/PnC structures are dynamically reconfigurable, both as switchable geometrical structures and as continuously tunable materials that can respond to a very wide range of physical and chemical stimuli.

The field of PhC research remains vibrant and is growing in new application areas for sensors and renewable energy. Entirely new photonic concepts are being explored in the area of optical metamaterials, including *PT*-symmetric materials. 3D PhC fabricated by colloidal self-assembly and 1D PhCs fabricated by BCP self-assembly lead in many sensor and display applications. In addition to self-assembly approaches, the introduction of non-conventional top-down techniques including IL, soft imprinting, and DW, and hybrid techniques overcome the tendency for inadvertent defect formation during self-assembly as well as the ability to precisely design a particular geometry and composition. The prominent characteristic of many of the PhCs fabricated to date focuses on structural color, yet there is much scope for the systematic and quantitative investigation of chemical and physical phenomena behind the dynamic responses of polymer based PhCs. With such efforts, PhC research will attract more attention from the industrial sector. The trend for engineering-oriented research to become more of a major player in PhC research is evident (Figure 2a). Indeed, research efforts on the engineering aspects of PhCs such as production yield, fabrication time, response time, and packaging, need more attention. This shift towards engineering can be a great opportunity to sustain and to further expand PhC research by encouraging the exchange

of knowledge between the traditional physical/optical and engineering communities.

PnCs are a more recent field of research and show strong growth similar to that of PhC research in the early 1990s. Polymers are more competitive for PnC applications due to their sufficiently high mechanical impedance to be able to open a complete phononic bandgap, compared to their relatively low refractive indices that leads to only partial optical bandgaps. In the current early stage of PnC research (Figure 2c), many developments for PnCs are following a similar track as for PhC; however, there are evidently exclusive aspects of PnC such as the more complex tensorial nature of elastic constants and the fundamental locality of phonons. With respect to fabrication, in contrast to the enormous efforts in the scale-down of PhC to achieve a complete PBG in the visible and telecommunication regimes, current fabrication techniques can readily create PnCs for nearly all regimes of elastic waves. Although PnCs for the audible regime will be mainly fabricated at the deep sub-wavelength scale in order to have a practical form factor, the volume of many PnCs (order of cm³), will be significantly larger than those of PhCs, so that polymers will likely be a major constituent material due to their lightweight and low cost. For frequencies below 1000 Hz, we envision that polymers would be particularly valuable since it is possible to modify their mechanical properties to engineer propagating acoustic waves in real time by use of the piezoelectric effect and an external driving signal. Therefore, we foresee that future PnCs especially for the audible frequencies will be device-like rather than material-like.

Acknowledgements

This article is part of an ongoing series celebrating the 25th anniversary of *Advanced Materials*. This work was supported by AOARD grants 114095 and 114078 by DTRA under contract 1–12–1–0008 and by the US Army Research Office through the Institute of Soldier Nanotechnology at MIT, under contract DAAD-19-02-D-0002.

Received: July 25, 2013
Published online:

- [1] E. Yablonovitch, *Phys. Rev. Lett.* **1987**, *58*, 2059.
- [2] S. John, *Phys. Rev. Lett.* **1987**, *58*, 2486.
- [3] H. Y. Chen, C. T. Chan, *Appl. Phys. Lett.* **2007**, *91*, 183518.
- [4] S. A. Cummer, B. I. Popa, D. Schurig, D. R. Smith, J. Pendry, M. Rahm, A. Starr, *Phys. Rev. Lett.* **2008**, *100*, 024301.
- [5] S. Zhang, C. G. Xia, N. Fang, *Phys. Rev. Lett.* **2011**, *106*, 024301.
- [6] X. D. Zhang, Z. Y. Liu, *Appl. Phys. Lett.* **2004**, *85*, 341.
- [7] M. H. Lu, C. Zhang, L. Feng, J. Zhao, Y. F. Chen, Y. W. Mao, J. Zi, Y. Y. Zhu, S. N. Zhu, N. B. Ming, *Nat. Mater.* **2007**, *6*, 744.
- [8] S. Zhang, L. L. Yin, N. Fang, *Phys. Rev. Lett.* **2009**, *102*, 194301.
- [9] N. Fang, D. J. Xi, J. Y. Xu, M. Ambati, W. Srituravanich, C. Sun, X. Zhang, *Nat. Mater.* **2006**, *5*, 452.
- [10] M. Maldoval, E. L. Thomas, *Appl. Phys. Lett.* **2006**, *88*, 251907.
- [11] W. Groh, A. Zimmermann, *Macromolecules* **1991**, *24*, 6660.
- [12] C. L. Lu, B. Yang, *J. Mater. Chem.* **2009**, *19*, 2884.
- [13] X. Li, J. P. Gao, L. J. Xue, Y. C. Han, *Adv. Funct. Mater.* **2010**, *20*, 259.
- [14] M. L. Williams, R. F. Landel, J. D. Ferry, *J. Am. Chem. Soc.* **1955**, *77*, 3701.
- [15] C. M. Roland, *Viscoelastic Behavior of Rubbery Materials*, Oxford University Press, New York **2011**.
- [16] C. Sun, N. Fang, D. M. Wu, X. Zhang, *Sens. Actuators, A* **2005**, *121*, 113.
- [17] W. N. Man, M. Megens, P. J. Steinhardt, P. M. Chaikin, *Nature* **2005**, *436*, 993.
- [18] L. F. Johnson, G. W. Kammlott, K. A. Ingersoll, *Appl. Opt.* **1978**, *17*, 1165.
- [19] M. Campbell, D. N. Sharp, M. T. Harrison, R. G. Denning, A. J. Turberfield, *Nature* **2000**, *404*, 53.
- [20] D. Mei, B. Cheng, W. Hu, Z. Li, D. Zhang, *Opt. Lett.* **1995**, *20*, 429.
- [21] X. Di, P. C. Kevin, H. Ahmad, L. Yuankun, *CLEO 2010*, CFF3.
- [22] T. Kondo, S. Matsuo, S. Juodkazis, H. Misawa, *Appl. Phys. Lett.* **2001**, *79*, 725.
- [23] D. Shir, H. W. Liao, S. Jeon, D. Xiao, H. T. Johnson, G. R. Bogart, K. H. A. Bogart, J. A. Rogers, *Nano Lett.* **2008**, *8*, 2236.
- [24] S. Yang, M. Megens, J. Aizenberg, P. Wiltzius, P. M. Chaikin, W. B. Russel, *Chem. Mater.* **2002**, *14*, 2831.
- [25] J. P. Singer, S. E. Kooi, E. L. Thomas, *Nanoscale* **2011**, *3*, 2730.
- [26] J. H. Jang, C. K. Ullal, M. Maldoval, T. Gorishnyy, S. Kooi, C. Y. Koh, E. L. Thomas, *Adv. Funct. Mater.* **2007**, *17*, 3027.
- [27] D. J. Shir, E. C. Nelson, D. Chanda, A. Brzezinski, P. V. Braun, J. A. Rogers, P. Wiltzius, *J. Vac. Sci. Technol. B* **2010**, *28*, 783.
- [28] J. Xu, R. Ma, X. Wang, W. Y. Tam, *Opt. Express* **2007**, *15*, 4287.
- [29] I. Bita, T. Choi, M. E. Walsh, H. I. Smith, E. L. Thomas, *Adv. Mater.* **2007**, *19*, 1403.
- [30] D. K. Cullen, Y. A. Xu, D. V. Reneer, K. D. Browne, J. W. Geddes, S. Yang, D. H. Smith, *Neuroimage* **2011**, *54*, S37.
- [31] D. K. Cullen, K. D. Browne, Y. A. Xu, S. Adeeb, J. A. Wolf, R. M. McCarron, S. Yang, M. Chavko, D. H. Smith, *J. Neurotrauma* **2011**, *28*, 2307.
- [32] T. Gorishnyy, C. K. Ullal, M. Maldoval, G. Fytas, E. L. Thomas, *Phys. Rev. Lett.* **2005**, *94*, 115501.
- [33] T. Gorishnyy, J. H. Jang, C. Koh, E. L. Thomas, *Appl. Phys. Lett.* **2007**, *91*, 121915.
- [34] J. H. Jang, C. K. Ullal, T. Gorishnyy, V. V. Tsukruk, E. L. Thomas, *Nano Lett.* **2006**, *6*, 740.
- [35] J. H. Jang, C. Y. Koh, K. Bertoldi, M. C. Boyce, E. L. Thomas, *Nano Lett.* **2009**, *9*, 2113.
- [36] L. Muller-Meskamp, Y. H. Kim, T. Roch, S. Hofmann, R. Scholz, S. Eckardt, K. Leo, A. F. Lasagni, *Adv. Mater.* **2012**, *24*, 906.
- [37] T. Bückmann, N. Stenger, M. Kadic, J. Kaschke, A. Fröhlich, T. Kennerknecht, C. Eberl, M. Thiel, M. Wegener, *Adv. Mater.* **2012**, *24*, 2710.
- [38] M. Kadic, T. Bückmann, N. Stenger, M. Thiel, M. Wegener, *Appl. Phys. Lett.* **2012**, *100*, 191901.
- [39] S. Maruo, K. Ikuta, *Appl. Phys. Lett.* **2000**, *76*, 2656.
- [40] J. Fischer, G. von Freymann, M. Wegener, *Adv. Mater.* **2010**, *22*, 3578.
- [41] M. Farsari, G. Filippidis, C. Fotakis, *Opt. Lett.* **2005**, *30*, 3180.
- [42] M. Deubel, G. von Freymann, M. Wegener, S. Pereira, K. Busch, C. M. Soukoulis, *Nat. Mater.* **2004**, *3*, 444.
- [43] M. Ma, K. Titievsky, E. L. Thomas, G. C. Rutledge, *Nano Lett.* **2009**, *9*, 1678.
- [44] C. N. LaFratta, J. T. Fourkas, T. Baldacchini, R. A. Farrer, *Angew. Chem. Int. Ed.* **2007**, *46*, 6238.
- [45] M. Thiel, J. Fischer, G. von Freymann, M. Wegener, *Appl. Phys. Lett.* **2010**, *97*, 221102.
- [46] K. K. Seet, S. Juodkazis, V. Jarutis, H. Misawa, *Appl. Phys. Lett.* **2006**, *89*, 024106.
- [47] M. Malinauskas, A. Zukauskas, G. Biekauskaitė, R. Gadonas, S. Juodkazis, *Opt. Express* **2010**, *18*, 10209.
- [48] T. F. Scott, B. A. Kowalski, A. C. Sullivan, C. N. Bowman, R. R. McLeod, *Science* **2009**, *324*, 913.

- [49] H. B. Sun, S. Kawata, in *NMR – 3D Analysis – Photopolymerization, Advances in Polymer Science, Vol. 170*, Springer-Verlag Berlin, Berlin 2004, 169.
- [50] L. Li, R. R. Gattass, E. Gershgoren, H. Hwang, J. T. Fourkas, *Science* 2009, 324, 910.
- [51] R. Wollhofen, J. Katzmann, C. Hrelescu, J. Jacak, T. A. Klar, *Opt. Express* 2013, 21, 10831.
- [52] A. Fröhlich, J. Fischer, T. Zebrowski, K. Busch, M. Wegener, *Adv. Mater.* 2013, 25, 3588.
- [53] J. Scrimgeour, D. N. Sharp, C. F. Blanford, O. M. Roche, R. G. Denning, A. J. Turberfield, *Adv. Mater.* 2006, 18, 1557.
- [54] J. P. Singer, J.-H. Lee, S. E. Kooi, E. L. Thomas, *Opt. Express* 2012, 20, 11097.
- [55] M. C. George, A. Mohraz, M. Piech, N. S. Bell, J. A. Lewis, P. V. Braun, *Adv. Mater.* 2009, 21, 66.
- [56] L. D. Zarzar, P. Kim, M. Kolle, J. Brinker, J. Aizenberg, B. Kaehr, *Angew. Chem. Int. Ed.* 2011, 50, 9356.
- [57] S. A. Pruzinsky, P. V. Braun, *Adv. Funct. Mater.* 2005, 15, 1995.
- [58] V. Ramanan, E. Nelson, A. Brzezinski, P. V. Braun, P. Wiltzius, *Appl. Phys. Lett.* 2008, 92, 173304.
- [59] S. A. Rinne, F. Garcia-Santamaria, P. V. Braun, *Nat. Photonics* 2008, 2, 52.
- [60] A. Ledermann, L. Cademartiri, M. Hermatschweiler, C. Toninelli, G. A. Ozin, D. S. Wiersma, M. Wegener, G. Von Freymann, *Nat. Mater.* 2006, 5, 942.
- [61] W. Monch, J. Dehnert, O. Prucker, J. Ruhe, H. Zappe, *Appl. Opt.* 2006, 45, 4284.
- [62] T. Komikado, S. Yoshida, S. Umegaki, *Appl. Phys. Lett.* 2006, 89, 061123.
- [63] L. Frezza, M. Patrini, M. Liscidini, D. Comoretto, *J. Phys. Chem. C* 2011, 115, 19939.
- [64] Z. H. Wang, J. H. Zhang, J. Xie, Z. Y. Wang, Y. S. Yin, J. X. Li, Y. F. Li, S. Liang, L. Zhang, L. Y. Cui, H. Zhang, B. Yang, *J. Mater. Chem.* 2012, 22, 7887.
- [65] L. M. Goldenberg, V. Lisinetskii, S. Schrader, *Laser Phys. Lett.* 2013, 10, 055808.
- [66] L. Zhai, A. J. Nolte, R. E. Cohen, M. F. Rubner, *Macromolecules* 2004, 37, 6113.
- [67] S. C. Olugefobola, S. W. Ryu, A. J. Nolte, M. F. Rubner, A. M. Mayes, *Langmuir* 2006, 22, 5958.
- [68] J. G. Son, J.-B. Chang, K. K. Berggren, C. A. Ross, *Nano Lett.* 2011, 11, 5079.
- [69] C. A. Ross, Y. S. Jung, V. P. Chuang, J. G. Son, K. W. Gotrik, R. A. Mickiewicz, J. K. W. Yang, J. B. Chang, K. K. Berggren, J. Gwyther, I. Manners, *Proc. SPIE* 2010, 7637, 76370H.
- [70] Y. S. Jung, W. Jung, C. A. Ross, *Nano Lett.* 2008, 8, 2975.
- [71] H.-W. Li, W. T. S. Huck, *Nano Lett.* 2004, 4, 1633.
- [72] I. Bita, J. K. W. Yang, Y. S. Jung, C. A. Ross, E. L. Thomas, K. K. Berggren, *Science* 2008, 321, 939.
- [73] A. F. Hannon, K. W. Gotrik, C. A. Ross, A. Alexander-Katz, *ACS Macro Lett.* 2013, 2, 251.
- [74] K. G. A. Tavakkoli, K. W. Gotrik, A. F. Hannon, A. Alexander-Katz, C. A. Ross, K. K. Berggren, *Science* 2012, 336, 1294.
- [75] B. H. Jones, T. P. Lodge, *ACS Nano* 2011, 5, 8914.
- [76] H.-J. Hung, P.-C. Yang, J.-H. Liu, *J. Appl. Polym. Sci.* 2008, 109, 3776.
- [77] A. C. Arsenault, T. J. Clark, G. Von Freymann, L. Cademartiri, R. Sapienza, J. Bertolotti, E. Vekris, S. Wong, V. Kitaev, I. Manners, R. Z. Wang, S. John, D. Wiersma, G. A. Ozin, *Nat. Mater.* 2006, 5, 179.
- [78] A. C. Arsenault, D. A. Rider, N. Tétreault, J. I. L. Chen, N. Coombs, G. A. Ozin, I. Manners, *J. Am. Chem. Soc.* 2005, 127, 9954.
- [79] Y. Wang, Y. Qin, A. Berger, E. Yau, C. He, L. Zhang, U. Gösele, M. Knez, M. Steinhart, *Adv. Mater.* 2009, 21, 2763.
- [80] P. Dobriyal, H. Q. Xiang, M. Kazuyuki, J. T. Chen, H. Jinnai, T. P. Russell, *Macromolecules* 2009, 42, 9082.
- [81] M. P. Stoykovich, H. Kang, K. C. Daoulas, G. Liu, C.-C. Liu, J. J. de Pablo, M. Müller, P. F. Nealey, *ACS Nano* 2007, 1, 168.
- [82] E. W. Edwards, M. F. Montague, H. H. Solak, C. J. Hawker, P. F. Nealey, *Adv. Mater.* 2004, 16, 1315.
- [83] C. De Rosa, C. Park, E. L. Thomas, B. Lotz, *Nature* 2000, 405, 433.
- [84] C. Osuji, P. J. Ferreira, G. P. Mao, C. K. Ober, J. B. Vander Sande, E. L. Thomas, *Macromolecules* 2004, 37, 9903.
- [85] M. Gopinadhan, P. W. Majewski, E. S. Beach, C. O. Osuji, *ACS Macro Lett.* 2012, 1, 184.
- [86] T. Xu, Y. Q. Zhu, S. P. Gido, T. P. Russell, *Macromolecules* 2004, 37, 2625.
- [87] D. E. Angelescu, J. H. Waller, D. H. Adamson, P. Deshpande, S. Y. Chou, R. A. Register, P. M. Chaikin, *Adv. Mater.* 2004, 16, 1736.
- [88] T. Hashimoto, J. Bodycomb, Y. Funaki, K. Kimishima, *Macromolecules* 1999, 32, 952.
- [89] B. C. Berry, A. W. Bosse, J. F. Douglas, R. L. Jones, A. Karim, *Nano Lett.* 2007, 7, 2789.
- [90] G. Singh, S. Batra, R. Zhang, H. Yuan, K. G. Yager, M. Cakmak, B. Berry, A. Karim, *ACS Nano* 2013, 7, 5291.
- [91] J. E. Seppala, R. L. Lewis, T. H. Epps, *ACS Nano* 2012, 6, 9855.
- [92] C. Park, C. De Rosa, E. L. Thomas, *Macromolecules* 2001, 34, 2602.
- [93] K. Hayashida, T. Dotera, A. Takano, Y. Matsushita, *Phys. Rev. Lett.* 2007, 98, 195502.
- [94] Y. Matsushita, K. Hayashida, T. Dotera, A. Takano, *J. Phys.: Condens. Matter* 2011, 23, 284111.
- [95] J. Zhang, F. S. Bates, *J. Am. Chem. Soc.* 2012, 134, 7636.
- [96] E. Kim, S. Y. Kim, G. Jo, S. Kim, M. J. Park, *ACS Appl. Mater. Inter.* 2012, 4, 5179.
- [97] H. S. Lim, J.-H. Lee, J. J. Walish, E. L. Thomas, *ACS Nano* 2012, 6, 8933.
- [98] B. Gauvreau, N. Guo, K. Schicker, K. Stoeffler, F. Boismenu, A. Ajji, R. Wingfield, C. Dubois, M. Skorobogatiy, *Opt. Express* 2008, 16, 15677.
- [99] M. S. Kang, A. Nazarkin, A. Brenn, P. S. J. Russell, *Nat. Phys.* 2009, 5, 276.
- [100] P. Dainese, P. S. J. Russell, G. S. Wiederhecker, N. Joly, H. L. Fragnito, V. Laude, A. Khelif, *Opt. Express* 2006, 14, 4141.
- [101] J. C. Knight, T. A. Birks, P. S. J. Russell, D. M. Atkin, *Opt. Lett.* 1996, 21, 1547.
- [102] M. L. Ma, E. L. Thomas, G. C. Rutledge, B. Yu, B. H. Li, Q. H. Jin, D. T. Ding, A. C. Shi, *Macromolecules* 2010, 43, 3061.
- [103] V. Kalra, P. A. Kakad, S. Mendez, T. Ivannikov, M. Kamperman, Y. L. Joo, *Macromolecules* 2006, 39, 5453.
- [104] E. B. Duoss, M. Twardowski, J. A. Lewis, *Adv. Mater.* 2007, 19, 3485.
- [105] G. M. Gratson, F. García-Santamaría, V. Lousse, M. Xu, S. Fan, J. A. Lewis, P. V. Braun, *Adv. Mater.* 2006, 18, 461.
- [106] D. J. Lorang, D. Tanaka, C. M. Spadaccini, K. A. Rose, N. J. Cherepy, J. A. Lewis, *Adv. Mater.* 2011, 23, 5055.
- [107] B. Y. Ahn, D. J. Lorang, J. A. Lewis, *Nanoscale* 2011, 3, 2700.
- [108] B. Y. Ahn, D. Shoji, C. J. Hansen, E. Hong, D. C. Dunand, J. A. Lewis, *Adv. Mater.* 2010, 22, 2251.
- [109] W. Wu, A. DeConinck, J. A. Lewis, *Adv. Mater.* 2011, 23, H178.
- [110] R. C. Hayward, D. A. Saville, I. A. Aksay, *Nature* 2000, 404, 56.
- [111] C. Y. Cho, J. H. Moon, *Adv. Mater.* 2011, 23, 2971.
- [112] J. Ye, R. Zentel, S. Arpiainen, J. Ahopelto, F. Jonsson, S. G. Romanov, C. M. Sotomayor Torres, *Langmuir* 2006, 22, 7378.
- [113] L. Mishchenko, B. Hatton, M. Kolle, J. Aizenberg, *Small* 2012, 8, 1904.
- [114] J. H. Holtz, S. A. Asher, *Nature* 1997, 389, 829.
- [115] A. C. Arsenault, D. P. Puzzo, I. Manners, G. A. Ozin, *Nat. Photonics* 2007, 1, 468.
- [116] W. Cheng, J. J. Wang, U. Jonas, G. Fytas, N. Stefanou, *Nat. Mater.* 2006, 5, 830.

- [117] W. Xiong, Y. S. Zhou, X. N. He, Y. Gao, M. Mahjouri-Samani, L. Jiang, T. Baldacchini, Y. F. Lu, *Light Sci. Appl.* **2012**, *1*, e6.
- [118] S. Jeon, J. U. Park, R. Cirelli, S. Yang, C. E. Heitzman, P. V. Braun, P. J. A. Kenis, J. A. Rogers, *Proc. Natl. Acad. Sci. USA* **2004**, *101*, 12428.
- [119] S. Jeon, D. J. Shir, Y. S. Nam, R. Nidetz, M. Highland, D. G. Cahill, J. A. Rogers, M. F. Su, I. F. El-Kady, C. G. Christodoulou, G. R. Bogart, *Opt. Express* **2007**, *15*, 6358.
- [120] A. Trabattoni, L. Maini, G. Benedek, *Opt. Express* **2012**, *20*, 28267.
- [121] K. Ueda, T. Dotera, T. Gemma, *Phys. Rev. B* **2007**, *75*, 11.
- [122] W. Steurer, D. Sutter-Widmer, *J. Phys. D: Appl. Phys.* **2007**, *40*, R229.
- [123] A. J. Jacobsen, W. Barvosa-Carter, S. Nutt, *Adv. Mater.* **2007**, *19*, 3892.
- [124] A. J. Jacobsen, W. Barvosa-Carter, S. Nutt, *Acta Mater.* **2008**, *56*, 1209.
- [125] T. A. Schaedler, A. J. Jacobsen, A. Torrents, A. E. Sorensen, J. Lian, J. R. Greer, L. Valdevit, W. B. Carter, *Science* **2011**, *334*, 962.
- [126] C. G. Xia, H. Lee, N. Fang, *J. Micromech. Microeng.* **2010**, *20*, 085030.
- [127] T. Watanabe, M. Akiyama, K. Totani, S. M. Kuebler, F. Stellacci, W. Wenseleers, K. Braun, S. R. Marder, J. W. Perry, *Adv. Funct. Mater.* **2002**, *12*, 611.
- [128] S. J. Jhaveri, J. D. McMullen, R. Sijbesma, L. S. Tan, W. Zipfel, C. K. Ober, *Chem. Mater.* **2009**, *21*, 2003.
- [129] T. A. Pham, D. P. Kim, T. W. Lim, S. H. Park, D. Y. Yang, K. S. Lee, *Adv. Funct. Mater.* **2006**, *16*, 1235.
- [130] J.-J. Park, P. Prabhakaran, K. K. Jang, Y. Lee, J. Lee, K. Lee, J. Hur, J.-M. Kim, N. Cho, Y. Son, D.-Y. Yang, K.-S. Lee, *Nano Lett.* **2010**, *10*, 2310.
- [131] S. Shukla, X. Vidal, E. P. Furlani, M. T. Swihart, K.-T. Kim, Y.-K. Yoon, A. Urbas, P. N. Prasad, *ACS Nano* **2011**, *5*, 1947.
- [132] H. S. Oh, H. Jee, A. Baev, M. T. Swihart, P. N. Prasad, *Adv. Funct. Mater.* **2012**, *22*, 5074.
- [133] M. Li, K. Douki, K. Goto, X. Li, C. Coenjarts, D. M. Smilgies, C. K. Ober, *Chem. Mater.* **2004**, *16*, 3800.
- [134] J. K. Bosworth, C. T. Black, C. K. Ober, *ACS Nano* **2009**, *3*, 1761.
- [135] J. P. Singer, K. W. Gotrik, J.-H. Lee, S. Kooi, C. A. Ross, E. L. Thomas, **2013**, Unpublished.
- [136] S. Lee, H. S. Kang, J.-K. Park, *Adv. Funct. Mater.* **2011**, *21*, 1770.
- [137] G. Decher, *Science* **1997**, *277*, 1232.
- [138] G. M. Nogueira, D. Banerjee, R. E. Cohen, M. F. Rubner, *Langmuir* **2011**, *27*, 7860.
- [139] R. Suntivich, O. Shchepelina, I. Choi, V. V. Tsukruk, *ACS Appl. Mater. Interfaces* **2012**, *4*, 3102.
- [140] B. Xu, F. Arias, S. T. Brittain, X. M. Zhao, B. Grzybowski, S. Torquato, G. M. Whitesides, *Adv. Mater.* **1999**, *11*, 1186.
- [141] X.-M. Zhao, Y. Xia, G. M. Whitesides, *J. Mater. Chem.* **1997**, *7*, 1069.
- [142] Y. Wu, G. Cheng, K. Katsov, S. W. Sides, J. Wang, J. Tang, G. H. Fredrickson, M. Moskovits, G. D. Stucky, *Nat. Mater.* **2004**, *3*, 816.
- [143] J.-H. Jang, S. J. Jhaveri, B. Rasin, C. Koh, C. K. Ober, E. L. Thomas, *Nano Lett.* **2008**, *8*, 1456.
- [144] J. Park, S. Wang, M. Li, C. Ahn, J. K. Hyun, D. S. Kim, D. K. Kim, J. A. Rogers, Y. Huang, S. Jeon, *Nat. Commun.* **2012**, *3*, 916.
- [145] R. H. Lambeth, J. Park, H. W. Liao, D. J. Shir, S. Jeon, J. A. Rogers, J. S. Moore, *Nanotechnology* **2010**, *21*, 6.
- [146] A. Honglawan, D. A. Beller, M. Cavallaro, R. D. Kamien, K. J. Stebe, S. Yang, *Proc. Natl. Acad. Sci. USA* **2013**, *110*, 34.
- [147] A. Honglawan, D. A. Beller, M. Cavallaro, R. D. Kamien, K. J. Stebe, S. Yang, *Adv. Mater.* **2011**, *23*, 5519.
- [148] J. Y. Cheng, C. A. Ross, E. L. Thomas, H. I. Smith, G. J. Vancso, *Appl. Phys. Lett.* **2002**, *81*, 3657.
- [149] C. Park, J. Yoon, E. L. Thomas, *Polymer* **2003**, *44*, 6725.
- [150] J. A. Radford, T. Alfrey, W. J. Schrenk, *Polym. Eng. Sci.* **1973**, *13*, 216.
- [151] T. Kazmierczak, H. M. Song, A. Hiltner, E. Baer, *Macromol. Rapid Commun.* **2007**, *28*, 2210.
- [152] K. Busch, S. John, *Phys. Rev. Lett.* **1999**, *83*, 967.
- [153] O. D. Lavrentovich, *Proc. Natl. Acad. Sci. USA* **2011**, *108*, 5143.
- [154] I.-C. Khoo, *Liquid Crystals*, Wiley, Hoboken **2007**.
- [155] A. Minovich, D. N. Neshev, D. A. Powell, I. V. Shadrivov, Y. S. Kivshar, *Appl. Phys. Lett.* **2010**, *96*, 193103.
- [156] E. Graugnard, S. N. Dunham, J. S. King, D. Lorang, S. Jain, C. J. Summers, *Appl. Phys. Lett.* **2007**, *91*, 111101.
- [157] W. Y. Cao, A. Munoz, P. Palffy-Muhoray, B. Taheri, *Nat. Mater.* **2002**, *1*, 111.
- [158] V. I. Kopp, B. Fan, H. K. M. Vithana, A. Z. Genack, *Opt. Lett.* **1998**, *23*, 1707.
- [159] Q. Zhao, L. Kang, B. Du, B. Li, J. Zhou, H. Tang, X. Liang, B. Z. Zhang, *Appl. Phys. Lett.* **2007**, *90*, 011112.
- [160] D. Shrekenhamer, W.-C. Chen, W. J. Padilla, *Phys. Rev. Lett.* **2013**, *110*, 177403.
- [161] S. M. Xiao, U. K. Chettiar, A. V. Kildishev, V. Drachev, I. C. Khoo, V. M. Shalaev, *Appl. Phys. Lett.* **2009**, *95*, 033115.
- [162] Y. H. Huang, Y. Zhou, C. Doyle, S. T. Wu, *Opt. Express* **2006**, *14*, 1236.
- [163] S. Furumi, S. Yokoyama, A. Otomo, S. Mashiko, *Appl. Phys. Lett.* **2004**, *84*, 2491.
- [164] G. Z. Han, Z. Y. Xie, D. Zheng, L. G. Sun, Z. Z. Gu, *Appl. Phys. Lett.* **2007**, *91*, 141114.
- [165] H. Coles, S. Morris, *Nat. Photonics* **2010**, *4*, 676.
- [166] L. T. de Haan, C. Sanchez-Somolinos, C. M. W. Bastiaansen, A. P. H. J. Schenning, D. J. Broer, *Angew. Chem. Int. Ed.* **2012**, *51*, 12469.
- [167] C. Liu, H. Qin, P. T. Mather, *J. Mater. Chem.* **2007**, *17*, 1543.
- [168] N. Liu, Q. Xie, W. M. Huang, S. J. Phee, N. Q. Guo, *J. Micromech. Microeng.* **2008**, *18*, 027001.
- [169] D. A. Mortimer, *Polym. Int.* **1991**, *25*, 29.
- [170] T. C. Wang, R. E. Cohen, M. F. Rubner, *Adv. Mater.* **2002**, *14*, 1534.
- [171] N. Tetreault, A. C. Arsenault, A. Mihi, S. Wong, V. Kitaev, I. Manners, H. Miguez, G. A. Ozin, *Adv. Mater.* **2005**, *17*, 1912.
- [172] C. Li, B. V. Lotsch, *Chem. Commun.* **2012**, *48*, 6169.
- [173] Y. Kang, J. J. Walish, T. Gorishny, E. L. Thomas, *Nat. Mater.* **2007**, *6*, 957.
- [174] K. Hwang, D. Kwak, C. Kang, D. Kim, Y. Ahn, Y. Kang, *Angew. Chem. Int. Ed.* **2011**, *50*, 6311.
- [175] J. J. Walish, Y. Kang, R. A. Mickiewicz, E. L. Thomas, *Adv. Mater.* **2009**, *21*, 3078.
- [176] M. F. Weber, C. A. Stover, L. R. Gilbert, T. J. Nevitt, A. J. Ouderkerk, *Science* **2000**, *287*, 2451.
- [177] Rainbow Winters webpage, <http://www.rainbowwinters.com/project6.html>, accessed: November 2013.
- [178] E. Adachi, United States Patent US 7,718,164 B2, **2010**.
- [179] L. D. Bonifacio, B. V. Lotsch, D. P. Puzzo, F. Scotognella, G. A. Ozin, *Adv. Mater.* **2009**, *21*, 1641.
- [180] G. R. Fowles, *Introduction to Modern Optics*, Dover Publisher Inc., New York, USA **1989**.
- [181] J. P. Ge, Y. D. Yin, *Angew. Chem. Int. Ed.* **2011**, *50*, 1492.
- [182] M. Maldovan, E. L. Thomas, *Periodic Materials and Interference Lithography for Photonics, Phononics and Mechanics*, Wiley-VCH, Weinheim, Germany **2009**.
- [183] Y. Fink, J. N. Winn, S. H. Fan, C. P. Chen, J. Michel, J. D. Joannopoulos, E. L. Thomas, *Science* **1998**, *282*, 1679.
- [184] K. M. Ho, C. T. Chan, C. M. Soukoulis, *Phys. Rev. Lett.* **1990**, *65*, 3152.
- [185] H. S. Sozuer, J. W. Haus, R. Inguva, *Phys. Rev. B* **1992**, *45*, 13962.
- [186] K. Busch, S. John, *Phys. Rev. E* **1998**, *58*, 3896.
- [187] Z. Y. Li, Z. Q. Zhang, *Phys. Rev. B* **2000**, *62*, 1516.

- [188] C. E. Finlayson, C. Goddard, E. Papachristodoulou, D. R. E. Snoswell, A. Kontogeorgos, P. Spahn, G. P. Hellmann, O. Hess, J. J. Baumberg, *Opt. Express* **2011**, *19*, 3144.
- [189] C. E. Finlayson, P. Spahn, D. R. E. Snoswell, G. Yates, A. Kontogeorgos, A. I. Haines, G. P. Hellmann, J. J. Baumberg, *Adv. Mater.* **2011**, *23*, 1540.
- [190] D. R. E. Snoswell, A. Kontogeorgos, J. J. Baumberg, T. D. Lord, M. R. Mackley, P. Spahn, G. P. Hellmann, *Phys. Rev. E* **2010**, *81*, 020401.
- [191] Y. S. Chan, C. T. Chan, Z. Y. Liu, *Phys. Rev. Lett.* **1998**, *80*, 956.
- [192] Z. V. Vardeny, A. Nahata, A. Agrawal, *Nat. Photonics* **2013**, *7*, 177.
- [193] E. Lidorikis, M. M. Sigalas, E. N. Economou, C. M. Soukoulis, *Phys. Rev. B* **2000**, *61*, 13458.
- [194] C. J. Jin, X. D. Meng, B. Y. Cheng, Z. L. Li, D. Z. Zhang, *Phys. Rev. B* **2001**, *63*, 195107.
- [195] D. Shechtman, I. Blech, D. Gratias, J. W. Cahn, *Phys. Rev. Lett.* **1984**, *53*, 1951.
- [196] A. Della Villa, S. Enoch, G. Tayeb, V. Pierro, V. Galdi, F. Capolino, *Phys. Rev. Lett.* **2005**, *94*, 183903.
- [197] W. Gellermann, M. Kohmoto, B. Sutherland, P. C. Taylor, *Phys. Rev. Lett.* **1994**, *72*, 633.
- [198] L. Dal Negro, C. J. Oton, Z. Gaburro, L. Pavesi, P. Johnson, A. Lagendijk, R. Righini, M. Colocci, D. S. Wiersma, *Phys. Rev. Lett.* **2003**, *90*, 055501.
- [199] X. B. Zeng, G. Ungar, Y. S. Liu, V. Percec, S. E. Dulcey, J. K. Hobbs, *Nature* **2004**, *428*, 157.
- [200] J. Mikhael, J. Roth, L. Helden, C. Bechinger, *Nature* **2008**, *454*, 501.
- [201] M. Notomi, H. Suzuki, T. Tamamura, K. Edagawa, *Phys. Rev. Lett.* **2004**, *92*, 123906.
- [202] D. Luo, Q. G. Du, H. T. Dai, H. V. Demir, H. Z. Yang, W. Ji, X. W. Sun, *Sci. Rep.* **2012**, *2*, 1.
- [203] M. D. Kelzenberg, S. W. Boettcher, J. A. Petykiewicz, D. B. Turner-Evans, M. C. Putnam, E. L. Warren, J. M. Spurgeon, R. M. Briggs, N. S. Lewis, H. A. Atwater, *Nat. Mater.* **2010**, *9*, 239.
- [204] H. W. Yin, B. Q. Dong, X. H. Liu, T. R. Zhan, L. Shi, J. Zi, E. Yablonovitch, *Proc. Natl. Acad. Sci. USA* **2012**, *109*, 10798.
- [205] J. H. Jang, C. K. Ullal, S. E. Kooi, C. Koh, E. L. Thomas, *Nano Lett.* **2007**, *7*, 647.
- [206] K. Edagawa, S. Kanoko, M. Notomi, *Phys. Rev. Lett.* **2008**, *100*, 013901.
- [207] P. W. Anderson, *Phys. Rev.* **1958**, *109*, 1492.
- [208] S. F. Liew, J. K. Yang, H. Noh, C. F. Schreck, E. R. Dufresne, C. S. O'Hern, H. Cao, *Phys. Rev. A* **2011**, *84*, 063818.
- [209] E. R. Dufresne, H. Noh, V. Saranathan, S. G. J. Mochrie, H. Cao, R. O. Prum, *Soft Matter* **2009**, *5*, 1792.
- [210] B. Q. Dong, X. H. Liu, T. R. Zhan, L. P. Jiang, H. W. Yin, F. Liu, J. Zi, *Opt. Express* **2010**, *18*, 14430.
- [211] J. Vörös, *Biophys. J.* **2004**, *87*, 553.
- [212] R. M. Kramer, W. J. Crookes-Goodson, R. R. Naik, *Nat. Mater.* **2007**, *6*, 533.
- [213] N. Kumano, T. Seki, M. Ishii, H. Nakamura, Y. Takeoka, *Angew. Chem. Int. Ed.* **2011**, *50*, 4012.
- [214] Y. Takeoka, M. Honda, T. Seki, M. Ishii, H. Nakamura, *ACS Appl. Mater. Inter.* **2009**, *1*, 982.
- [215] J. D. Forster, H. Noh, S. F. Liew, V. Saranathan, C. F. Schreck, L. Yang, J. G. Park, R. O. Prum, S. G. J. Mochrie, C. S. O'Hern, H. Cao, E. R. Dufresne, *Adv. Mater.* **2010**, *22*, 2939.
- [216] I. Lee, D. Kim, J. Kal, H. Baek, D. Kwak, D. Go, E. Kim, C. Kang, J. Chung, Y. Jang, S. Ji, J. Joo, Y. Kang, *Adv. Mater.* **2010**, *22*, 4973.
- [217] K. Michielsen, D. G. Stavenga, *J. R. Soc. Interface* **2008**, *5*, 85.
- [218] V. Saranathan, C. O. Osuji, S. G. J. Mochrie, H. Noh, S. Narayanan, A. Sandy, E. R. Dufresne, R. O. Prum, *Proc. Natl. Acad. Sci. USA* **2010**, *107*, 11676.
- [219] J. W. Galusha, L. R. Richey, M. R. Jorgensen, J. S. Gardner, M. H. Bartl, *J. Mater. Chem.* **2010**, *20*, 1277.
- [220] P. Vukusic, J. R. Sambles, *Nature* **2003**, *424*, 852.
- [221] R. Hanlon, *Curr. Biol.* **2007**, *17*, R400.
- [222] S. Johnsen, H. M. Sosik, *Limnol. Oceanogr.* **2003**, *48*, 1277.
- [223] S. Kinoshita, S. Yoshioka, *ChemPhysChem* **2005**, *6*, 1442.
- [224] T. J. Wardill, P. T. Gonzalez-Bellido, R. J. Crook, R. T. Hanlon, *Proc. Roy. Soc. B* **2012**, *279*, 4243.
- [225] M. Saba, M. Thiel, M. D. Turner, S. T. Hyde, M. Gu, K. Grosse-Brauckmann, D. N. Neshev, K. Mecke, G. E. Schröder-Turk, *Phys. Rev. Lett.* **2011**, *106*, 103902.
- [226] T. Hahn, U. Shmueli, A. A. J. C. Wilson, E. Prince, *International Tables for Crystallography*, D. Reidel Publishing Company, **2005**.
- [227] R. A. Potyrailo, H. Ghiradella, A. Vertiatchikh, K. Dovidenko, J. R. Cournoyer, E. Olson, *Nat. Photonics* **2007**, *1*, 123.
- [228] O. Sato, S. Kubo, Z. Z. Gu, *Acc. Chem. Res.* **2009**, *42*, 1.
- [229] A. R. Parker, H. E. Townley, *Nat. Nanotechnol.* **2007**, *2*, 347.
- [230] M. B. Christiansen, A. Kristensen, S. S. Xiao, N. A. Mortensen, *Appl. Phys. Lett.* **2008**, *93*, 231101.
- [231] J. Yoon, W. Lee, E. L. Thomas, *Nano Lett.* **2006**, *6*, 2211.
- [232] S. Furumi, H. Fudouzi, H. T. Miyazaki, Y. Sakka, *Adv. Mater.* **2007**, *19*, 2067.
- [233] K. Min, Y. K. Choi, H. Jeon, *Opt. Express* **2012**, *20*, 2452.
- [234] J. Yoon, W. Lee, J. M. Caruge, M. Bawendi, E. L. Thomas, S. Kooi, P. N. Prasad, *Appl. Phys. Lett.* **2006**, *88*, 091102.
- [235] J. Yoon, W. Lee, E. L. Thomas, *Macromolecules* **2008**, *41*, 4582.
- [236] E. P. Chan, J. J. Walish, E. L. Thomas, C. M. Stafford, *Adv. Mater.* **2011**, *23*, 4702.
- [237] J. P. Dowling, M. Scalora, M. J. Bloemer, C. M. Bowden, *J. Appl. Phys.* **1994**, *75*, 1896.
- [238] H. Finkelmann, S. T. Kim, A. Munoz, P. Palffy-Muhoray, B. Taheri, *Adv. Mater.* **2001**, *13*, 1069.
- [239] A. D. Ford, S. M. Morris, M. N. Pivnenko, H. J. Coles, *Proc. SPIE* **2004**, *5289*, 213.
- [240] A. Urbas, R. Sharp, Y. Fink, E. L. Thomas, M. Xenidou, L. J. Fetter, *Adv. Mater.* **2000**, *12*, 812.
- [241] S. Yokoyama, S. Mashiko, H. Kikuchi, K. Uchida, T. Nagamura, *Adv. Mater.* **2006**, *18*, 48.
- [242] S.-T. Hur, B. R. Lee, M.-J. Gim, K.-W. Park, M. H. Song, S.-W. Choi, *Adv. Mater.* **2013**, *25*, 3002.
- [243] J. Li, C. H. Wen, S. Gauza, R. B. Lu, S. T. Wu, *IEEE J. Disp. Technol.* **2005**, *1*, 51.
- [244] G. Li, R. Zhu, Y. Yang, *Nat. Photonics* **2012**, *6*, 153.
- [245] W. L. Min, B. Jiang, P. Jiang, *Adv. Mater.* **2008**, *20*, 3914.
- [246] J. Zhu, C. M. Hsu, Z. F. Yu, S. H. Fan, Y. Cui, *Nano Lett.* **2010**, *10*, 1979.
- [247] D. Madzharov, R. Dewan, D. Knipp, *Opt. Express* **2011**, *19*, A95.
- [248] I. Suemune, *Opt. Express* **2013**, *21*, A539.
- [249] J. N. Munday, H. A. Atwater, *Nano Lett.* **2011**, *11*, 2195.
- [250] M. A. Green, S. Pillai, *Nat. Photonics* **2012**, *6*, 130.
- [251] D. E. Markov, E. Amsterdam, P. W. M. Blom, A. B. Sieval, J. C. Hummelen, *J. Phys. Chem. A* **2005**, *109*, 5266.
- [252] P. E. Shaw, A. Ruseckas, I. D. W. Samuel, *Adv. Mater.* **2008**, *20*, 3516.
- [253] G. Yu, J. Gao, J. C. Hummelen, F. Wudl, A. J. Heeger, *Science* **1995**, *270*, 1789.
- [254] M. C. Scharber, D. Wuhlacher, M. Koppe, P. Denk, C. Waldauf, A. J. Heeger, C. L. Brabec, *Adv. Mater.* **2006**, *18*, 789.
- [255] D. H. Ko, J. R. Tumbleston, L. Zhang, S. Williams, J. M. DeSimone, R. Lopez, E. T. Samulski, *Nano Lett.* **2009**, *9*, 2742.
- [256] L. Z. Chen, W. E. I. Sha, W. C. H. Choy, *Opt. Express* **2012**, *20*, 8175.
- [257] K. Tvingstedt, N. K. Persson, O. Inganäs, A. Rahachou, I. V. Zozoulenko, *Appl. Phys. Lett.* **2007**, *91*, 113514.
- [258] S. I. Na, S. S. Kim, J. Jo, S. H. Oh, J. Kim, D. Y. Kim, *Adv. Funct. Mater.* **2008**, *18*, 3956.
- [259] J. Y. Kim, K. Lee, N. E. Coates, D. Moses, T. Q. Nguyen, M. Dante, A. J. Heeger, *Science* **2007**, *317*, 222.

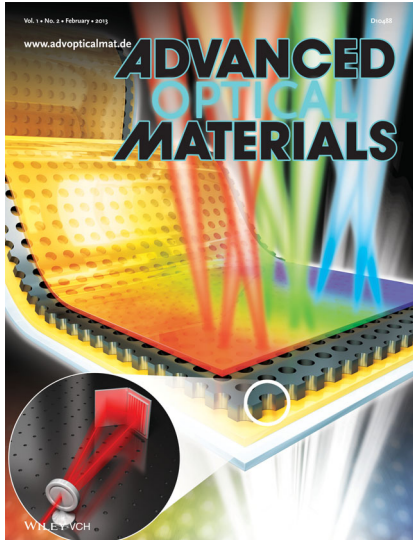
- [260] J. R. Tumbleston, D. H. Ko, E. T. Samulski, R. Lopez, *Appl. Phys. Lett.* **2009**, *94*, 043305.
- [261] S. Kassegne, K. Moon, P. Martin-Ramos, M. Majzoub, G. Ozturk, K. Desai, M. Parikh, B. Nguyen, A. Khosla, P. Chamorro-Posada, J. *Micromech. Microeng.* **2012**, *22*, 115015.
- [262] C. Bauer, H. Giessen, *Opt. Express* **2013**, *21*, A363.
- [263] L. Jia, I. Bita, E. L. Thomas, *Adv. Funct. Mater.* **2012**, *22*, 1150.
- [264] S. H. Park, A. Roy, S. Beaupre, S. Cho, N. Coates, J. S. Moon, D. Moses, M. Leclerc, K. Lee, A. J. Heeger, *Nat. Photonics* **2009**, *3*, 297.
- [265] E. J. W. Crossland, M. Kamperman, M. Nedelcu, C. Ducati, U. Wiesner, D. M. Smilgies, G. E. S. Toombes, M. A. Hillmyer, S. Ludwigs, U. Steiner, H. J. Snaith, *Nano Lett.* **2009**, *9*, 2807.
- [266] N. Sary, F. Richard, C. Brochon, N. Leclerc, P. Leveque, J. N. Audinot, S. Berson, T. Heiser, G. Hadzioannou, R. Mezzenga, *Adv. Mater.* **2010**, *22*, 763.
- [267] X. M. He, F. Gao, G. L. Tu, D. Hasko, S. Huttner, U. Steiner, N. C. Greenham, R. H. Friend, W. T. S. Huck, *Nano Lett.* **2010**, *10*, 1302.
- [268] S. Guldin, S. Huttner, M. Kolle, M. E. Welland, P. Muller-Buschbaum, R. H. Friend, U. Steiner, N. Tetreault, *Nano Lett.* **2010**, *10*, 2303.
- [269] P. Zavala-Rivera, K. Channon, V. Nguyen, E. Sivaniah, D. Kabra, R. H. Friend, S. K. Nataraj, S. A. Al-Muhtaseb, A. Hexemer, M. E. Calvo, H. Miguez, *Nat. Mater.* **2012**, *11*, 53.
- [270] H. Li, J. X. Wang, Z. L. Pan, L. Y. Cui, L. A. Xu, R. M. Wang, Y. L. Song, L. Jiang, *J. Mater. Chem.* **2011**, *21*, 1730.
- [271] I. A. Levitsky, W. B. Euler, N. Tokranova, A. Rose, *Appl. Phys. Lett.* **2007**, *90*, 041904.
- [272] K. H. Jensen, M. N. Alam, B. Scherer, A. Lambrecht, N. A. Mortensen, *Opt. Commun.* **2008**, *281*, 5335.
- [273] M. Karaman, S. E. Kooi, K. K. Gleason, *Chem. Mater.* **2008**, *20*, 2262.
- [274] R. A. Barry, P. Wiltzius, *Langmuir* **2006**, *22*, 1369.
- [275] L. Hu, M. J. Serpe, *Chem. Commun.* **2013**, *49*, 2649.
- [276] K. Lee, S. A. Asher, *J. Am. Chem. Soc.* **2000**, *122*, 9534.
- [277] C. E. Reese, M. E. Baltusavich, J. P. Keim, S. A. Asher, *Anal. Chem.* **2001**, *73*, 5038.
- [278] H. Saito, Y. Takeoka, M. Watanabe, *Chem. Commun.* **2003**, 2126.
- [279] J. H. Holtz, J. S. Holtz, C. H. Munro, S. A. Asher, *Anal. Chem.* **1998**, *70*, 780.
- [280] O. B. Ayyub, M. B. Ibrahim, R. M. Briber, P. Kofinas, *Biosens. Bioelectron.* **2013**, *46*, 124.
- [281] K. Yoshino, Y. Kawagishi, M. Ozaki, A. Kose, *Jpn. J. Appl. Phys. Part 2* **1999**, *38*, L786.
- [282] C. Osuji, C. Y. Chao, I. Bita, C. K. Ober, E. L. Thomas, *Adv. Funct. Mater.* **2002**, *12*, 753.
- [283] Y. Takeoka, M. Watanabe, *Adv. Mater.* **2003**, *15*, 199.
- [284] Y. D. Hu, J. Y. Wang, H. Wang, Q. Wang, J. T. Zhu, Y. J. Yang, *Langmuir* **2012**, *28*, 17186.
- [285] E. T. Tian, J. X. Wang, Y. M. Zheng, Y. L. Song, L. Jiang, D. B. Zhu, *J. Mater. Chem.* **2008**, *18*, 1116.
- [286] Z. H. Wang, J. H. Zhang, J. Xie, C. A. Li, Y. F. Li, S. Liang, Z. C. Tian, T. Q. Wang, H. Zhang, H. B. Li, W. Q. Xu, B. Yang, *Adv. Funct. Mater.* **2010**, *20*, 3784.
- [287] P. Puligundla, J. Jung, S. Ko, *Food Control* **2012**, *25*, 328.
- [288] M. Xu, A. V. Goponenko, S. A. Asher, *J. Am. Chem. Soc.* **2008**, *130*, 3113.
- [289] Y. J. Lee, P. V. Braun, *Adv. Mater.* **2003**, *15*, 563.
- [290] J. Shin, P. V. Braun, W. Lee, *Sens. Actuators B* **2010**, *150*, 183.
- [291] J. T. Zhang, L. L. Wang, J. Luo, A. Tikhonov, N. Kornienko, S. A. Asher, *J. Am. Chem. Soc.* **2011**, *133*, 9152.
- [292] Q. Z. Cui, W. Wang, B. H. Gu, L. Y. Liang, *Macromolecules* **2012**, *45*, 8382.
- [293] M. M. W. Muscatello, S. A. Asher, *Adv. Funct. Mater.* **2008**, *18*, 1186.
- [294] S. A. Asher, A. C. Sharma, A. V. Goponenko, M. M. Ward, *Anal. Chem.* **2003**, *75*, 1676.
- [295] B.-F. Ye, F. Rong, H. Gu, Z. Xie, Y. Cheng, Y. Zhao, Z.-Z. Gu, *Chem. Commun.* **2013**, *49*, 5331.
- [296] C. E. Reese, S. A. Asher, *Anal. Chem.* **2003**, *75*, 3915.
- [297] S. A. Asher, S. F. Peteu, C. E. Reese, M. Lin, D. Finegold, *Anal. Bioanal. Chem.* **2002**, *373*, 632.
- [298] A. V. Goponenko, S. A. Asher, *J. Am. Chem. Soc.* **2005**, *127*, 10753.
- [299] N. Dave, M. Y. Chan, P.-J. J. Huang, B. D. Smith, J. Liu, *J. Am. Chem. Soc.* **2010**, *132*, 12668.
- [300] A. Ono, H. Togashi, *Angew. Chem. Int. Ed.* **2004**, *43*, 4300.
- [301] C. Ma, Y. N. Jiang, X. D. Yang, C. X. Wang, H. Li, F. X. Dong, B. Yang, K. Yu, Q. Lin, *ACS Appl. Mater. Interfaces* **2013**, *5*, 1990.
- [302] D. Arunbabu, A. Sannigrahi, T. Jana, *Soft Matter* **2011**, *7*, 2592.
- [303] C. Fenzl, S. Wilhelm, T. Hirsch, O. S. Wolfbeis, *ACS Appl. Mater. Interfaces* **2013**, *5*, 173.
- [304] S. A. Asher, V. L. Alexeev, A. V. Goponenko, A. C. Sharma, I. K. Lednev, C. S. Wilcox, D. N. Finegold, *J. Am. Chem. Soc.* **2003**, *125*, 3322.
- [305] V. L. Alexeev, S. Das, D. N. Finegold, S. A. Asher, *Clin. Chem.* **2004**, *50*, 2353.
- [306] V. L. Alexeev, A. C. Sharma, A. V. Goponenko, S. Das, I. K. Lednev, C. S. Wilcox, D. N. Finegold, S. A. Asher, *Anal. Chem.* **2003**, *75*, 2316.
- [307] M. Ben-Moshe, V. L. Alexeev, S. A. Asher, *Anal. Chem.* **2006**, *78*, 5149.
- [308] X. P. Yang, X. H. Pan, J. Blyth, C. R. Lowe, *Biosens. Bioelectron.* **2008**, *23*, 899.
- [309] S. Kim, A. N. Mitropoulos, J. D. Spitzberg, H. Tao, D. L. Kaplan, F. G. Omenetto, *Nat. Photonics* **2012**, *6*, 817.
- [310] E. P. Chan, J. J. Walish, A. M. Urbas, E. L. Thomas, *Adv. Mater.* **2013**, *25*, 3934.
- [311] Y. Iwayama, J. Yamanaka, Y. Takiguchi, M. Takasaka, K. Ito, T. Shinohara, T. Sawada, M. Yonese, *Langmuir* **2003**, *19*, 977.
- [312] S. H. Foulger, P. Jiang, A. Lattam, D. W. Smith, J. Ballato, D. E. Dausch, S. Grego, B. R. Stoner, *Adv. Mater.* **2003**, *15*, 685.
- [313] K. Sumioka, H. Kayashima, T. Tsutsui, *Adv. Mater.* **2002**, *14*, 1284.
- [314] J. Li, Y. Wu, J. Fu, Y. Cong, J. Peng, Y. C. Han, *Chem. Phys. Lett.* **2004**, *390*, 285.
- [315] H. Fudouzi, T. Sawada, *Langmuir* **2006**, *22*, 1365.
- [316] O. L. J. Pursiainen, J. J. Baumberg, K. Ryan, J. Bauer, H. Winkler, B. Viel, T. Ruhl, *Appl. Phys. Lett.* **2005**, *87*, 101902.
- [317] C. G. Schäfer, M. Gallo, J. Zahn, J. Engelhardt, G. P. Hellmann, M. Rehahn, *Chem. Mater.* **2013**, DOI: 10.1021/cm400911j.
- [318] M. Kolle, A. Lethbridge, M. Kreysing, J. J. Baumberg, J. Aizenberg, P. Vukusic, *Adv. Mater.* **2013**.
- [319] M. A. Haque, G. Kamita, T. Kurokawa, K. Tsujii, J. P. Gong, *Adv. Mater.* **2010**, *22*, 5110.
- [320] J. Sussman, D. Snoswell, A. Kontogeorgos, J. J. Baumberg, P. Spahn, *Appl. Phys. Lett.* **2009**, *95*, 173116.
- [321] M. C. Chiappelli, R. C. Hayward, *Adv. Mater.* **2012**, *24*, 6100.
- [322] J. H. Kang, J. H. Moon, S. K. Lee, S. G. Park, S. G. Jang, S. Yang, S. M. Yang, *Adv. Mater.* **2008**, *20*, 3061.
- [323] P. D. Hustad, G. R. Marchand, E. I. Garcia-Mein, P. L. Roberts, J. D. Weinhold, *Macromolecules* **2009**, *42*, 3788.
- [324] M. Honda, T. Seki, Y. Takeoka, *Adv. Mater.* **2009**, *21*, 1801.
- [325] E. Kim, C. Kang, H. Baek, K. Hwang, D. Kwak, E. Lee, Y. Kang, E. L. Thomas, *Adv. Funct. Mater.* **2010**, *20*, 1728.
- [326] Y. J. Lu, H. W. Xia, G. Z. Zhang, C. Wu, *J. Mater. Chem.* **2009**, *19*, 5952.
- [327] D. P. Puzzo, A. C. Arsenault, I. Manners, G. A. Ozin, *Angew. Chem. Int. Ed.* **2009**, *48*, 943.
- [328] Y. Ahn, E. Kim, J. Hyon, C. Kang, Y. Kang, *Adv. Mater.* **2012**, *24*, Op127.
- [329] J. Q. Xia, Y. R. Ying, S. H. Foulger, *Adv. Mater.* **2005**, *17*, 2463.
- [330] T. S. Shim, S. H. Kim, J. Y. Sim, J. M. Lim, S. M. Yang, *Adv. Mater.* **2010**, *22*, 4494.
- [331] P. Jiang, D. W. Smith, J. M. Ballato, S. H. Foulger, *Adv. Mater.* **2005**, *17*, 179.

- [332] H. Fudouzi, Y. N. Xia, *Adv. Mater.* **2003**, *15*, 892.
[333] H. Fudouzi, Y. N. Xia, *Langmuir* **2003**, *19*, 9653.
[334] H. Fudouzi, Y. Lu, Y. N. Xia, *ACS Symp. Ser.* **2005**, *888*, 329.
[335] J. Pendry, *Phys. Rev. Lett.* **2000**, *85*, 3966.
[336] J. B. Pendry, D. Schurig, D. R. Smith, *Science* **2006**, *312*, 1780.
[337] H. Y. Chen, C. T. Chan, P. Sheng, *Nat. Mater.* **2010**, *9*, 387.
[338] D. A. Genov, S. Zhang, X. Zhang, *Nat. Phys.* **2009**, *5*, 687.
[339] E. E. Narimanov, A. V. Kildishev, *Appl. Phys. Lett.* **2009**, *95*, 041106.
[340] K. Hur, Y. Francescato, V. Giannini, S. A. Maier, R. G. Hennig, U. Wiesner, *Angew. Chem. Int. Ed.* **2011**, *50*, 11985.
[341] S. Salvatore, A. Demetriadou, S. Vignolini, S. S. Oh, S. Wuestner, N. A. Yuja, M. Stefk, U. Wiesner, J. J. Baumberg, O. Hess, U. Steiner, *Adv. Mater.* **2013**.
[342] D. R. Smith, J. B. Pendry, M. C. K. Wiltshire, *Science* **2004**, *305*, 788.
[343] E. Cubukcu, K. Aydin, E. Ozbay, S. Fotinopoulou, C. M. Soukoulis, *Nature* **2003**, *423*, 604.
[344] P. V. Parimi, W. T. T. Lu, P. Vodo, S. Sridhar, *Nature* **2003**, *426*, 404.
[345] S. T. Wu, M. S. Li, A. Y. G. Fuh, *Appl. Phys. Lett.* **2007**, *91*, 251117.
[346] G. Dolling, M. Wegener, S. Linden, *Opt. Lett.* **2007**, *32*, 551.
[347] J. Valentine, S. Zhang, T. Zentgraf, E. Ulin-Avila, D. A. Genov, G. Bartal, X. Zhang, *Nature* **2008**, *455*, 376.
[348] D. Chanda, K. Shigeta, S. Gupta, T. Cain, A. Carlson, A. Mihi, A. J. Baca, G. R. Bogart, P. Braun, J. A. Rogers, *Nat. Nanotechnol.* **2011**, *6*, 402.
[349] M. S. Rill, C. E. Kriegler, M. Thiel, G. von Freymann, S. Linden, M. Wegener, *Opt. Lett.* **2009**, *34*, 19.
[350] S. M. Xiao, V. P. Drachev, A. V. Kildishev, X. J. Ni, U. K. Chettiar, H. K. Yuan, V. M. Shalaev, *Nature* **2010**, *466*, 735.
[351] C. M. Bender, S. Boettcher, *Phys. Rev. Lett.* **1998**, *80*, 5243.
[352] S. Klaiman, U. Guenther, N. Moiseyev, *Phys. Rev. Lett.* **2008**, *101*.
[353] C. E. Rüter, K. G. Makris, R. El-Ganainy, D. N. Christodoulides, M. Segev, D. Kip, *Nat. Phys.* **2010**, *6*, 192.
[354] Z. Lin, H. Ramezani, T. Eichelkraut, T. Kottos, H. Cao, D. N. Christodoulides, *Phys. Rev. Lett.* **2011**, *106*, 213901.
[355] A. Regensburger, C. Bersch, M. A. Miri, G. Onishchukov, D. N. Christodoulides, U. Peschel, *Nature* **2012**, *488*, 167.
[356] J. Mei, G. C. Ma, M. Yang, Z. Y. Yang, W. J. Wen, P. Sheng, *Nat. Commun.* **2012**, *3*, 756.
[357] Z. Y. Liu, X. X. Zhang, Y. W. Mao, Y. Y. Zhu, Z. Y. Yang, C. T. Chan, P. Sheng, *Science* **2000**, *289*, 1734.
[358] J. S. Li, L. Fok, X. B. Yin, G. Bartal, X. Zhang, *Nat. Mater.* **2009**, *8*, 931.
[359] L. Fok, M. Ambati, X. Zhang, *MRS Bull.* **2008**, *33*, 931.
[360] N. P. Nelson RB, *J. Acoust. Soc. Am.* **1975**, *57*, 773.
[361] M. S. Kushwaha, P. Halevi, L. Dobrzynski, B. Djafari-Rouhani, *Phys. Rev. Lett.* **1993**, *71*, 2022.
[362] M. Sigalas, E. N. Economou, *Solid State Commun.* **1993**, *86*, 141.
[363] E. N. Economou, M. M. Sigalas, *Phys. Rev. B* **1993**, *48*, 13434.
[364] R. Martinez-Sala, J. Sancho, J. V. Sanchez, V. Gomez, J. Llinares, F. Meseguer, *Nature* **1995**, *378*, 241.
[365] J. V. Sanchez-Perez, D. Caballero, R. Martinez-Sala, C. Rubio, J. Sanchez-Dehesa, F. Meseguer, J. Llinares, F. Galvez, *Phys. Rev. Lett.* **1998**, *80*, 5325.
[366] F. R. M. de Espinosa, E. Jimenez, M. Torres, *Phys. Rev. Lett.* **1998**, *80*, 1208.
[367] W. M. Robertson, J. F. Rudy, *J. Acoust. Soc. Am.* **1998**, *104*, 694.
[368] J. O. Vasseur, P. A. Deymier, B. Chenni, B. Djafari-Rouhani, L. Dobrzynski, D. Prevost, *Phys. Rev. Lett.* **2001**, *86*, 3012.
[369] A. Khelif, A. Choujaa, B. Djafari-Rouhani, M. Wilm, S. Ballandras, V. Laude, *Phys. Rev. B* **2003**, *68*, 214301.
[370] E. L. Thomas, T. Gorishnyy, M. Maldovan, *Nat. Mater.* **2006**, *5*, 773.
[371] T. T. Wu, L. C. Wu, Z. G. Huang, *J. Appl. Phys.* **2005**, *97*, 094916.
[372] S. Benchabane, A. Khelif, J. Y. Rauch, L. Robert, V. Laude, *Phys. Rev. E* **2006**, *73*, 065601.
[373] I. El-Kady, R. H. Olsson, J. G. Fleming, *Appl. Phys. Lett.* **2008**, *92*, 233504.
[374] D. F. Goettler, M. F. Su, C. M. Reinke, S. Alaie, P. E. Hopkins, R. H. Olsson, I. El-Kady, Z. C. Leseman, *AIP Adv.* **2011**, *1*, 042001.
[375] W. Cheng, N. Gomopoulos, G. Fytas, T. Gorishnyy, J. Walish, E. L. Thomas, A. Hiltner, E. Baer, *Nano Lett.* **2008**, *8*, 1423.
[376] N. Gomopoulos, D. Maschke, C. Y. Koh, E. L. Thomas, W. Tremel, H. J. Butt, G. Fytas, *Nano Lett.* **2010**, *10*, 980.
[377] P. M. Walker, J. S. Sharp, A. V. Akimov, A. J. Kent, *Appl. Phys. Lett.* **2010**, *97*, 073106.
[378] D. Torrent, J. Sanchez-Dehesa, *New. J. Phys.* **2008**, *10*, 063015.
[379] Y. Cheng, F. Yang, J. Y. Xu, X. J. Liu, *Appl. Phys. Lett.* **2008**, *92*, 151913.
[380] M. Farhat, S. Enoch, S. Guenneau, A. B. Movchan, *Phys. Rev. Lett.* **2008**, *101*, 134501.
[381] N. Stenger, M. Wilhelm, M. Wegener, *Phys. Rev. Lett.* **2012**, *108*, 014301.
[382] B. I. Popa, L. Zigoneanu, S. A. Cummer, *Phys. Rev. Lett.* **2011**, *106*, 253901.
[383] A. M. Urbas, E. L. Thomas, H. Kriegs, G. Fytas, R. S. Penciu, L. N. Economou, *Phys. Rev. Lett.* **2003**, *90*, 108302.
[384] D. Schneider, F. Liaqat, E. H. El Boudouti, Y. El Hassouani, B. Djafari-Rouhani, W. Tremel, H. J. Butt, G. Fytas, *Nano Lett.* **2012**, *12*, 3101.
[385] A. Sato, Y. Pennec, N. Shingne, T. Thurn-Albrecht, W. Knoll, M. Steinhart, B. Djafari-Rouhani, G. Fytas, *ACS Nano* **2010**, *4*, 3471.
[386] L. F. Wang, K. Bertoldi, *Int. J. Solids Struct.* **2012**, *49*, 2881.
[387] F. Göncü, S. Lüding, K. Bertoldi, *J. Acoust. Soc. Am.* **2012**, *131*, EL475.
[388] J. F. Robillard, O. B. Matar, J. O. Vasseur, P. A. Deymier, M. Stippinger, A. C. Hladky-Hennion, Y. Pennec, B. Djafari-Rouhani, *Appl. Phys. Lett.* **2009**, *95*, 124104.
[389] J. Y. Yeh, *Physica B* **2007**, *400*, 137.
[390] K. Bertoldi, P. M. Reis, S. Willshaw, T. Mullin, *Adv. Mater.* **2010**, *22*, 361.
[391] C. Y. Koh, Ph.D. Thesis, *Massachusetts Institute of Technology* **2011**, <http://hdl.handle.net/1721.1/69791>.
[392] V. Leroy, A. Bretagne, M. Fink, H. Willaime, P. Tabeling, A. Tourin, *Appl. Phys. Lett.* **2009**, *95*, 171904.
[393] M. Devaud, T. Hocquet, J. C. Bacri, V. Leroy, *Eur. J. Phys.* **2008**, *29*, 1263.
[394] A. Bretagne, A. Tourin, V. Leroy, *Appl. Phys. Lett.* **2011**, *99*, 221906.
[395] U. Ingard, *J. Acoust. Soc. Am.* **1953**, *25*, 1037.
[396] S. Singamaneni, K. Bertoldi, S. Chang, J. H. Jang, S. L. Young, E. L. Thomas, M. C. Boyce, V. V. Tsukruk, *Adv. Funct. Mater.* **2009**, *19*, 1426.
[397] O. Thorp, M. Ruzzene, A. Baz, *Smart Mater. Struct.* **2001**, *10*, 979.
[398] L. Airoldi, M. Ruzzene, *New. J. Phys.* **2011**, *13*, 113010.
[399] A. Sato, W. Knoll, Y. Pennec, B. Djafari-Rouhani, G. Fytas, M. Steinhart, *J. Chem. Phys.* **2009**, *130*, 111102.
[400] U. Leonhardt, *Science* **2006**, *312*, 1777.
[401] D. Schurig, J. J. Mock, B. J. Justice, S. A. Cummer, J. B. Pendry, A. F. Starr, D. R. Smith, *Science* **2006**, *314*, 977.
[402] G. W. Milton, M. Briane, J. R. Willis, *New. J. Phys.* **2006**, *8*, 248.
[403] J. S. Li, J. B. Pendry, *Phys. Rev. Lett.* **2008**, *101*, 203901.
[404] R. Liu, C. Ji, J. J. Mock, J. Y. Chin, T. J. Cui, D. R. Smith, *Science* **2009**, *323*, 366.

ADVANCED OPTICAL MATERIALS

Editorial Advisory Board

Hatice Altug
Richard Averitt
Paul Braun
Mark Brongersma
Timothy J. Bunning
Cornelia Denz
Harald Giessen
Peter Günter
Zhi-Yuan Li
David Lidsey
Luis Liz-Marzán
Cefe López
Stefan Maier
Holger Moench
Dan Oron
Albert Polman
Ulrich Steiner
Jianfang Wang
Ralf Wehrspohn
Martin Wegener



Cover picture by Byeong-Kwon Ju,
Kyung Cheol Choi and co-workers
DOI: 10.1002/adom.201200021

Opt In for
Free Access
until Jan 2015

Advanced Optical Materials is an international, interdisciplinary forum for peer-reviewed papers dedicated to breakthrough discoveries and fundamental research in the field of optical materials. The scope of the journal covers all aspects of light-matter interactions including metamaterials and plasmonics, optical nanostructures, optical devices, photonics and more.

Volume 1, 12 issues in 2013.
Online ISSN: 2195-1071

Submit your manuscript for
Advanced Optical Materials online

www.edmgr.com/advopticalmat

Examples of excellent papers published in *Advanced Optical Materials*:



Magnetoplasmonics: Combining Magnetic and Plasmonic Functionalities

Gaspar Armelles, Alfonso Cebollada*,
Antonio García-Martín, María Ujué González

<http://onlinelibrary.wiley.com/doi/10.1002/adom.201200011/full>



ZnO p-n Homojunction Random Laser Diode Based on Nitrogen-Doped p-type Nanowires

J. Huang, S. Chu, J. Kong, L. Zhang, C. M. Schwarz,
G. Wang, L. Chernyak, Z. Chen, J. Liu

<http://onlinelibrary.wiley.com/doi/10.1002/adom.201200062/full>



Optically Reconfigurable Reflective/Scattering States Enabled with Photosensitive Cholesteric Liquid Crystal Cells

J. P. Vernon, U. A. Hrozhyk, S. V. Serak, V. P. Tondiglia,
T. J. White, N. V. Tabiryan, T. J. Bunning

<http://onlinelibrary.wiley.com/doi/10.1002/adom.201200014/full>



Broadband and Efficient Diffraction

C. Ribot, M.-S. Laure Lee, S. Collin, S. Bansropun,
P. Plouhinec, D. Thenot, S. Cassette, B. Loiseaux, P. Lalanne

<http://onlinelibrary.wiley.com/doi/10.1002/adom.201300215/full>



Fast and Low-Power All-Optical Tunable Fano Resonance in Plasmonic Microstructures

Y. Zhu, X. Hu, Y. Huang, H. Yang, Q. Gong

<http://onlinelibrary.wiley.com/doi/10.1002/adom.201200025/full>



Spoof Plasmon Surfaces: A Novel Platform for THz Sensing

Binghao Ng, Jianfeng Wu, Stephen M. Hanham,
Antonio I. Fernández-Domínguez, Norbert Klein,
Yun Fook Liew, Mark B. H. Breese, Minghui Hong,
Stefan A. Maier*

<http://onlinelibrary.wiley.com/doi/10.1002/adom.201300146/full>

WILEY-VCH

www.advopticalmat.de